UNDERSTANDING THE MECHANISM OF RNA-PROTEIN INTERACTION INVOLVED IN THE PROTEIN TRANSLOCATION IN ARCHAEA

Thesis submitted for the degree of

Doctor of Philosophy (Science)

In

Life Science and Biotechnology

By

Sayandeep Gupta

(Index No. 203/18/Life Sc./26 of 2018)

Department of Life Science and Biotechnology

Jadavpur University

2022

Dedicated to …

Alexandra Elbakyan

the torchbearer who single-handedly revolutionized the hierarchy of academic publication

&

Katalin Kariko

whose undying dedication and perseverance in research won against all patriarchal bigotry

ACKNOWLEDGEMENT

"Happiness can be found even in the darkest of times,
if one only remembers to turn on the light"

It was an evening in mid-December 2013 when I just had my first meeting with a tall man. A man who, for the next eight years, would be my friend, philosopher, and guide, in every possible way. Dr. Abhrajyoti Ghosh, whom we affectionately call "Abhra da", believed in me at a time when others could barely do so. Having suffered from a stale and toxic research environment in past years, I was dredging for a start-over, desperate to try my puny worth in this field. Eight years later, I still cannot say for sure that I have become worthy enough, because of the benchmark set by my PI. "My boss is flawless" – said no scholar ever (and vice-versa)! But if there is a true amalgamation of humility and scientific prowess, this man would come very close to it. A formal expression of gratitude or respect would never be enough for the countless brainstorming sessions we shared during coffee breaks or the pep-talks that followed each of my failed experiments. Thank you, boss.

Doctoral research is not just a set of routine works, but a journey that bleeds you, makes you stronger and more determined. And my journey has been fueled by the constant support from my parents. Mani and Baba have worked hard to bless me with the privilege which has helped me to cross most hurdles. Penning this long piece of labor has been possible only because my mother struggled all the odds in the world and continues to do so. I will never be able to live up to her spirit, but I hope to be able to honor it, someday. I would also like to thank all my immediate relatives who always respected my choice without a second thought. There is one person I would like to acknowledge specially – Mr. Sunil Gupta, or "kakudadu" as we call him. Of all my family members, he is the only man who truly feels the depth and excitement of a job that requires critical thinking. Every time we meet, he would remind me that to be a small part in a bigger problem, one needs to turn away from

small problems. I wish I could have the zeal and wisdom of this nonagenarian fellow when I be his age!

They say home is where the heart is. With each failure, each little moment of triumph, and all the mundane chores, my heart has always found comfort in the coziness of Archaea Lab and its inmates. Chandrima, Mousam, Shayantan and me started our journey together, and the whole concept of a research group was born with us. In time, we have been joined by Ivy di, Somi di, Triparna di, Arghya, Koustav and Sangita. I had the best of my moments with these people, and their mere presence soothed me in my worsts. Be it an academic discussion or a drinking session, I always had the best company to cherish it for good. My research acumen has greatly benefited as I kept learning from these guys, especially from Mousam. His unparalleled skill in critical thinking surely makes him one of the finest teachers I have ever had. I wish the youngest members, Agnita and Sangita will enjoy the privileges of Archaea Lab, much like I did.

It would be unfair to not mention my buddies from Dr. Anupama Ghosh's research group. Dibya, Udita, Rahul, Aroni, Shubhasish and Anisha have been an integral part of my professional life. From an early-morning walk in the hills to sharing deepest regrets in confidence, we grew up to be a family, divided by a few floors. I wish it remains like that as long as the labs stand.

A research is made successful by the right kind of academic help and collaboration. In that regard, I am immensely grateful to Dr. Anupama Ghosh, for she has always been insightful to my professional endeavor. I am equally thankful to Dr. Ankan Banerjee for his valuable help in structural analyses and Dr. Dhritiman Dey for all his efforts in tutoring me to hone new skills.

I would like to express my deepest gratitude to Dr. Souvik Sinha for all his professional help, and I am sure he will be highly amused! Souvik has been a constant fuel to my scientific quest. Sharing research ideology to chatting about every little wonders of science – his words have kept my chords tuned of late, amidst all the cacophony of life. I am also thankful to Dr. Sayani Sarkar as her influence has been instrumental to my personal growth. She introduced me to a new

diversity of arts, cuisines, and science literatures that shaped my taste over time. Things may not have ended to the best of our terms, but the moments shared have been among the bests in my life.

I would also like to pay my warmest gratitude to Mr. Anargha Biswas for the fantastic cover illustration. He suffered the anxiety of a doctoral student twice and survived!

I feel fortunate to have more than a few set of shoulders that I can rest upon when the storm hits hard. Naming them all is surely a mammoth task but not to mention a few, who witnessed the struggle and nursed the wounds, would be unfair as well. Suvankar and Ipsita have always been the best critics and the strongest pillars whereas Debroop has totally redefined brotherhood in terms of blind support. He, along with Upasana and Priyanka, practically encroached my college memory! Life would have meant nothing without their crazy jokes and cozy hugs.

I must offer the best of my respects to the staffs at the Department of Biochemistry and Central Instrument Facility, Bose Institute, whose active cooperation was a key factor to my progress. I am equally thankful to all the members of the Bose Institute Scholars' Forum who always made the annual events a success and taught me the nuances of teamwork and leadership.

I have been a part of a few serious cultural activities lately, and that satiated my mind even when the chores became strenuous. I am thankful to Antar Ranga, an intimate theatre group, and Silly Point, an online literary portal, for shaping my intellectual self and helping me discover the skill for popular science writing.

Finally, I would like to thank my Alma Mater, Jodhpur Park Boys' School for the fondest memories and the finest teachers that made me what I am today. It was the first home away from home, and it would remain so. Always.

(If you have been patient enough to take the blabber for three long pages, remember, I did it for eight years!)

Sayandeep Gupta

February 2022

ABBREVIATIONS

PCR	Polymerase Chain Reaction
SDS	Sodium Dodecyl Sulphate
PAGE	Polyacrylamide Gel Electrophoresis
EDTA	Ethylenediamine tetra-acetic acid
PMSF	Phenylmethylsulphonyl fluoride
CD	Circular dichroism
SAXS	Small-angle X-ray scattering
DMSO	Dimethyl sulphoxide
IPTG	Isopropyl-1-thio-β-D-galactopyranoside
kDa	kilo Dalton
kb	kilo base
µL	Microliter
µM	Micromolar
ml	Millilitre
mM	Millimolar
min	Minutes
M	Molar
FITC	Fluorescein isothiocyanate
TRITC	Tetramethylrhodamine-5-isothiocyanate
DPH	1,6-diphenyl-1,3,5-hexatriene
SRP	Signal recognition particle
SR	SRP receptor
Ni-NTA	Nickel-nitrilotriacetic acid
KCl	Potassium chloride
MOPS	3-(N-morpholino) propanesulfonic acid
APS	Ammonium persulfate
Tris	2-Amino-2-hydroxymethyl-propane-1,3-diol
GTP	Guanosine triphosphate

CONTENTS

Chapter no.	Chapter name	Page no.
I	**General introduction and objectives**	**1 - 28**
	1.1 Why archaea?	2
	1.2 *Sulfolobus* – a thermophilic acidophile	3
	1.3 Signal recognition particle	4
	1.4 SRP receptor	13
	1.5 Archaeal Sec translocon	15
	1.6 Future questions	18
	1.7 Aims of the study	19
	1.8 Bibliography	21
II	**General methods and materials**	**29 - 46**
III	**Biochemical and biophysical characterization of the purified SRP components**	**47 - 74**
	3.1 Introduction	48
	3.2 Materials & methods	51
	3.3 Results	55
	3.4 Discussion	68
	3.5 Conclusion	70
	3.6 Bibliography	71
IV	**Characterization of the functional targeting complex in archaea and the role of SRP components in facilitating the event at high temperature**	**75 - 103**
	4.1 Introduction	76
	4.2 Materials & methods	78

	4.3 Results	85
	4.4 Discussion	96
	4.5 Conclusion	98
	4.6 Bibliography	100
V	**Role of archaeal membrane and the structural domains of the SRP receptor in the activity of targeting complex at high temperature**	**105 - 132**
	5.1 Introduction	106
	5.2 Materials & methods	109
	5.3 Results	113
	5.4 Discussion	124
	5.5 Conclusion	127
	5.6 Bibliography	127
VI	**Final summary**	**133 - 135**
	List of publications	**137**

CHAPTER 1

INTRODUCTION TO PROTEIN TRANSLOCATION IN THE THIRD DOMAIN OF LIFE: INSIGHTS INTO THE BACKGROUND AND THE OBJECTIVE OF THE PRESENT STUDY

Protein translocation is a key process in the maintenance of cellular life. Proteins are sorted to various intracellular destinations or secreted into the extracellular space from their sites of synthesis. Gunter Blobel and David Sabatini, in the early 1970s, proposed the hypothesis of "molecular zip codes" in terms of intrinsic signal sequences that drive the transport and localization of secretory proteins (Blobel & Sabatini, 1971). In the following years, a series of publications by Blobel et al. provided insight into a signal sequence binding factor – Signal Recognition Particle (SRP). This discovery was a milestone in the molecular analysis of protein translocation across cellular membranes, and as expected, fetched a Nobel Prize (1999) for Gunter Blobel! However, the discovery of signal sequence and its binding factor was the key to explaining the previous finding that secreted proteins must cross the endoplasmic reticulum (ER) membrane readily after or during their synthesis. These proteins are subsequently sequestered into vesicles and secreted in the exterior environment. But how does that explain the event in prokaryotes? There must be a similar mechanism at play in the bacterial membrane. That was the only parallel concern until Carl Woese thought otherwise.

1.1 WHY ARCHAEA?

The world was at peace with the dichotomy of only two kinds of life forms, prokaryotic and eukaryotic, before 1977. Later in that year, Carl Woese's proposal of Archaea as the third domain of life brought a huge paradigm shift in the scientific community. Archaea, having differed in the small subunit rRNA sequence from that of the Bacteria and Eukarya, showed specific features from both domains in its cellular build-up (Woese & Fox, 1977; Woese et al., 1990). Evolution of domain-specific and individual ribosomal RNA and proteins were found to be in tandem as soon as the correlations between their signatures were established. This brought the domain Archaea in a close evolutionary relationship with Eukarya, so much so that the origin of eukaryotes, to date, is debated to have commenced from an ancestor common to both domains or the fusion of an archaeon with a bacterium (Jarrell et al., 2011). Nevertheless, archaea remained a true mosaic of biochemical and genomic characteristics comprising the other two domains, while presenting unique cellular

features of its own. The presence of glycoproteins in the archaeal cell wall S-layer, ether-linked diphytanylglycerol molecules in the membrane bilayer, eukaryotic ESCRT homologs involved in the archaeal cell division, unique cellular appendages, and many other interesting features have contributed to their ability to survive in extreme habitats as well as to exploit unique metabolic pathways (Jarrell et al., 2011). Thus, archaea became an important tool to address fundamental questions about the molecular evolution of the cell.

1.2 *Sulfolobus* – A THERMOPHILIC ACIDOPHILE

Initially, during the time they were introduced to the scientific community, archaea were largely represented by the methanogens. Within a few years, they were joined by thermoacidophiles and extreme halophiles. Over time and with discoveries of newer archaeal species from usual to extreme habitats, the Domain Archaea were further divided into four phyla – Euryarchaeota, Crenarchaeota, Nanoarchaeota, and Korarchaeota. Euryarchaeota includes methanogens and halophiles mostly, whereas Crenarchaeota comprises most of the mesophiles and acidophilic hyperthermophiles. Interestingly, these two phyla contain the best culturable archaeal species.

Sulfolobus is a genus belonging to Crenarchaeota that can thrive in an extremely acidic and hot environment. Usually, the phylum Crenarchaeota is more closely related to eukaryotes concerning their genomic signatures. The very first member of the *Sulfolobus* genus to be isolated from the Solfatara volcano is *Sulfolobus solfataricus*. However, initial studies were based upon Thomas Brock's experiments with *Sulfolobus acidocaldarius*, isolated from the Yellowstone National Park (USA). *S. acidocaldarius* is characterized by spherical cells (0.8-1.0 μM diameter) with an irregular shape and frequent lobes. The optimal condition for cellular growth includes 70-75 °C temperature and pH 3.0-4.0. This species is frequently used in research since genetic manipulation is easier in this organism due to the availability of a genetic toolbox (Leigh et al., 2011; Wagner et al., 2012).

In the past decade, genetic techniques for archaeal research have undergone revolutionary development. Such advancement results in an increased understanding of the role of this group of organisms in different environmental processes. In recent years, the research community has successfully established genetic experimentations in at least four groups of related archaeal organisms, namely, the methanogens, halophiles, *Thermococcales*, and *Sulfolobales*. The euryarchaeota phylum contains many genetically tractable methanogens (including members of the phylogenetically diverse *Methanosarcinales*, and *Methanococcales*), several haloarchaea, and members of *Thermococcales*. Amongst members of crenarchaeota, *Sulfolobales* (*S. solfataricus*, *S. acidocaldarius*, and *S. islandicus*) is the only genetically accessible group, and as such, the genetic studies are currently restricted to hyperthermoacidophilic crenarchaeota (Leigh et al., 2011; Wagner et al., 2012).

1.3 SIGNAL RECOGNITION PARTICLE

The SRP, a ribonucleoprotein complex, plays an important role in executing protein sorting and translocation in all three domains of life. It is a universally conserved protein-targeting machine that binds to a specific peptide sequence at the N-terminus of the nascent polypeptide chain and delivers it to the translocation system for further processing (Halic et al., 2004; Grudnik et a., 2009). The SRP-ribosome-nascent polypeptide complex (RNC) attaches to the cognate SRP receptor (SR) located on the targeted membrane (Egea et al., 2004). The interaction between the GTPase domains associated with both the SR and SRP allows the delivery of the concerned protein into the adjacent protein conducting channel (PCC). The process is empowered by GTP hydrolysis and the SRP is recycled for another round of targeting process (Koch et al., 2003; Nagai et al., 2003).

In general, protein translocation occurs either in a co- or post-translational manner in all three domains of life (Fig. 1.1). In eukaryotes, with few exceptions like fission yeast, proteins are transported co-translationally into the lumen of the endoplasmic reticulum (ER). In this mode, a signal peptide that emerges from the ribosome is bound by SRP (Noriega et al., 2014). Binding of SRP to the signal peptide arrests the

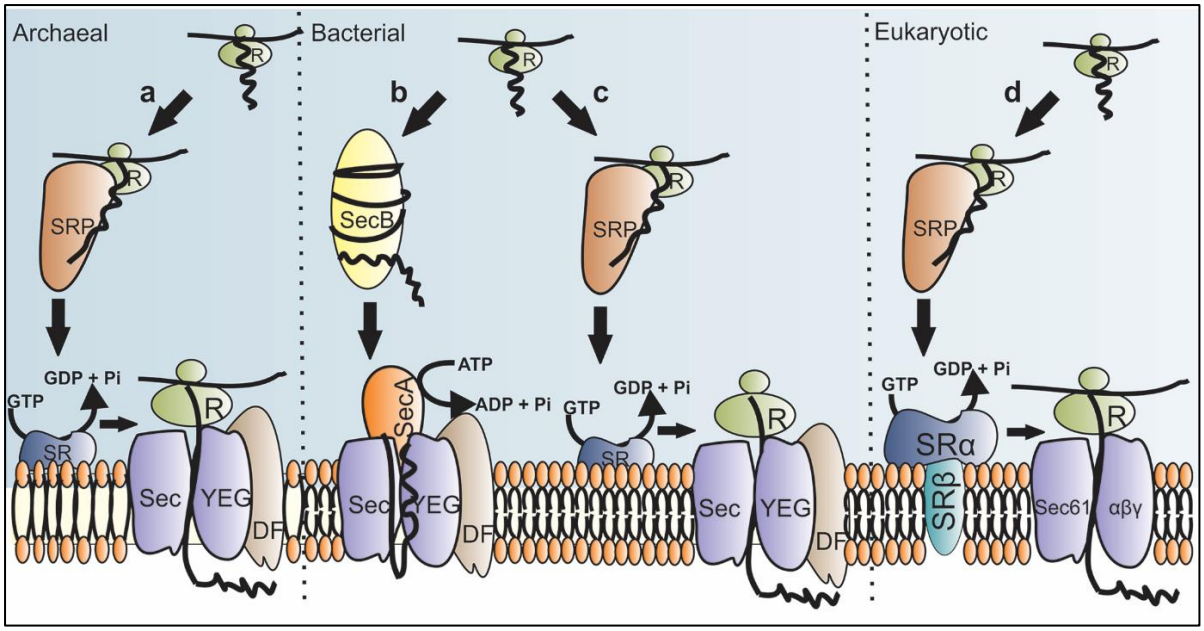

Figure 1.1. The Sec translocase can participate in both co-translational and post-translational translocation of proteins. The main components of Sec translocase involved in co-translational translocation are shown in archaea (a) bacteria (c) and eukaryotes (d). Post-translational translocation in bacteria is shown in (b).

protein translation and the entire RNC is targeted to the ER membrane, where this complex interacts with the SRP receptors SRα and SRβ. Finally, at ER membrane the ribosome docks onto the protein translocation channel (Sec61αβγ), and SRP is released from the nascent polypeptide chain (Fig. 1.1c). In bacteria and archaea, while membrane proteins are translocated in a co-translational manner, most of the secreted proteins are translocated in a post-translational manner (Fig. 1.1). Bacterial secretory proteins, after synthesis in the cytoplasm, are kept in a translocation-competent state and targeted to the cell membrane with the help of cytosolic chaperone, SecB. Upon arrival, these proteins are delivered to the peripheral membrane protein SecA. SecA is a secretion family ATPase that provides the driving force for the secretion process by pushing the secretory proteins into the translocation channel (SecYEG) (Fig. 1.1). Bacterial membrane proteins however are transported through SRP-mediated co-translational pathways like eukaryotes (Fig. 1.1b) (Bercovich-Kinori & Bibi, 2015; Gupta et al., 2016). In archaea, although both co- and post-translational translocations have been reported, no SecB or SecA homologs have yet been identified (Haney et al., 1999; Ortenberg & Mevarech, 2000;

Irhimovitch & Eichler, 2003). The protein translocation in archaea, therefore, seems solely dependent on the SRP machinery (Fig. 1.1a).

In different domains of life, the SRP shares similarities in its structural components as well as its mode of action. In eukaryotes, the SRP consists of a 7S RNA and six proteins, namely, SRP68, SRP72, SRP54, SRP19, SRP14, and SRP9 (Keenan et al., 2001) (Fig. 1.2). On contrary, bacteria have only one protein, Ffh (an SRP54 homolog) and a 4.5S RNA (Batey et al., 2000; Buskiewicz et al., 2005) (Fig. 1.2). Together they constitute the functional SRP and function together with the bacterial SRP receptor FtsY to incorporate the proteins into the plasma membrane (Ulbrandt et al., 1997). The SRP in archaea is composed of a 7S RNA of about 300 nucleotide residues and two protein components, e.g., SRP54 and SRP19 (Bhuiyan et al., 2000; Zwieb & Eichler, 2002). These components highly resemble their eukaryotic homologs. Nuclease treatment studies on SRP-complex reveal the presence of eukaryote-like Alu domain and S domain in archaeal SRP-RNA; the Alu domain comprises helices 1-5 and the S domain comprises a small portion of helix 5 and helices 6-8. Of these secondary RNA structures, helices 6-8 are bound by SRP19 and helix 8 is contacted by SRP54 (Gupta et al., 2016) (Fig. 1.2). In general, SRP54 (bacterial homolog Ffh) performs the main role by binding the nascent polypeptide and the SR (Romisch et al., 1989). The SRP19 is believed to provide a minor regulatory function in archaea, since, unlike the eukaryotic counterpart; it is easily dispensable in archaeal SRP assembly and protein sorting (Diener & Wilson, 2000; Yurist et al., 2007). The archaeal SRP is thus a true mosaic of eukaryotic and bacterial features along with certain unique attributes exclusive to this domain.

1.3.1 SRP RNA

The archaeal SRP RNA forms secondary stem-loop structures that contain extensive base pairing. These secondary structures include a prominent central helix flanked by two stem-loop-containing domains: a large S domain and a small Alu domain (Fig. 1.2). A helical section formed upon pairing of the 5′ and 3′ termini of SRP RNA, designated as Helix 1 is present only in archaeal and some bacterial (*Bacillus, Listeria* and *Staphylococcus*) SRP RNAs (Fig. 1.2) (Kempf et al., 2014).

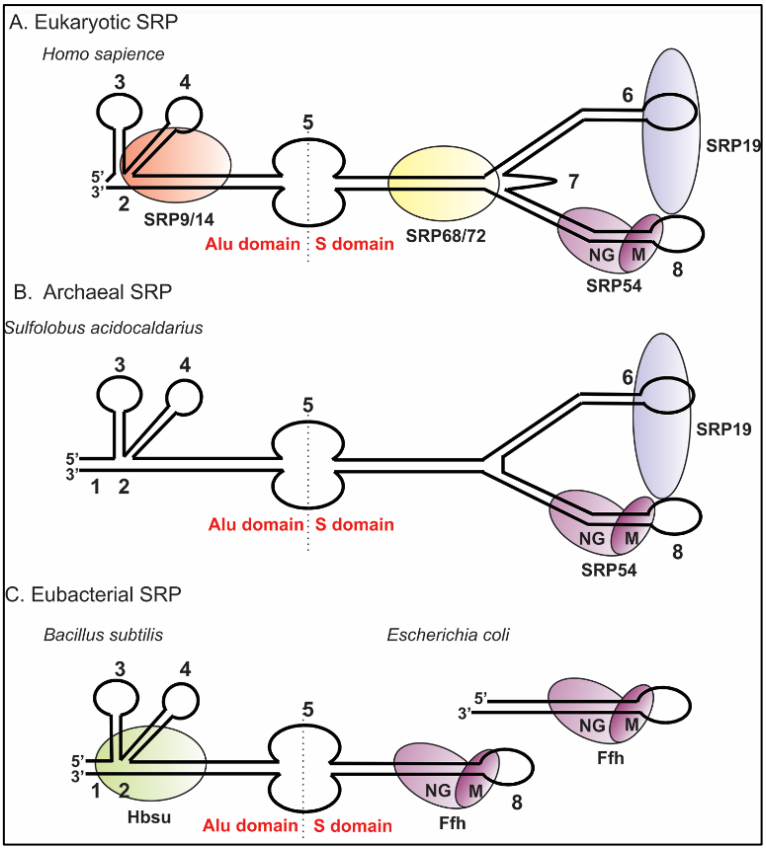

Figure 1.2. Signal Recognition Particle (SRP) across the evolution. Schematic illustrations of eukaryotic (human), archaeal (*S. acidocaldarius*), and bacterial (*B. subtilis* and *E. coli*) SRP complex are presented. The numbered helices of SRP RNA are indicated.

The number of base pairs that constitute Helix 1 also varies from one organism to another. For instance, *Pyrodictium occultum* SRP RNA Helix 1 contains only three base pairs whereas, in the case of *Methanococcus jannaschii*, it is 13 base pairs. Since this helical region holds the 5′ and 3′ ends of the SRP RNA together, the most likely function of this region could be protection against unfolding in response to extreme environmental conditions (Zwieb & Bhuiyan, 2010). Another notable feature of archaeal SRP RNA is the absence of helix 7 which is present only in eukaryotes (Fig. 1.2).

Helices 6 and 8 are the most prominent features of the SRP RNA (Fig. 1.2). These helices are held in proximity via interactions at two distinct sites. The first site of extensive base and backbone interactions comprises the tips of the helices, which have conserved bases at their respective tetraloops. In helix 6 two looped out, consecutive adenines, A176, and A177 interact with the base pairs in the asymmetric

loop of helix 8 through an A-minor motif. In general, the A-minor motif involves the insertion of the smooth, minor groove edges of adenines into the minor groove of neighboring helices, preferentially at the C–G base pairs, where they form hydrogen bonds with one or both 20 OHs of those pairs (Nissen et al., 2001). In the SRP RNA, bases in the short strand of the asymmetric loop base-pair continuously, while base stacking is interrupted in the long strand. Three unpaired nucleotides of this loop, A195, C196, and C197, point towards the interior of the helix (Hainzl et al., 2005). Helix 6 is exclusively present in eukaryotes and archaea. The apical tetraloop of this region has a GNAR consensus sequence, where N is any nucleotide and R is a purine. The SRP 19 mainly contacts the phosphoribosyl surface of this motif (Hainzl et al., 2002; Wild et al., 2010). Helix 8 similarly contains a usual GNRA motif at its tetraloop position. In *M. jannaschii*, GUAG tetraloop (helix 6) adopts a closed conformation where the first and fourth bases (G163 & G166) form a direct nucleotide interaction. It was also observed that the third and fourth bases (A165 and G166) of this tetraloop interact with the tetraloop A212-G209 pair and the tetraloop-closing G213-C208 pair at the helix 8 minor groove (Hainzl et al., 2002). Helix 8 is divided into sections 8a and 8b by an asymmetric loop. There is an atypical invariant A-C pair and two highly conserved G-G and G-A pairs within section 8b. Together they form a flattened minor groove to facilitate interaction with SRP54 (Batey et al., 2000). The RNA-M domain interaction alleviates the GTP hydrolysis by the NG domain. As evident from the study in *E. coli*, domain IV of 4.5S RNA forms a protein-interacting pocket in between an asymmetric and a symmetric internal loop. The terminal loop of helix 8 has a GRRA motif, almost always starting with guanosine and ending with highly conserved adenosine (Kuglstatter et al., 2002). The two adenosines of the apical tetraloops of helices 6 and 8 are involved in hydrogen bonding, as was first observed in *M. jannaschii* (Hainzl et al., 2005).

In hyperthermophilic crenarchaeon *Thermoproteus tenax*, the canonical SRP RNA gene has not been identified, while all the other archaeal components of the SRP complex (e.g., SRP19 and SRP54) are present in the genome (Plagens et al., 2015). It has been shown recently that, the 50 - and 30 -termini of this SRP RNA are located close to a functionally important loop present in all known SRP RNAs. These termini

are ligated together by a tRNA splicing endonuclease to generate a circular SRP RNA molecule that binds SRP54 and SRP19. The formation of such permuted circular RNA has been proposed to provide an evolutionary advantage to this thermophilic crenarchaeon (Plagens et al., 2015).

Since many archaea are characterized by higher optimal growth temperature (OGT), marks of thermal adaptations are supposed to be evident at their molecular level. Several studies have been made to instigate the level of thermal adaptation at the transcriptomic and proteomic levels. Transcriptome analyses have established that there is a positive correlation between the GC content of the double-stranded regions of structural RNAs and the OGT of prokaryotes (Nakashima et al., 2003). Thus, an increase in the GC content of nucleic acid stem results in the strengthening of the stability of its secondary structures. Therefore, in organisms living in a habitat of high-temperature natural selection would favor the increase in the GC content on the stem regions. In a recent phylogenetic-independence contrast (PIC) analysis, which is a comparative method for testing hypotheses of how organisms are adapted to their environment (Groussin & Gouy, 2011), a strong positive correlation was proposed between the stems GC content of archaeal SRP RNA and the OGT of respective organisms (Miralles F, 2011). In general, however, the only correlation that exists between OGT and the complete genome is in terms of the purine (A+G) content.

1.3.2 SRP19

The SRP19 of archaea is similar to the eukaryotic homolog and absent in bacteria. The NMR structure of SRP19 of *Archaeoglobus fulgidus* has been solved (Pakhomova et al., 2002). In addition, the crystal structures of both RNA-bound and free SRP19 have been elucidated by various research groups (Hainzl et al., 2007; Wild et al., 2010). Besides acting as an adapter to connect helices 6 and 8, through reconstitution studies in *A. fulgidus,* SRP 19 has been shown to aid in the binding of SRP54 to helix (Bhuiyan et al., 2000; Rose & Pohlschroder, 2002). The side-by-side alignment of the two crucial RNA helices, 6 and 8, is induced by SRP19 and in effect, brings about the conformational changes in the asymmetric loop of helix 8 necessary for SRP54

binding. This was evident both in the case of archaea and mammals. However, SRP19-independent tight binding has been presented in most of the other studies, including one in *Haloferax volcanii*, which suggests that SRP19 is rather a dispensable part of the archaeal SRP complex (Maeshima et al., 2001; Tozik et al., 2002). Egea *et al.* solved the crystal structure of *Pyrococcus furiosus* SRP19 and reported a βαββα fold adopted by the protein. A similar structure could be detected in the RNP domains of various RNA-binding proteins including the anticodon-binding domains of a few aminoacyl-tRNA synthetases (Egea et al., 2008). The reported structure also contains two loops- L1 and L2 (Fig. 3a). The L1 region is rigid, well-defined, and acts as the primary RNA binding surface. The SRP19 bridges the tetraloops of the helices when bound to the RNA molecule. It binds to the distal minor groove on helix 8 and the major groove at the tip of helix 6. In *M. jannaschii*, the helix 6 GNAR tetraloop has an open-loop conformation formed by U164 (Hainzl et al., 2002). This surface-exposed position is extensively stabilized by interactions with Met1, Tyr68, Asp67, and Lys69 of SRP19 via pseudo-Watson-Crick interactions. The loop closing base pair U162-G167 and the base of G163 are stabilized via extensive hydrogen bonding with Lys19 and Lys72 of SRP19 (Hainzl et al., 2005). There are two conserved Pro54 and Lys51 in the *M. jannaschii* complexes that occupy important positions. The Pro54 –carbonyl contacts G215 and its side chain are forced between helices 6 and 8. On the other hand, Lys51 makes hydrogen bonds with G209 which resides in the proposed signal sequence binding interface in the helix 8 backbone (Batey et al., 2000; Hainzl et al., 2002). The relatively disordered L2 region refolds upon contacting the SRP RNA. Such structural rearrangements induce the RNA to attain a conformation that accepts SRP54. This observation supports the idea that SRP19 may act as a molecular scaffold and a chaperone. It helps the SRP RNA in adopting the conformation necessary for its interaction with SRP54 (Egea et al., 2008).

Further experiments with *A. fulgidus* SRP show that for a compact arrangement of the SRP domain, the conserved adenosine in the GNAR tetraloop of helix 6, rather than SRP19, is responsible (Yin et al., 2004). In *H. volcanii* deletion of SRP19 did not affect protein translocation or membrane insertion (Yurist et al., 2007). Such SRP19-independent binding of archaeal SRP-RNA and SRP54 suggests a highly stable SRP

complex which may be required for growth under extreme environmental conditions (Diener & Wilson, 2000).

1.3.3 SRP54

SRP54 is a highly conserved multi-domain protein present in all organisms (Fig. 3). It is the most important component of the SRP complex. Deletion of SRP54 gene *ffh* (*f*ifty-*f*our *h*omolog, as named to describe the similarities between the eukaryotic SRP54 and its bacterial counterpart) in *H. volcanii* leads to cell death (Rose & Pohlschroder, 2002; Yurist et al., 2007). SRP54/Ffh is employed, not only in the interaction with SRP RNA but also in the binding of a signal peptide with the SRP receptor. The high-resolution crystal structure of this protein has been elucidated in various archaeal species, notably in *M. jannaschii* (Hainzl et al., 2007), *P. furiosus* (Egea et al., 2008), and *Sulfolobus solfataricus* (Rosendal et al., 2003). These structural insights revealed the presence of three domains in SRP54/Ffh - N domain, G domain, and M domain (Fig. 3b). The acidic N-terminal (N) domain is composed of four α-helices and is tightly associated with the central Ras-like GTPase (G) domain. Together they form a structural and functional catalytic unit (NG domain). The NG domain is connected to the C-terminal methionine-rich (M) domain via a flexible linker. This flexible linker region has the consensus sequence RXLGXGD (Fig. 3b). The conserved glycines within the linker region allow the RNA-bound SRP54 to undergo conformational rearrangements upon binding to the signal sequence (Rosendal et al., 2003). The glycine residues provide the articulation point between the NG core and M domain. Although the residues at the tip of the N domain and those in the M domain and its finger loop are reported to be in close interactions in *M. jannaschii* and *S. solfataricus* (Rosendal et al., 2003; Hainzl et al., 2007), studies in *P. furiosus* SRP54 showed no such interactions (Egea et al., 2008).

The G domain is homologous to the classical P-loop GTPase fold and contains an additional I-box insertion domain (IBD) of βαβα motif that can serve as a guanine nucleotide exchange factor (GEF) and stabilize the nucleotide-free protein (Moser et al., 1997). Inside IBD, an insertion loop contains multiple catalytic residues and represents a probable switch II region as found in Ras-like GTPases (Freymann et al.,

1997; Montoya et al., 1997). The interaction of nucleotide with the protein is mediated via the intricate hydrogen bonding network between the residues in the conserved motifs I, II, IV, and V. Just as in small GTPases, the P-loop or G1 region forms intricate hydrogen bonding with the G3 region and with the IBD.

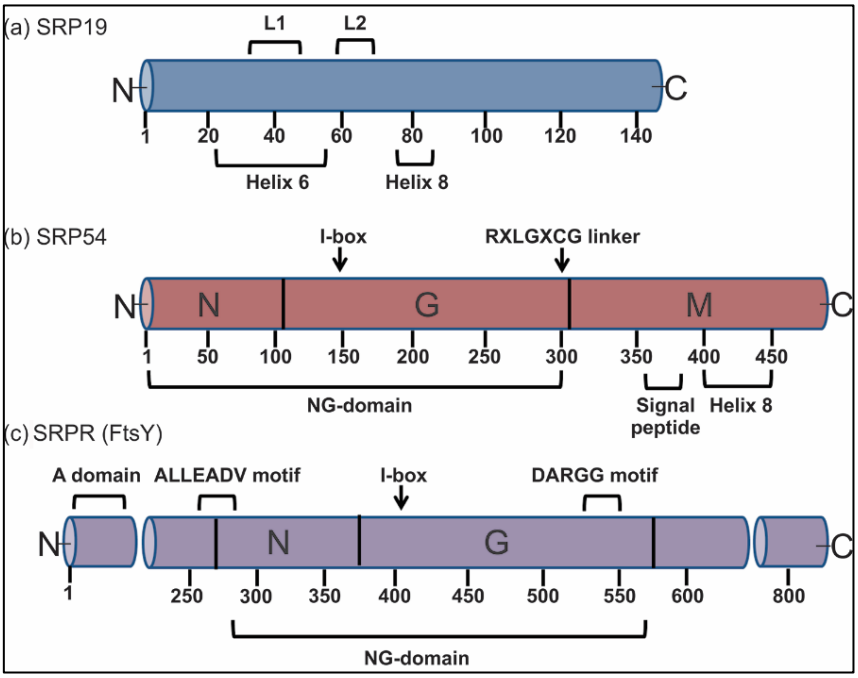

Figure 1.3. Features of (a) SRP19, (b) SRP54, and the (c) SRP receptor (FtsY). Indicated are the N- and C-termini. All the important and conserved residues are marked in the schematic representation. Regions and sites which interact with other SRP components, or the signal sequence, are marked with brackets below each panel.

In a study by Montoya et al., the nucleotide-binding site of *Acidianus ambivalens*-SRP54 was shown to have hydrogen bonding between Gln107 in G1 and Arg138 in IBD and weak interaction between Thr112 and Asp187 (Montoya et al., 1997). One single Thr112 to Ala mutation was shown to paralyze the GTP hydrolyzing ability of the NG core. From the studies performed on *S. solfataricus* and *A. ambivalens*, it was observed that the SRP54-NG domain of these organisms contains unique GY dipeptide insertion in the switch II region (Montoya et al., 2000; Rosendal et al., 2003). Such insertion is supposed to be present only in Crenarchaeota since *T. aquaticus* Ffh structure did not show such motif (Freymann et al., 1997). In *A. ambivalens*, this tyrosine (Tyr194) is engaged in a network of hydrogen bonds with Val106, Gly108, and Thr110 in the P-loop. Following such interactions, it has been

proposed that Tyr194 might be able to sense the conformational changes in the active site and communicate with the G1, G4, and I-box regions (Montoya et al., 2000). Eukaryotic SRP54 has a conserved threonine at the GTP binding site which is missing in some archaeal SRP54 proteins. This hints at some unique mechanism of GTP hydrolysis in the archaeal SRP system unlike that in the eukaryote. Though the 7S.S RNA is known to contact SRP54 at its M domain, contributions from the NG domain also play a role. As for the fact, such association is supposed to stimulate the SRP-SR dual GTPase activity.

The M domain has an all-helical fold and is composed of seven α-helices. Within the SRP core, the M domain contacts the helix 8 of the SRP RNA and on the other hand, interacts with the signal peptide via its C-terminal portion (Rosendal et al., 2003) (Fig. 3b). Signal sequences engaging the SRP have, in general, a core of 8-12 hydrophobic residues that preferentially adopts α-helical structure (Gierasch LM, 1989; Grudnik et al., 2009). The signal sequence is accepted in a groove formed by a finger-loop segment of the M domain that connects the α1 and α2 helices bordering the bottom of the groove (Keenan et al., 1998; Janda et al., 2010). In *Pfu* SRP54, the groove is covered by helices α10, α11, and α14 (Egea et al., 2008) and in *Ssol* SRP54, by αM1, αM2 and the C-terminal αM5 (Rosendal et al., 2003). The groove is lined by flexible hydrophobic residues that contribute to the structural plasticity required to bind signal peptides of different lengths and amino acid composition (Keenan et al., 1998). Portions of the finger loop may adopt α-helical conformation to favor the binding of a signal sequence by the M domain (Janda et al., 2010). N domain may also influence signal sequence binding by the M domain since mutations in the ALLEADV motif in the N domain severely impaired signal sequence binding (Newitt & Bernstein, 1997).

1.4 SRP RECEPTOR

Unlike the eukaryotic SRP receptor, which is composed of SRα and SRβ proteins, the archaeal SRP receptor shares similarities with the bacterial SRP receptor FtsY, which itself is a homolog of SRα (Miller et al., 1994) (Fig. 3c). Archaeal FtsY has a conserved NG domain shared with NG of SRP54, including the I-box, and may or may not

contain an N-terminal acidic (A) domain (Fig. 3c). The A domain may play a role in recruiting SRP to the archaeal membrane as observed in *H. volcanii* (Lichi et al., 2004; Haddad et al., 2005). However, proteolytic cleavage of the A domain from the NG catalytic core does not affect receptor function (Herskovits et al., 2001). The N domain of *P. furiosus* is elongated and lacks the N-terminal extension found in bacterial FtsY. Instead, it is characterized by a long N-terminal helix αN1, which is positively charged and might constitute the primary membrane interaction site. The site supports the initial attachment of the targeting system to the membrane and interaction with the translocon, as evident from the crystal structure analysis (Egea et al., 2008). Besides, the N domain of *Pfu*-FtsY was found to be very rich in charged residues (30 acidic and 25 basic amino acid residues), which contribute to the high thermostability of the protein through an intricate meshwork of intra-molecular salt bridges and hydrogen bonds stabilizing the N domain. The C-terminal end of helix αN1 also contains extended ion-pair networks to further facilitate thermo-stability.

Both the SRP54 and FtsY possess a central GTPase domain. The classical GTPase motifs I-IV (Bourne et al., 1991) are present in both SRP GTPases along with four additional elements, the I-box domain, the closing loop, the DARGG motif, and the ALLEADV motif for essential function (Keenan et al., 2001) (Fig. 3c). Contrary to the classical GTPases, SRP GTPases interact directly to stimulate concomitant hydrolysis of GTP and do not require a guanine nucleotide exchange factor for nucleotide release (Powers & Walter, 1995; Jagath et al., 2000). The crystal structure of *Pfu*-FtsY (Egea et al., 2008) reveals two nucleotide molecules, one at the catalytic site and the other at the protein surface next to the IBD motif. The RNC-SRP complex is targeted to the membrane through a dynamic GTP-dependent interaction between the NG domains of SRP54 and FtsY. These two GTPases interact tightly through the so-called "twinning" of their GTP substrates (Egea et al., 2004; Focia et al., 2004). Following this reciprocal GTP hydrolysis, the SRP54-FtsY complex dissociates, inducing the transfer of the ribosome-nascent chain complex to the translocon.

Another crystal structure consisting of *E. coli* Ffh-FtsY complex bound with 4.5S RNA from *D. radiodurans* explains how the different residues of the distal end of the

RNA are contacted by the Ffh-FtsY NG heterodimer (Ataide et al., 2011). C86 of the GUGCCG conserved motif in the distal portion of 4.5S RNA is contacted by Lys278 and Glu277 from Ffh-NG and Leu198 and Phe137 (IBD motif) of FtsY-NG. The M domain of Ffh also interacts with the domain IV of RNA (Buskiewicz et al., 2005). The tetraloop end of the RNA accelerates the initial assembly of the Ffh:FtsY complex, while the distal end facilitates the GTPase activation. The extensive interaction between FtsY and the distal end of the RNA is favored as part of the GTP-activated twin complex but never in the free state of the SRP receptor. The cryo-EM structure of the SRP–FtsY complex with a GTP analog in the presence of actively translating ribosome (translating a signal sequence) from *E. coli* revealed a complex interaction between the Ffh-M domain with the ribosome-nascent chain complexes (RNC) and signal sequence (von Loeffelholz et al., 2015). Furthermore, the single-molecule FRET and gold-labeling experiments showed that the NG domain contacts the RNA tetraloop at the early state of the complex formation (Kuhn et al., 2015; von Loeffelholz et al., 2015). In the activated state, however, the NG domain moves away from the tetra loop towards the distal end of the RNA.

SRP-SR interaction exposes the translocation binding site in the ribosome while associating with the RNC complex. In presence of SR in mammals, the S domain of RNA rotates itself with respect to the 60S subunit. As a result, the S domain moves closure to the ribosome and away from the peptide exit site (Luirink & Sinning, 2004). This is followed by the release of SRP-ribosome binding which exposes a site composed of ribosomal proteins L23e and L35 (L23p and L29p in *E. coli*). This serves as a major binding site for the translocon.

1.5 ARCHAEAL SEC TRANSLOCON

The three-dimensional structure of the *M. jannaschii* Sec translocon (SecYEG) has been solved and has provided valuable insights into the protein translocation in archaea (Van den Berg et al., 2004). Interestingly, archaeal Sec translocon components have emerged to be a link between bacterial and eukaryotic components. For example, *in silico* analysis of SecE of *S. solfataricus* revealed that it has sequence similarity to eukaryotic Sec61γ, which was previously considered to be

a distinct protein as compared to SecE in prokaryotes (Hartmann et al., 1994). On other hand, both bacterial and archaeal SecY shows similarity to Sec6α, with the archaeal proteins more closely related to their eukaryotic counterpart (Rensing & Maier, 1994). The complementation experiment with *M. vanielii* SecY homolog in the temperature-sensitive mutant of *E. coli* revealed that the archaeal SecY could functionally replace its bacterial counterpart even in the absence of the unique ether-linked phospholipid environment (Auer et al., 1991). Unlike SecY (Sec61α) or SecE (Sec61γ), the archaeal SecG shows little sequence similarity to its functional analogs in other two domains of life and has been identified from *in silico* analysis (Matlack et al., 1998; Cao & Saier, 2003).

Both in eukaryotes and bacteria, the Sec61αβγ/SecYEG translocon is associated with accessory components. In eukaryotes, the Sec61αβγ complex is associated with TRAM (Gorlich et al., 1992) or the Sec62/Sec63 (Deshaies et al., 1991) complex. The SecYEG complex in bacteria was detected in association with SecDFyajC (Duong & Wickner, 1997) or YidC (Scotti et al., 2000; Seitl et al., 2014; Kumazaki et al., 2014). In archaea, however, no auxiliary translocon components have yet been identified (Pohlschroder et al., 2005; Calo & Eichler, 2011). *In silico* analyses have confirmed the presence of genes encoding SecDF or YidC in archaea (Calo & Eichler, 2011). However, their functional role remained elusive. In bacteria, SecDF has been proposed to modulate the behavior of SecA, the ATPase that drives post-translational translocation (Economou et al., 1995; Duong & Wickner, 1997). In archaea, as no SecA has been identified, the function of SecDF remains an enigma (Pohlschroder et al., 1997). Nonetheless, the involvement of archaeal SecDF in Sec-mediated protein translocation has been verified by the generation of *secDF* deletion in *H.volcanii* (Hand et al., 2006). The YidC protein has been shown to participate in the membrane insertion of certain bacterial proteins (Samuelson et al., 2000). *In silico* analysis has identified YidC (Oxa/Alb3) homologs in some archaea but no functional confirmation is yet available for this protein in this domain (Luirink et al., 2001; Zhang et al., 2009).

One important question that arises, regarding the translocon, is how it interacts with the SRP-RNC-SRP receptor complex and facilitates entry of the nascent polypeptide chain. SecYEG is suggested to contact the L23 ribosomal protein and the signal sequence in vivo and the unloading of cargo into the translocon happens after the exquisitely timed event of concomitant GTP hydrolysis by SRP-SRP receptor complex (Shen et al., 2012). It has recently been shown in a study on bacterial Ffh-FtsY system that the RNC-induced delay in GTPase activation in the SRP-FtsY complex followed by the pause in the sliding over the RNA to the distal loop [99] is completely taken care of by the SecYEG translocon. The translocon reverses the cargo-induced pausing in vitro and restores efficient GTP hydrolysis. It never displaces the RNC from the docking site but displaces the GTPase complex from the proximal site and prolongs docking at the RNA distal site.

The mechanism of cargo loading from the SRP complex to the translocon has always been of huge interest. Several studies have demonstrated that SRP delivers RNCs directly to the FtsY, associated in a complex with the translocon. Recently, an in vitro site-directed cross-linking study using Forster resonance energy transfer (FRET) (Kuhn et al., 2015) indicated that the FtsY–SecY interaction is rather strong and GTP-independent, however, requires the association of phospholipids. The conserved lipid-binding helix of FtsY undergoes a random coil-to-helix transition upon induction by anionic phospholipids (Stjepanovic et al., 2011). The interaction between the A domain of FtsY with the membrane phospholipid as well as the SecYEG translocon has also been demonstrated recently (Lakomek et al., 2016). A domain of FtsY is shown to be highly flexible and intrinsically disordered. The positively charged N-terminal region and the C-terminal membrane targeting region of the A domain were shown to be in contact with the phospholipids in an alpha-helical conformation. The negatively charged central region is, however, found to be associated with the positively charged translocon non-specifically, suggesting that electrostatic force might be the driving factor for SecY–FtsY interaction.

The nascent chain enters the translocon via the opening of a lateral gate following a 'crack' in the translocation channel. The cytoplasmic C-terminal helix of *Pfu* SecY

seems likely to interact with the signal sequence in the nascent chain. This interaction induces the cytosolic vestibule to widen up and the lateral gate is open, without much conformational rearrangement (Egea & Stroud, 2010). Transmembrane helices 1 and 2, present in the SecYE complex, form a central helical plug and together with the ring region maintain a membrane seal that may act to prevent ion and solute leakage (Egea & Stroud, 2010). SecE exerts a clamping effect on the SecY subunit that is released upon lateral opening of SecY. The substrate then enters the vestibule and gradually dislocates the central plug. Such a process also allows interaction of the membrane phospholipids with the nascent chain within the translocon channel.

1.6 FUTURE QUESTIONS

Over the years, several interesting features of archaeal SRP-mediated protein translocation and membrane insertion have been elucidated. The SRPs of the crenarchaeon *A. ambivalens* and euryarchaea *A. fulgidus*, *P. furiosus*, and *H. volcanii* have been reconstituted, and the ability of the archaeal SRP54 to recognize and bind signal sequence has been established (Moll et al., 1999; Maeshima et al., 2001; Tozik et al., 2002). Besides, several crystal structures (SRP54, SRP19, FtsY, SecYEG, SRP54 with helix 8 of SRP RNA, SRP54 with a signal peptide, and SRP19 with 6th and 8th SRP RNA helices) concerning archaeal SRP complex were solved (Gupta et al., 2016). However, the lack of detailed biochemical analyses and limited availability of the genetic and cell-biological tools have restricted our progress in understanding the *in vivo* role of SRP in archaea. It remains unclear whether the translocation of secretory and membrane proteins display similar relations to protein translation in archaea and what role does SRP plays in these processes. Although the SRP is involved in the translocation of both membrane and secreted proteins in eukaryotes, SRP seems necessary for insertion of a sub-set of inner-membrane proteins in *E.coli*, and possibly for targeting of some secreted proteins (Denks et al., 2014). In archaea, evidence for both co-translational and post-translational protein translocation has been furnished, but to what extent these findings are representative remains to be

investigated (Dale & Krebs, 1999; Ortenberg & Mevarech, 2000; Irihimovich & Eichler, 2003).

The present work embarks on a journey to explore the biochemical basis underlying the macromolecular interaction associated with archaeal protein targeting. Within the limited frame of doctoral research, it tries to address a few basic questions, such as, the role of 7S RNA in the functionality of SRP54, how the concomitant GTP hydrolyses by SRP54 and FtsY is regulated, what factors govern the successful assembly of a targeting complex and if the archaeal membrane has any role in that.

1.7 AIM OF THE STUDY

The present thesis is divided into three major objectives aiming to characterize the signal recognition particle system in thermoacidophilic crenarchaea and to elucidate the intricate nature of protein-RNA and protein-protein interaction that govern this process.

1.7.1 *Biochemical and biophysical characterization of the purified SRP components*

Archaeal SRP is a ribonucleoprotein complex consisting of two proteins, SRP54 and SRP19, and a 7S RNA. SRP19 contacts helices 6 and 8 in the smaller S domain of the SRP RNA and possibly bring out specific conformational changes that widen the minor groove of the helix 8. This widened groove serves as the binding pocket for the M domain of SRP54. Lack of biochemical evidence has hindered our understanding of the protein targeting system in archaea, hence we sought to characterize the components of this pathway by biochemical as well as computational means. The RNA-binding ability of the two proteins was investigated by electrophoretic mobility shift assay and a computational model was also generated to identify key residues participating in this interaction. Mutations were introduced in the M domain of SRP54 based on that prediction and their effect on RNA binding was further tested. The intrinsic GTPase activity of SRP54 was also characterized considering the natural habitat of our model organism, *Sulfolobus acidocaldarius*.

1.7.2 *Characterization of the functional targeting complex in archaea and the role of SRP components in facilitating the event at high temperature*

The targeting complex (TC) can be defined as the functional association between SRP54 and its receptor FtsY that successfully mediates the process of cargo unloading and GTP hydrolysis. TC has been extensively studied in bacterial SRP systems and recently a detailed structural investigation into the *Sulfolobus* FtsY has provided the necessary support to elucidate the same in the archaeal domain. By the virtue of the FRET technique, we sought to characterize the role of SRP RNA in facilitating the formation of archaeal TC. Kinetic analyses using sub-optimal substrate concentration were employed to characterize the reciprocal GTP hydrolyzing activity by the participating GTPases by generating a battery of G domain mutants.

1.7.3 *Role of archaeal membrane and the structural domains of the SRP receptor in the activity of targeting complex at high temperature*

The components of TC have an intrinsic affinity toward the membrane phospholipid, especially the tetraether lipids in the archaeal plasma membrane. Since archaeal FtsY lacks any membrane-spanning domain, the possible dynamics of its membrane association remains elusive. Structural studies have implicated that the N terminal alpha helices and the acidic A domain have major roles to play in SRP54 association as well as membrane targeting. We, therefore, generated differentially truncated versions of FtsY and investigated their role in membrane association and SRP54 binding by using various biophysical techniques such as FRET, circular dichroism, small-angle X-ray scattering, and molecular dynamic simulation. The dual GTPase characteristic of the TC was also tested for the mutual affinity of the participating proteins.

1.8 BIBLIOGRAPHY

Akopian, D., Dalal, K., Shen, K., Duong, F., & Shan, S. O. (2013). SecYEG activates GTPases to drive the completion of cotranslational protein targeting. *Journal of Cell Biology*, *200*(4), 397–405.

Akopian, D., Shen, K., Zhang, X., & Shan, S. (2013). Signal recognition particle: an essential protein-targeting machine. In *Annual review of biochemistry* (Vol. 82).

Althoff, S. M., Stevens, S. W., & Wise, J. A. (1994). The Srp54 GTPase is essential for protein export in the fission yeast Schizosaccharomyces pombe. *Molecular and Cellular Biology*, *14*(12), 7839–7854.

Althoff, S., Selinger, D., & Wise, J. A. (1994). Molecular evolution of SRP cycle components: Functional implications. *Nucleic Acids Research*, *22*(11), 1933–1947.

Ataide, S. F., Ataide, S. F., Schmitz, N., Shen, K., Ke, A., Shan, S., Doudna, J. A., & Ban, N. (2012). *The Crystal Structure of the Signal with Its Receptor*. *881*(2011).

Auer, J., Spicker, G., & Böck, A. (1991). Presence of a gene in the archaebacterium Methanococcus vannielii homologous to secY of eubacteria. *Biochimie*, *73*(6), 683–688.

Batey, R. T., Rambo, R. P., Lucast, L., Rha, B., & Doudna, J. A. (2000). Crystal structure of the ribonucleoprotein core of the signal recognition particle. *Science*, *287*(5456), 1232–1239.

Bercovich-Kinori, A., & Bibi, E. (2015). Co-translational membrane association of the Escherichia coli SRP receptor. *Journal of Cell Science*, *128*(7), 1444–1452.

Bhuiyan, S. H., Gowda, K., Hotokezaka, H., & Zwieb, C. (2000). Assembly of archaeal signal recognition particle from recombinant components. *Nucleic Acids Research*, *28*(6), 1365–1373.

Blobel, G., & Sabatini, D. D. (1971). Ribosome-Membrane Interaction in Eukaryotic Cells. *Biomembranes*, 193–195.

Bourne, H. R., Sanders, D. A., & McCormick, F. (1991). The GTPase superfamily: conserved structure and molecular mechanism. *Nature*, *349*(6305), 117–127.

Buskiewicz, I., Kubarenko, A., Peske, F., Rodnina, M. V., & Wintermeyer, W. (2005). Domain rearrangement of SRP protein Ffh upon binding 4.5S RNA and the SRP receptor FtsY. *Rna*, *11*(6), 947–957.

Buskiewicz, I., Peske, F., Wieden, H. J., Gryczynski, I., Rodnina, M. V., & Wintermeyer, W. (2005). Conformations of the signal recognition particle protein Ffh from Escherichia coli as determined by FRET. *Journal of Molecular Biology*, *351*(2), 417–430.

Calo, D., & Eichler, J. (2011). Crossing the membrane in Archaea, the third domain of life. *Biochimica et Biophysica Acta - Biomembranes*, *1808*(3), 885–891.

Cao, T. B., & Saier, M. H. (2003). The general protein secretory pathway: phylogenetic analyses leading to evolutionary conclusions. *Biochimica et Biophysica Acta*, *1609*(1), 115–125.

Dale, H., & Krebs, M. P. (1999). Membrane insertion kinetics of a protein domain in vivo. The bacterioopsin n terminus inserts co-translationally. *The Journal of Biological Chemistry*, *274*(32), 22693–22698.

Denks, K., Vogt, A., Sachelaru, I., Petriman, N. A., Kudva, R., & Koch, H. G. (2014). The Sec translocon mediated protein transport in prokaryotes and eukaryotes. *Molecular Membrane Biology*, *31*(2–3), 58–84.

Deshaies, R. J., Sanders, S. L., Feldheim, D. A., & Schekman, R. (1991). Assembly of yeast Sec proteins involved in translocation into the endoplasmic reticulum into a membrane-bound multisubunit complex. *Nature*, *349*(6312), 806–808.

Diener, J. L., & Wilson, C. (2000). Role of SRP19 in assembly of the Archaeoglobus fulgidus signal recognition particle. *Biochemistry*, *39*, 12862–12874.

Duong, F., & Wickner, W. (1997a). Distinct catalytic roles of the SecYE, SecG and SecDFyajC subunits of preprotein translocase holoenzyme. *The EMBO Journal*, *16*(10), 2756–2768.

Duong, F., & Wickner, W. (1997b). The SecDFyajC domain of preprotein translocase controls preprotein movement by regulating SecA membrane cycling. *The EMBO Journal*, *16*(16), 4871–4879.

Economou, A., Pogliano, J. A., Beckwith, J., Oliver, D. B., & Wickner, W. (1995). SecA membrane cycling at SecYEG is driven by distinct ATP binding and hydrolysis events and is regulated by SecD and SecF. *Cell*, *83*(7), 1171–1181.

Egea, P. F., Napetschnig, J., Walter, P., & Stroud, R. M. (2008). Structures of SRP54 and SRP19, the two proteins that organize the ribonucleic core of the signal recognition particle from Pyrococcus furiosus. *PLoS ONE*, *3*(10).

Egea, P. F., Shan, S. O., Napetschnig, J., Savage, D. F., Walter, P., & Stroud, R. M. (2004). Substrate twinning activates the signal recognition particle and its receptor. *Nature*, *427*(6971), 215–221.

Egea, P. F., & Stroud, R. M. (2010). Lateral opening of a translocon upon entry of protein suggests the mechanism of insertion into membranes. *Proceedings of the National Academy of Sciences of the United States of America*, *107*(40), 17182–17187.

Egea, P. F., Tsuruta, H., de Leon, G. P., Napetschnig, J., Walter, P., & Stroud, R. M. (2008). Structures of the signal recognition particle receptor from the archaeon Pyrococcus furiosus: implications for the targeting step at the membrane. *PloS One*, *3*, e3619.

Focia, P. J., Shepotinovskaya, I. V., Seidler, J. A., & Freymann, D. M. (2004). Heterodimeric GTPase Core of the SRP Targeting Complex. *Science*, *303*(5656), 373–377.

Freymann, D. M., Keenan, R. J., Stroud, R. M., & Walter, P. (1997). Structure of the conserved GTPase domain of the signal recognition particle. *Nature*, *385*(6614), 361–364.

Gierasch, L. M. (1989). Signal sequences. *Biochemistry*, *28*(3), 923–930.

Görlich, D., Hartmann, E., Prehn, S., & Rapoport, T. A. (1992). A protein of the endoplasmic reticulum involved early in polypeptide translocation. *Nature*, *357*(6373), 47–52.

Groussin, M., & Gouy, M. (2011). Adaptation to environmental temperature is a major determinant of molecular evolutionary rates in archaea. *Molecular Biology and Evolution*, *28*(9), 2661–2674.

Grudnik, P., Bange, G., & Sinning, I. (2009). Protein targeting by the signal recognition particle. *Biological Chemistry*, *390*(8), 775–782.

Haddad, A., Rose, R. W., & Pohlschröder, M. (2005). The Haloferax volcanii FtsY homolog is critical for haloarchaeal growth but does not require the A domain. *Journal of Bacteriology*, *187*, 4015–4022.

Hainzl, T., Huang, S., & Sauer-Eriksson, A. E. (2007). Interaction of signal-recognition particle 54 GTPase domain and signal-recognition particle RNA in the free signal-recognition particle. *Proceedings of the National Academy of Sciences of the United States of America*, *104*(38), 14911–14916.

Hainzl, T., Huang, S., & Sauer-Eriksson, A. E. (2002). Structure of the SRP19 RNA complex and implications for signal recognition particle assembly. *Nature*, *417*, 767–771.

Hainzl, T., Huang, S., & Sauer-Eriksson, A. E. (2005). Structural insights into SRP RNA: An induced fit mechanism for SRP assembly. *Rna*, *11*(7), 1043–1050.

Hand, N. J., Klein, R., Laskewitz, A., & Pohlschröder, M. (2006). Archaeal and bacterial SecD and SecF homologs exhibit striking structural and functional conservation. *Journal of Bacteriology*, *188*(4), 1251–1259.

Hartmann, E., Sommer, T., Prehn, S., Görlich, D., Jentsch, S., & Rapoport, T. A. (1994). Evolutionary conservation of components of the protein translocation complex. *Nature*, *367*(6464), 654–657.

Herskovits, A. A., Seluanov, A., Rajsbaum, R., Ten Hagen-Jongman, C. M., Henrichs, T., Bochkareva, E. S., Phillips, G. J., Probst, F. J., Nakae, T., Ehrmann, M., Luirink, J., & Bibi, E. (2001). Evidence for coupling of membrane targeting and function of the signal recognition particle (SRP) receptor FtsY. *EMBO Reports*, *2*(11), 1040–1046.

Ilangovan, U., Bhuiyan, S. H., Hinck, C. S., Hoyle, J. T., Pakhomova, O. N., Zwieb, C., & Hinck, A. P. (2008). A. fulgidus SRP54 M-domain. *Journal of Biomolecular NMR*, *41*(4), 241–248.

Irihimovitch, V., & Eichler, J. (2003). Post-translational secretion of fusion proteins in the halophilic archaea Haloferax volcanii. Journal of Biological Chem 278(15):12881–12887

Jagath, J. R., Rodnina, M. V, & Wintermeyer, W. (2000). Conformational changes in the bacterial SRP receptor FtsY upon binding of guanine nucleotides and SRP. *Journal of Molecular Biology*, *295*, 745–753.

Janda, C. Y., Li, J., Oubridge, C., Hernández, H., Robinson, C. V., & Nagai, K. (2010). Recognition of a signal peptide by the signal recognition particle. *Nature*, *465*(7297), 507–510.

Jarrell, K. F., Walters, A. D., Bochiwal, C., Borgia, J. M., Dickinson, T., & Chong, J. P. J. (2011). Major players on the microbial stage: Why Archaea are important. *Microbiology*, *157*(4), 919–936.

Keenan, R. J., Freymann, D. M., Stroud, R. M., & Walter, P. (2001). The signal recognition particle. *Annual Review of Biochemistry*, *70*, 755–775.

Keenan, Robert J., Freymann, D. M., Walter, P., & Stroud, R. M. (1998). Crystal structure of the signal sequence binding subunit of the signal recognition particle. *Cell*, *94*(2), 181–191.

Kuglstatter, A., Oubridge, C., & Nagai, K. (2002). Induced structural changes of 7SL RNA during the assembly of human signal recognition particle. *Nature Structural Biology*, *9*(10), 740–744.

Kuhn, P., Draycheva, A., Vogt, A., Petriman, N. A., Sturm, L., Drepper, F., Warscheid, B., Wintermeyer, W., & Koch, H. G. (2015). Ribosome binding induces repositioning of the signal recognition particle receptor on the translocon. *The Journal of Cell Biology*, *211*(1), 91–104.

Kumazaki, K., Kishimoto, T., Furukawa, A., Mori, H., Tanaka, Y., Dohmae, N., Ishitani, R., Tsukazaki, T., & Nureki, O. (2014). Crystal structure of Escherichia coli YidC, a membrane protein chaperone and insertase. *Scientific Reports*, *4*.

Lakomek, N. A., Draycheva, A., Bornemann, T., & Wintermeyer, W. (2016). Electrostatics and Intrinsic Disorder Drive Translocon Binding of the SRP Receptor FtsY. *Angewandte Chemie (International Ed. in English)*, *55*(33), 9544–9547.

Leigh, J. A., Albers, S. V., Atomi, H., & Allers, T. (2011). Model organisms for genetics in the domain Archaea: methanogens, halophiles, Thermococcales and Sulfolobales. *FEMS Microbiology Reviews*, *35*(4), 577–608.

Lichi, T., Ring, G., & Eichler, J. (2004). Membrane binding of SRP pathway components in the halophilic archaea Haloferax volcanii. *European Journal of Biochemistry / FEBS*, *271*, 1382–1390.

Luirink, J., Samuelsson, T., & De Gier, J. W. (2001). YidC/Oxa1p/Alb3: evolutionarily conserved mediators of membrane protein assembly. *FEBS Letters*, *501*(1), 1–5.

Luirink, J., & Sinning, I. (2004). SRP-mediated protein targeting: Structure and function revisited. *Biochimica et Biophysica Acta - Molecular Cell Research*, *1694*(1-3 SPEC.ISS.), 17–35.

Maeshima, H., Okuno, E., Aimi, T., Morinaga, T., & Itoh, T. (2001). An archaeal protein homologous to mammalian SRP54 and bacterial Ffh recognizes a highly conserved region of SRP RNA. *FEBS Letters*, *507*(3), 336–340. https://doi.org/10.1016/S0014-5793(01)02996-9

Matlack, K. E. S., Mothes, W., & Rapoport, T. A. (1998). Protein translocation: tunnel vision. *Cell*, *92*(3), 381–390.

Miller, J. D., Bernstein, H. D., & Walter, P. (1994). Interaction of E. coli Ffh/4.5S ribonucleoprotein and FtsY mimics that of mammalian signal recognition particle and its receptor. *Nature*, *367*(6464), 657–659.

Miralles, F. (2011). Compositional and structural features related to thermal stability in the archaea SRP19 and SRP54 signal recognition particle proteins. *Journal of Molecular Evolution*, *72*(5–6), 450–465.

Moll, R., Schmidtke, S., & Schäfer, G. (1999). Domain structure, GTP-hydrolyzing activity and 7S RNA binding of Acidianus ambivalens ffh-homologous protein suggest an SRP-like complex in archaea. *European Journal of Biochemistry / FEBS*, *259*(1–2), 441–448.

Montoya, G., Svensson, C., Luirink, J., & Sinning, I. (1997). Crystal structure of the NG domain from the signal-recognition particle receptor FtsY. *Nature*, *385*(6614), 365–368.

Montoya, G., Te Kaat, K., Moll, R., Schäfer, G., & Sinning, I. (2000). The crystal structure of the conserved GTPase of SRP54 from the archaeon Acidianus ambivalens and its comparison with related structures suggests a model for the SRP-SRP receptor complex. *Structure*, *8*(5), 515–525.

Moser, C., Mol, O., Goody, R. S., & Sinning, I. (1997). The signal recognition particle receptor of Escherichia coli (FtsY) has a nucleotide exchange factor built into the GTPase domain. *Proceedings of the National Academy of Sciences of the United States of America*, *94*(21), 11339–11344.

Nakashima, H., Fukuchi, S., & Nishikawa, K. (2003). Compositional changes in RNA, DNA and proteins for bacterial adaptation to higher and lower temperatures. *Journal of Biochemistry*, *133*(4), 507–513.

Newitt, J. A., & Bernstein, H. D. (1997). The N-domain of the signal recognition particle 54-kDa subunit promotes efficient signal sequence binding. *European Journal of Biochemistry*, *245*(3), 720–729.

Nissen, P., Ippolito, J. A., Ban, N., Moore, P. B., & Steitz, T. A. (2001). RNA tertiary interactions in the large ribosomal subunit: the A-minor motif. *Proceedings of the National Academy of Sciences of the United States of America*, *98*(9), 4899–4903.

Noriega, T. R., Tsai, A., Elvekrog, M. M., Petrov, A., Neher, S. B., Chen, J., Bradshaw, N., Puglisi, J. D., & Walter, P. (2014). Signal recognition particle-ribosome binding is sensitive to nascent chain length. *Journal of Biological Chemistry*, *289*(28), 19294–19305.

Ortenberg, R., & Mevarech, M. (2000). Evidence for post-translational membrane insertion of the integral membrane protein bacterioopsin expressed in the heterologous halophilic archaeon Haloferax volcanii. *The Journal of Biological Chemistry*, *275*(30), 22839–22846.

Pakhomova, O. N., Deep, S., Huang, Q., Zwieb, C., & Hinck, A. P. (2002). Solution structure of protein SRP19 of Archaeoglobus fulgidus signal recognition particle. *Journal of Molecular Biology*, *317*(1), 145–158.

Plagens, A., Daume, M., Wiegel, J., & Randau, L. (2015). Circularization restores signal recognition particle RNA functionality in Thermoproteus. *ELife*, *4*(OCTOBER2015).

Pohlschröder, M., Giménez, M. I., & Jarrell, K. F. (2005). Protein transport in Archaea: Sec and twin arginine translocation pathways. *Current Opinion in Microbiology*, *8*(6), 713–719.

Pohlschröder, M., Prinz, W. A., Hartmann, E., & Beckwith, J. (1997). Protein translocation in the three domains of life: variations on a theme. *Cell*, *91*(5), 563–566.

Powers, T., & Walter, P. (1995). Reciprocal stimulation of GTP hydrolysis by two directly interacting GTPases. *Science*, *269*(5229), 1422–1424.

Rensing, S. A., & Maier, U. G. (1994). The SecY protein family: comparative analysis and phylogenetic relationships. *Molecular Phylogenetics and Evolution*, *3*(3), 187–191.

Rose, R. W., & Pohlschröder, M. (2002). In vivo analysis of an essential archaeal signal recognition particle in its native host. *Journal of Bacteriology*, *184*(12), 3260–3267.

Rosendal, K. R., Wild, K., Montoya, G., & Sinning, I. (2003). Crystal structure of the complete core of archaeal signal recognition particle and implications for interdomain communication. *Proceedings of the National Academy of Sciences of the United States of America*, *100*(25), 14701–14706.

Samuelson, J. C., Chen, M., Jiang, F., Möller, I., Wiedmann, M., Kuhn, A., Phillips, G. J., & Dalbey, R. E. (2000). YidC mediates membrane protein insertion in bacteria. *Nature*, *406*(6796), 637–641.

Scotti, P. A., Urbanus, M. L., Brunner, J., De Gier, J. W. L., Von Heijne, G., Van Der Does, C., Driessen, A. J. M., Oudega, B., & Luirink, J. (2000). YidC, the Escherichia coli homologue of mitochondrial Oxa1p, is a component of the Sec translocase. *The EMBO Journal*, *19*(4), 542–549.

Seitl, I., Wickles, S., Beckmann, R., Kuhn, A., & Kiefer, D. (2014). The C-terminal regions of YidC from Rhodopirellula baltica and Oceanicaulis alexandrii bind to ribosomes and partially substitute for SRP receptor function in Escherichia coli. *Molecular Microbiology*, *91*(2), 408–421.

Shen, K., Arslan, S., Akopian, D., Ha, T., & Shan, S. O. (2012). Activated GTPase movement on an RNA scaffold drives co-translational protein targeting. *Nature*, *492*(7428), 271–275.

Shen, K., Wang, Y., Hwang Fu, Y. H., Zhang, Q., Feigon, J., & Shan, S. O. (2013). Molecular Mechanism of GTPase Activation at the Signal Recognition Particle (SRP) RNA Distal End. *Journal of Biological Chemistry*, *288*(51), 36385–36397.

Stjepanovic, G., Kapp, K., Bange, G., Graf, C., Parlitz, R., Wild, K., Mayer, M. P., & Sinning, I. (2011). Lipids Trigger a Conformational Switch That Regulates Signal Recognition Particle (SRP) -mediated Protein Targeting. *Journal of Biological Chemistry*, *286*(26), 23489–23497.

Tozik, I., Huang, Q., Zwieb, C., & Eichler, J. (2002). Reconstitution of the signal recognition particle of the halophilic archaeon Haloferax volcanii. *Nucleic Acids Research*, *30*(19), 4166–4175.

Van Den Berg, B., Clemons, W. M., Collinson, I., Modis, Y., Hartmann, E., Harrison, S. C., & Rapoport, T. A. (2004). X-ray structure of a protein-conducting channel. *Nature*, *427*(6969), 36–44.

Von Loeffelholz, O., Jiang, Q., Ariosa, A., Karuppasamy, M., Huard, K., Berger, I., Shan, S. O., & Schaffitzel, C. (2015). Ribosome-SRP-FtsY cotranslational targeting complex in the closed state. *Proceedings of the National Academy of Sciences of the United States of America*, *112*(13), 3943–3948.

Wagner, M., van Wolferen, M., Wagner, A., Lassak, K., Meyer, B. H., Reimann, J., & Albers, S. V. (2012). Versatile Genetic Tool Box for the Crenarchaeote Sulfolobus acidocaldarius. *Frontiers in Microbiology*, *3*(JUN).

Wild, Klemens, Bange, G., Bozkurt, G., Segnitz, B., Hendricks, A., & Sinning, I. (2010). Structural insights into the assembly of the human and archaeal signal recognition particles. *Acta Crystallographica Section D: Biological Crystallography*, *66*(3), 295–303.

Wild, Klemens, Bange, G., Motiejunas, D., Kribelbauer, J., Hendricks, A., Segnitz, B., Wade, R. C., & Sinning, I. (2016). Structural Basis for Conserved Regulation and Adaptation of the Signal Recognition Particle Targeting Complex. *Journal of Molecular Biology*, *428*(14), 2880–2897.

Woese, C. R., Kandler, O., & Wheelis, M. L. (1990). Towards a natural system of organisms: proposal for the domains Archaea, Bacteria, and Eucarya. *Proceedings of the National Academy of Sciences*, *87*(12), 4576–4579.

Woese, C. R., & Fox, G. E. (1977). Phylogenetic structure of the prokaryotic domain: The primary kingdoms. *Proceedings of the National Academy of Sciences*, *74*(11), 5088–5090.

Yin, J., Huang, Q., Pakhomova, O. N., Hinck, A. P., & Zwieb, C. (2004). The conserved adenosine in helix 6 of Archaeoglobus fulgidus signal recognition particle RNA initiates SRP assembly. *Archaea*, *1*(4), 269–275.

Yurist, S., Dahan, I., & Eichler, J. (2007). SRP19 is a dispensable component of the signal recognition particle in Archaea. *Journal of Bacteriology*, *189*(1), 276–279.

Zhang, Y. J., Tian, H. F., & Wen, J. F. (2009). The evolution of YidC/Oxa/Alb3 family in the three domains of life: a phylogenomic analysis. *BMC Evolutionary Biology*, *9*(1).

CHAPTER 2

An account of reagents, resources, strains, clones and experimental methods used in the study

2.1 MATERIALS

2.1.1 Bacterial strains used in the study

Bacterial strains	Relevant characteristics	Source or reference
E. coli XL1Blue	recA1 endA1 gyrA96 thi-1 hsdR17 supE44 relA1 lac [F´ proAB lacIq ZΔM15 Tn10 (Tet^r)]	Stratagene
E. coli BL21(DE3)-RIL	B F-ompT hsdS(rB−mB−) dcm+Tetr *E. coli* gal λ (DE3) endA Hte [argU ileY leuW Cam^r]	Stratagene
Sulfolobus acidocaldarius DSM639	Hyper-thermoacidophilic crenarchaeon which grows optimally at 80 °C and pH 2–3	DSMZ
Haloferax volcanii H53	Δ*pyrE2* Δ*trpA* (background strain DS70)	72

Tet^r, tetracycline-resistant; Cam^r, chloramphenicol resistant.

2.1.2 Primers used in the study

Primers	Salient features	Source or reference
12	5′-CCCCCGGTACCATGGTCAGGTAGGG-3′ Forward primer for Saci_0095 with KpnI cut site	Present study
13	5′-CCCCCAAGCTTGTCAGCTCCCCTATG-3′ Reverse primer for Saci_0095 with HindIII cut site	Present study
14	5′-GGGGGAATTCGATGAGCTTAAGAG-3′ Forward primer for Saci_0759 with EcoRI cut site	Present study
15	5′-GGGGGAAGCTTCTATTTATTCTTTTCTAATTC-3′ Reverse primer for Saci_0759 with HindIII cut site	Present study
16	5′-CCCCCGGATCCGTTGTTAGATGGTCTAAG-3′ Forward primer for Saci_1310 with BamHI cut site	Present study
17	5′-CCCCCAAGCTTTTATTGATTACTTCCG-3′ Reverse primer for Saci_1310 with HindIII cut site	Present study

18	5′- ATGCGTCCGGCGTAGAG-3′	Present
	Forward sequencing primer for MCS1 of pETDuet-1	study
19	5′- GATTATGCGGCCGTGTACAA-3′	Present
	Reverse sequencing primer for MCS1 of pETDuet-1	study
20	5′- TTGTACACGGCCGCATAATC-3′	Present
	Forward sequencing primer for MCS2 of pETDuet-1	study
21	5′- GCTAGTTATTGCTCAGCGG-3′	Present
	Reverse sequencing primer for MCS2 of pETDuet-1	study
452	5′- CCATGGGCATAATTTGTTTTGATAG-3′	Present
	Forward primer for Saci_1462 with NcoI cut site	study
165	5′- GGGGGCTCGAGACTACTGAATATCCTTTCTAC-3′	Present
	Reverse primer for Saci_1462 with XhoI cut site	study

2.1.3 Plasmid used in the study

Plasmids	Relevant characteristics	Source or reference
pET28a	Kan^r, Bacterial expression vector with T7 promoter, replicon ColE1 (pBR322), and one MCS.	Novagen
pGEM-3Z	Amp^r, bacterial transcription vector with T7 RNA polymerase promoter, replicon ColE1 (pUC18), and one MCS	Promega
pETDuet1	Amp^r, Bacterial expression vector with T7 promoter, replicon ColE1 (pBR322), and two MCS	Novagen
pAG3	Amp^r, pETDuet1 carrying N terminal His-tagged Saci_1310 (SRP54) using restriction sites BamHI-HindIII	Present study
pAG5	Kan^r, pGEM-3Z carrying Saci_0095 (7S SRP RNA) using restriction sites KpnI-HindIII	Present study
pAG13	Amp^r, pETDuet1 carrying N terminal His-tagged Saci_0759 (SRP19) using restriction sites NdeI-XhoI	Present study

pAG21	Kan^r, pGEM3Z carrying 133-228 nucleotide of *Saci_0095* (S domain, SRP RNA) using KpnI/HindIII	Present study
pAG351	Kan^r, pET28a carrying C terminal His-tagged Saci_1462 (FtsY) using restriction sites NcoI-XhoI	Present study

Kan^r, kanamycin-resistant; Amp^r, ampicillin-resistant

2.1.4 Growth medium used

2.1.4.1 Luria Bertini (LB) medium

Tryptone – 10 gm/lit

Yeast extract -5 gm/lit

Sodium chloride- 10 gm/lit

All components were dissolved, and volume made up to the desired amount. The pH was adjusted to pH 7.0 by the addition of 5N NaOH before volume adjustment.

2.1.4.2 *Sulfolobus acidocaldarius* growth media

Trace elements (2000X)	**Brock I (1000X)**	**Brock II (100X)**	**Brock III (200X)**	**Fe-Solution (1000x)**
$MnCl_2$, 4 H_2O – 3.6 gm/L $Na_2B_4O_7$, 10 H_2O – 9.0 gm/L $ZnSO_4$, 7 H_2O – 0.44 gm/L $CuCl_2$, 2 H_2O – 0.10 gm/L $NaMoO_4$, 2 H_2O – 0.06 gm/L $VOSO_4$, 2 H_2O – 0.06 gm/L	$CaCl_2$, $2H_2O$ – 70 gm/lit	$(NH_4)_2SO_4$ – 130 gm/L $MgSO_4$, $7H_2O$ – 25 gm/L 1.5 ml H_2SO_4 – 1:1	KH_2PO_4 Trace Elements 1.5 ml H_2SO_4 – 1:1	$FeCl_2$ or $FeCl_3$, $6H_20$–20gm/L

$CuSO_4$, 7 H_2O – 0.2 gm/L

Final composition:

Components	1 L culture
Brock I	1 ml
Brock II	10 ml
Brock III	5 ml
Fe 2+	1 ml
Trypton (20%)	10 ml
Sucrose (20%)	10 ml
Yeast (10%)	10 ml

Adjust pH to 3.5 with H_2SO_4

2.1.4.3 *Haloferax volcanii* growth medium

Salt	1 L
NaCl	240 gm
$MgCl_2$, $6H_2O$	30 gm
$MgSO_4$, $7H_2O$	35 gm
KCl	7 gm
$CaCl_2$, $2H_2O$ (added from 1 M stock)	5 ml (0.5gm/L)

2.1.4.4 23% Modified Growth Medium

Components	1 L
Saltwater	767 ml
Pure water	200 ml
Peptone	5 gm
Yeast extract	1 gm

2.1.5 Buffers and solutions

2.1.5.1 *Competent cell preparation*

MOPS buffer stock solution (pH 7.0)	Aqueous solution of 1 M MOPS
MOPS buffer stock solution (pH 6.5)	Aqueous solution of 1 M MOPS
Rubidium chloride stock solution ($RbCl_2$)	0.1 M aqueous solution
Calcium chloride stock solution ($CaCl_2$)	0.5 M aqueous solution
Solution I	0.5 ml MOPS (pH 7.0) +5 ml $RbCl_2$+ 44.5 ml autoclaved water
Solution II	1 ml MOPS (pH 6.5) +10 ml $RbCl_2$+10 ml $CaCl_2$ +79 ml autoclaved water
Solution III	2 ml glycerol + 10 ml Solution III

2.1.5.2 *Plasmid isolation by alkaline lysis*

Solution I	50 mM glucose, 25 mM Tris-HCl (pH 8.0), 1 mM EDTA
Solution II	0.2 mM NaOH, 1% SDS
Solution III	3 M Sodium acetate, pH 4.8
RNase A	10 mg/ml
Phenol: chloroform: isoamyl alcohol	A mixture of phenol, chloroform, isoamyl alcohol in 25:24:1 ratio, saturated with Tris-HCl (50 mM pH 8.0)
TE buffer	10 mM Tris-HCl (pH 8.0), 1 mM EDTA

2.1.5.3 *SDS-polyacrylamide gel electrophoresis (PAGE) for protein*

30:0.8 acrylamide: bis-acrylamide solution (100 ml)	30 gm acrylamide and 0.8 gm bis-acrylamide dissolved in deionised water

Buffer for resolving gel	1.5 M Tris-HCl pH 8.8
Buffer for stacking gel	0.5 M Tris-HCl pH 6.8
5X Loading dye	0.0625 M Tris-HCl (pH 6.8), 15% glycerol, 0.1% SDS, 1% β-mercaptoethanol, 0.001% bromophenol blue
5X running buffer	15 gm Tris, 72 gm glycine, and 5 gm SDS dissolved in 1000 lit of water
Staining solution	0.1 % Coomassie blue R-250 dissolved in 50: 10: 40 methanol, acetic acid, and water solution
De-staining solution	methanol: acetic acid: water in 40:10:50 ratios

2.1.5.4 ***Agarose gel electrophoresis for nucleic acid***

10X TBE (1 L)	108 gm Tris-base, 55 gm boric acid, 7.2 gm $Na_2EDTA, 2H_2O$
Agarose solution	The required amount of agarose was suspended in 0.5X TBE, melted, and cooled to 55 °C before pouring in the casting block
Ethidium Bromide (EtBr) solution.	0.1 gm of EtBr was dissolved in 10 ml of water
6X loading dye	0.5X TBE, 30% glycerol, 0.05% bromophenol blue

2.1.5.5 ***Native gel electrophoresis for protein-nucleic acid binding***

50X TAE (1 L)	242gm Tris-base, 57.1ml glacial acetic acids and 37.2gm Na_2EDTA, $2H_2O$.
30:0.8 acrylamide: bis-acrylamide solution	As described in 2.1.5.x
10X Native gel loading dye	50% glycerol, 1mM EDTA, 0. 25% bromophenol blue and 0. 25% xylene cyanol.
Gel solution preparation	The required amount of stock solution was taken in 1X TAE, additionally, glycerol at a final of 5% concentration was added. Volume was made up with deionized water, degassed and TEMED and APS were added to it.

2.1.5.6 ***Urea polyacrylamide gel electrophoresis (PAGE) for RNA***

10X TBE	As described in 2.1.5.4
19:1 acrylamide: bis-acrylamide solution	19 gm acrylamide and 1 gm bis-acrylamide dissolved in deionized water and volume made up to 100 ml
2X RNA loading dye	80% (v/v) formamide, 1mM EDTA (pH 8.0), 0.1% bromophenol blue and 0.1% xylene cyanol.
Gel solution preparation	The required amount of stock acrylamide solution was taken in 1X TBE and the required amount of urea was added so that the final concentration becomes 8M urea. The required amount of APS and TEMED

	was added after volume makeup with deionized water.

2.1.5.7 *Overexpression of protein*

IPTG solution	1 M (0.238 gm/ml) aqueous solution
Kanamycin solution	50 mg/ml aqueous solution
Chloramphenicol solution	35 mg/ml ethanol solution
Ampicillin solution	100 mg/ml aqueous solution

2.1.5.8 *Purification of overexpressed protein*

Lysozyme solution	10 mg/ml aqueous solution
PMSF solution	100 mM in isopropanaol
Imidazole solution	1 M aqueous solution pH 8.0
Cell resuspension buffer	50 mM Tris-Cl (pH 8.0), 150 mM KCl
Lysis buffer	Cell resuspension buffer + 1 mM PMSF + 1 mM Lysozyme
Wash buffer I	Cell resuspension buffer + 10 mM imidazole
Wash buffer II	Cell resuspension buffer + 20 mM imidazole
Elution buffer I	Cell resuspension buffer + 100 mM imidazole
Elution buffer II	Cell resuspension buffer + 200 mM imidazole
Elution buffer III	Cell resuspension buffer + 300 mM imidazole
Elution buffer IV	Cell resuspension buffer + 400 mM imidazole

Elution buffer V	Cell resuspension buffer + 500 mM imidazole
Dialysis buffer	50 mM Tris-Cl (pH 8.0), 150 mM KCl, 10% glycerol

2.1.6 Commonly used commercial reagents

2.1.6.1 *Reagents for cloning*

Reagents	Manufacturers
NcoI	Thermo Scientific
XhoI	Thermo Scientific
KpnI	Thermo Scientific
HindIII	Thermo Scientific
BamHI	Thermo Scientific
EcoRI	Thermo Scientific
Tango buffer	Thermo Scientific
T4 DNA Ligase	Thermo Scientific
$MgCl_2$	Thermo Scientific
DMSO	Thermo Scientific
dNTPs	Thermo Scientific
Nuclease free water	Ambion
Taq polymerase	Invitrogen & TaKaRa
Phusion polymerase	Thermo Scientific
Pfu Polymerase	Thermo Scientific

2.1.6.2 *Reagents for in vitro transcription*

Reagents	Manufacturers
T7 RNA polymerase	Thermo Scientific
RNase inhibitor (RiboLock)	Thermo Scientific
DNase I	Thermo Scientific

5X Transcription buffer	Thermo Scientific
NTPs	Thermo Scientific
α^{32}P-UTP	BRITT

2.1.6.3 ***Additional reagents***

Name of the reagent	**Manufacturers**
IPTG	Calbiochem
Kanamycin	Calbiochem
Chloramphenicol	Calbiochem
Tetracycline	Calbiochem
Ampicillin	Calbiochem
Bradford Reagent	Bio-Rad
Bicinchoninic acid protein estimation kit	Thermo Scientific
Ni-NTA Agarose	Qiagen & TaKaRa
Coomassie brilliant blue r-250	Sigma-Aldrich
Ethidium bromide	HiMedia
Methanol	Merck Millipore
Glacial acetic acid	Merck Millipore
Hydrochloric acid	Merck Millipore
Sodium Hydroxide	Merck Millipore
Potassium chloride	Merck Millipore
Tris Base	Merck Millipore
Glycine	Merck Millipore
Acrylamide	Bio-Rad
Bis-acrylamide	Bio-Rad
Diethyl pyrocarbonate (DEPC)	Sigma-Aldrich

2.1.7 Instruments

Name of the instrument	Manufacturers
Spectrophotometer (U-2900)	Hitachi, Japan
Spectrophotometer (Halo XB-10)	Dynamica, UK
Spectrofluorometer (FP-8500)	Jasco, Japan
Circular Dichroism Spectrophotometer (Jasco-150)	Jasco, Japan
Cold Centrifuge (Sorvall ST8R)	Thermo Scientific
Vertical Gel electrophoresis system (Mini Protean tetra cell)	Bio-Rad
Horizontal gel electrophoresis system	Bio-Rad
Gel documentation system	Bio-Rad
Polymerase chain reaction (PCR) machine	Applied Biosystem
FPLC (ÄKTA Start)	GE Healthcare

2.1.8 Software used in the study

Name of the software	Developers
SigmaPlot	Systat Software Inc.
Microsoft office	Microsoft Corporation
Adobe Photoshop	Adobe, Inc.
CorelDRAW	Corel
ImageJ	National Institute of Health, USA
Quantity One	Bio-Rad
Igor Pro	Wave Metrics, Portland, USA
Chimera	Resource for Biocomputing, Visualization, and Informatics (RBVI), UCSF
Pymol	Schrödinger, Inc.
BESTSEL	Micsonai et al
Clone manager	Sci-Ed Software

GENtle	Manske M, Germany

2.2 METHODS

2.2.1 Competent Cell preparation

A. Preparation of bacterial culture

A single colony of bacteria was inoculated into 10 ml of LB media and incubated overnight at 37 °C as a starter culture. 2 ml of the starter culture was used to inoculate 200 ml of LB media as a growth culture. The growth culture was incubated at 37 °C until the OD600 reaches 0.6. Everything after this point was performed in a cold environment with pre-chilled supplies.

B. Treatment of bacterial cells

Bacterial cells were pelleted down by centrifuging at 6000 rpm for 10 mins at 4 °C. Pellets were resuspended in 50 ml solution I followed by centrifugation at 7500 rpm for 7 mins at 4 °C. Pellets were resuspended in 80 ml solution II and kept on ice for 30 mins. Cells were further pelleted down by centrifuging at 7500 rpm for 7 mins at 4 °C. Finally, pellets were resuspended in 12 ml of Solution III.

C. Freezing and storage of competent cells

Competent cells were distributed in 100 µL aliquots in small microcentrifuge tubes. Liquid nitrogen was used to snap freeze the cells before storing them at - 80 °C freezer.

2.2.2 Transformation

Competent cells were thawed on ice and desired plasmid (50-100 ng) was added into the cells and gently mixed. This mixture was incubated on ice for 30 mins. Heat shock was applied by incubating cells at 42 °C for 90 secs. After heat shock, the mixture was further incubated on ice for another 5 mins. 500 µL of LB media was added into the mixture as recovery and incubation were carried out for 45 mins at 37 °C. After incubation, 50-100 µL of the mixture was spread on a LA plate containing desired antibiotics. The spread plate was incubated overnight at 37 °C.

2.2.3 Plasmid isolation

A single colony of transformed bacteria containing the desired plasmid was inoculated into 5 ml of LB media with appropriate antibiotic and incubated overnight at 37 °C. The next day, cells were pelleted down by centrifugation at 6000 rpm for 6 mins. The pellet was resuspended in 100 µL solution 1 and kept on ice for 5 mins. 200 µL of freshly prepared solution II was added into the cell suspension and mixed thoroughly by inversion before incubating at room temperature for 5 mins. 150 µL of solution III was added into the solution and mixed properly followed by another 15 mins of incubation on ice. After incubation, centrifugation was carried out at 10000 rpm for 15 mins and the supernatant was transferred carefully into a fresh microcentrifuge tube. RNase A was added into the solution with a final concentration of 2 mg/ml and incubation was carried out for 15 mins at 37°C. An equal volume of phenol: chloroform: isoamyl alcohol (25:24:1) mixture was added into the solution and mixed by using a vortex. The resulting aqueous and the organic phase was separated by centrifugation at 10000 rpm for 3 mins. The aqueous phase was transferred into a fresh tube and plasmid DNA was precipitated by adding 2.5 volumes of absolute ethanol. The tube was kept at -20 °C for 30 mins to allow complete precipitation. Centrifugation was carried out at 12000 rpm for 15 mins at 4 °C and the DNA pellet was washed twice with 70 % ethanol. Finally, the DNA was vacuum dried and resuspended in 50 µL of TE buffer.

2.2.4 Overexpression of recombinant protein

10 µL of required antibiotic [kanamycin (50 mg/ml) or ampicillin (100 mg/ml)] was added into 10 ml of LB medium and a single transformed colony was transferred into the medium. Then it was incubated at 37 °C under shaking conditions for 16 hours. 10 ml of this primary culture was then added into 1 lit of LB medium, containing 1 ml of the same antibiotic solution previously used and incubated at 37 °C under shaking condition until the OD_{600} reaches 0.6.

500 µL IPTG (1 M Stock) was added into the culture for induction and incubated at 37°C (for SRP54, SRP19) or 16°C (for FtsY) for 16 hours under shaking conditions.

Induction was checked by lysing the cell and then running the cell lysate on an SDS page. A cell lysate of uninduced culture was used as the control.

2.2.5 Protein purification by affinity chromatography

After 16 hours of incubation of the induced culture centrifugation was carried out at 6000 rpm for 8 mins to pellet down the cells. The cell pellet was dissolved in cell resuspension buffer and followed by the addition of 1 mM lysozyme and 1 mM PMSF into it. The Cell was lysed using a sonicator (Soniprep 150). Pulses of 30 secs were used to lyse the cells with a 1 min break between two pulses. Pulses were continued until the cell suspension became clear indicating lysis of cells. Then centrifugation was performed at 15000 rpm for 30 mins to separate cell debris and the supernatant was collected in a sterile centrifuge tube. This supernatant was incubated at 65 °C using a hot water bath to remove all the bacterial proteins. It was then subjected to the same centrifugation cycle of 15000 rpm for 30 mins and the supernatant was collected and placed in ice.

The FPLC system was equilibrated with filtered and degassed water and resuspension buffer (see 2.1.5.8). Prepacked Ni-NTA agarose column was assembled and washed with 20 column volume (cv) of water followed by equilibration with resuspension buffer. Beads were further washed with 10 cv of wash buffer I (see 2.1.5.8). The collected cell lysate was loaded upon the column and the flow-through was collected. The affinity column was washed with a 20 column volume of wash buffer I and wash buffer II to remove nonspecific proteins. The protein of interest was eluted in a stepwise manner by adding elution buffers (I to V) with increasing concentration of imidazole, at a flow rate of 1 ml/min.

All the washed and eluted fractions along with the lysate and the flow-through were analyzed by running an SDS-PAGE. Eluted fractions with considerable purity were selected for dialysis.

2.2.6 Buffer exchange

A dialysis bag with either 3 kDa or 12 kDa cut off (depending on the size of the protein) was boiled in distilled water containing 1 mM EDTA for 10 mins. Then it was rinsed

with distilled water and again boiled for 10 mins without EDTA. A final rinsing was done with cold distilled water before adding protein into it. After securing both ends of the dialysis bag with a dialysis clip, it was placed into a beaker containing the dialysis buffer. Dialysis was continued for 3 hours followed by replacing the old buffer with a fresh one. After the addition of the fresh buffer, dialysis was continued overnight.

A spin column with an appropriate cut-off was used to increase the protein concentration when needed. The spin column was first equilibrated with dialysis buffer before the addition of the protein. Centrifugation was performed at 5000g for 15 mins to concentrate the protein. This step was continued until the desired concentration was achieved. Protein concentration was measured using either Bradford or BCA method.

2.2.7 Protein purification by size exclusion chromatography

To achieve further purification size exclusion chromatography was performed. For this purification, at first, buffer and water were filtered and degassed. Then the gel filtration column (Sephacryl S-300 HR) was washed with water at a 0.5 ml/min flow rate either in an FPLC machine (ÄKTA Start) or using a peristaltic pump, followed by washing with the buffer (same as the dialysis buffer) at the same flow rate. After that protein was loaded into the column and ran at a 0.5 ml/min flow rate. Fractions were collected in microcentrifuge tubes and absorption at 280 nm was measured to select protein-containing fractions. An SDS-PAGE was run to analyze the fractions and protein concentration of the desired fractions was measured by either Bradford or BCA methods. Protein was then concentrated using a spin column until the desired concentration was achieved.

For long-term storage of the purified protein, it was distributed in small aliquots in microcentrifuge tubes. Liquid nitrogen was used to snap freeze the protein to avoid ice crystal formation before storing the aliquots in a - 80 °C freezer.

2.2.8 Synthesis and purification of the RNA transcript

2.2.8.1 *Preparation of RNA transcript by run-off transcription*

Run-off transcription reaction was set up for small-scale production of radiolabeled RNA using T7 RNA polymerase. The following components were added in order of their occurrence and the reaction was incubated for 3 hrs at room temperature.

Transcription buffer (5X)	1X final concentration
Linearized template DNA	1 µg
ATP, GTP, CTP	2 mM each (for unlabeled RNA) or, 0.5 mM each (for labeled RNA)
UTP	2 mM (for unlabeled RNA) or, 12 µM (for labeled RNA)
α^{32}P-UTP	10 µCi (for radiolabeled RNA)
RNase Inhibitor	20 U
T7 RNA polymerase	20 U

2.2.8.2 *Elution of RNA*

Radiolabeled RNA was separated in denaturing polyacrylamide gel. The RNA was located by autoradiography (30sec) and the band was excised. RNA was eluted from the excised gel slice into 0.4ml RNA elution buffer by incubating at room temperature overnight in a vertical cyclo-mixture. Elution was centrifuged and the supernatant was collected. RNA was extracted with phenol and ethanol precipitated from the supernatant.

2.2.8.3 *Purification of in vitro transcribed RNA*

To the IVT reaction mix, 3 M sodium acetate solution (pH 5.0) was added to the final concentration of 0.3 M. the rest of the volume was made up of DEPC-treated water. An equal volume of phenol-chloroform-isoamyl alcohol (25:24:1) solution was added to the reaction tube and mixed gently. The content was centrifuged at 10,000 rpm for 5 mins and the upper aqueous layer was separated. An equal volume of chloroform

was added to this layer and centrifuged at 10,000 rpm for 5 mins; the upper aqueous layer is collected and separated. Ethanol (100%) was added as three times the volume of the aqueous layer, mixed thoroughly, and kept at – 20 °C for overnight. On the following day, the tube was centrifuged at 15,000 rpm for 40 mins, the supernatant was discarded, and the pellet was washed with 500 µl of ethanol (70%). The sample was further centrifuged at 15,000 rpm for 20 mins and the pellet was dried using vacuum centrifugation or by incubating at 45 °C for 15 mins.

2.2.9 SDS-polyacrylamide discontinuous gel

The required concentration of polyacrylamide gel was prepared according to Laemmlie's protocol (1970) taking polyacrylamide bis-acrylamide solution (30:0.8), 1.5M Tris-HCl (pH 8.8), 10% SDS, and water. The required amount of TEMED and 30µg/ml APS was added to it for polymerization and poured into the casting chamber. For stacking gel 1M Tris-HCl (6.8) was used instead of 1.5M Tris-HCl, pH 8.8. The protein sample is suspended in an SDS-sample buffer, boiled in the water bath for 3min and loaded in gel. The gel was run in an SDS-PAGE running buffer at a constant 2 mA/lane until bromophenol blue dye reached the bottom. The gel was fixed in fixing solution, stained with 0.1% Coomassie Blue and distained with a de-staining solution.

CHAPTER 3

Biochemical and biophysical characterization of the purified SRP components

3.1 INTRODUCTION

In all three domains of life, three ribonucleoprotein complexes are universally conserved. These are the RNase P, ribosome, and the signal recognition particle (SRP). SRP plays a critical role, both in prokaryotes and eukaryotes, to facilitate the co-translational protein targeting across the plasma membrane and ER membrane (Grudnik et al., 2009; Akopian et al., 2013). The signal sequence located at the N terminus of the newly synthesized protein, emerging from the ribosome, is recognized by SRP. The whole ribosome-nascent-chain complex (RNC) is transferred to the protein conducting channel by the interaction of SRP with its cognate receptor; SR in eukaryotes, FtsY in prokaryotes (Pohlschroder et al., 2003; Halic et al., 2006). SRP is an ensemble of non-coding RNA and one or more proteins. The bacterial SRP consists of only one protein, Ffh, and a 4.5S SRP RNA (Poritz et al., 1990; Batey et al., 2000) whereas the eukaryotic SRP employs a 7S RNA molecule associated with six proteins – SRP68, SRP72, SRP54, SRP19, SRP14 and SRP9 (Keenan et al., 2001). Interestingly, archaeal SRP retains the 7S RNA despite its robustness and two proteins from the eukaryotic line-up – SRP54 and SRP19 (Gupta et al., 2016).

Several features of archaeal SRP RNA distinguish it from that of the other two domains, most notably the helical arrangements in its secondary structure (Zwieb & Bhuiyan, 2010). Helix 1 of the SRP RNA is typically present in all archaea and a few bacteria, whereas helix 7 is only found in archaea, but none of them are ever found in eukaryotes (Kempf et al., 2014). Though, the presence of helix 6 is shared among archaea and eukaryotes. This is because SRP19 is present in both domains which contact the SRP RNA at helices 6 and 8 (Hainzl et al., 2005; Gupta et al., 2016). SRP54 (Ffh in bacteria) associates with the RNA at the helix 8 via its C terminal M domain. The SRP RNA acts as a scaffold that undergoes structural rearrangements to favor the binding of other constituent proteins that helps in the overall function of SRP. Crystal structure analyses of the SRP19-bound 7S RNA from *M. jannaschii* reveal the conformational changes in the RNA induced by the interaction with SRP19. When compared with the solution structure of 7S.S RNA (S domain of 7S RNA consisting of helices 6 and 8), the binding of SRP19 at the tips of two helices shows substantial

restructuring in the helix 6. The tetraloop bases of this helical region are looped-out and reoriented to facilitate an increase in the fraction of surface-exposed bases in the distal asymmetric loop of helix 8 (Hainzl et al., 2005). In the absence of any protein, the unpaired bases of this loop are directed toward the helical axis but the binding of SRP19 inverts the loop backbone and the bases now face the outside of the RNA helix. Such profound conformational changes enhance the affinity of SRP54 for the RNA, a fact that was also supported by biochemical study (Hainzl et al., 2005) and free-state characterization of an SRP54-SRP19-SRP RNA complex crystal structure (Hainzl et al., 2007). The binding of the SRP54-M domain not only reorients the helix 8 but also displaces the nucleotides at the G domain binding site. The intricate intermolecular interface, including base-specific interactions, that mediates the M domain recognition is not present in the NG domain-RNA interface. Nevertheless, the RNA contacts the NG domain via its sugar-phosphate backbone (Hainzl et al., 2007). Similar structural studies with SRP54 from *S. solfataricus* reveal that the flexible hinge region in the G-M domain interface may play a critical role in the necessary conformational rearrangements (Rosendal et al., 2003). The signal peptide binding to the M domain finger-loop region induces the repositioning of the G domain (Hainzl et al., 2007; Janda et al., 2010) which contains conserved Ras-like classical P-loop GTPase motifs. Therefore, RNA binding may directly influence the GTPase activity of SRP54 in the complex. Evidence from biochemical studies on the *E. coli* Ffh-GTPase activity in the presence and absence of 4.5S RNA provides direct confirmation of this hypothesis. The bacterial SRP RNA has been found to increase the enzymatic GTP hydrolysis rate of the Ffh alone by a few folds but by more than 100 folds when measured in combination with the SRP-receptor, FtsY (Powers & Walter, 1995; Peluso et al., 2000; Peluso et al., 2001). More recent studies have established that the RNA tetraloop mediated Ffh-FtsY assembly relocates to the distal end of the RNA, induced by a defined bend in the RNA backbone. This repositioning of the GTPase complex is crucial for the concomitant GTP hydrolysis at the end of the protein targeting process (Shen et al., 2013; Voights-Hoffmann et al., 2013).

Although a plethora of experimental findings help us to understand the molecular mechanism underlying the bacterial SRP assembly and its precise role in the protein targeting process, such biochemical evidence is lacking in archaeal SRP research. An initial analysis of the RNA-binding and the GTPase activity of SRP54 from the hyperthermophilic archaeon *A. ambivalens* (Moll et al., 1999), followed by a thorough reconstitution experiment with the mesophilic *H. volcanii* SRP assembly (Tozik et al., 2002) provide necessary information regarding the archaeal SRP system. Another hyperthermophilic, sulfate-reducing archaeon, *Archaeoglobus fulgidus* has been studied to establish the precise role of SRP19 in facilitating the SRP54-7S RNA interaction (Diener & Wilson, 2000). Together these data comprise a nominal representation of the co-translational translocation machinery in the vast milieu of the archaeal diversity. Thus, the very first objective of this study is to elucidate the nature of intramolecular interactions within the SRP assembly in the thermoacidophilic crenarchaeon *Sulfolobus acidocaldarius*. With the help of both biochemical and biophysical tools, the different components of the functional SRP complex have been cloned, expressed, purified, and studied for their intrinsic activities. Members of the genus *Sulfolobus* thrive at extremely high temperatures of 70-80 °C and acidic pH of 2-3. Their natural habitats include hot solfataric springs where the conditions are highly fluctuating due to volcanic activity. *Sulfolobus* requires unique strategies to survive in such extremely adverse conditions and therefore is a very suitable candidate for studying molecular mechanisms considering evolution and stress response. The broader aim of this dissertation has therefore been directed to unravel any mechanistic detail that contributes to the evolutionary importance of the archaeal domain in the prokaryotic to eukaryotic transition.

3.2 MATERIALS & METHODS

3.2.1 Construction of overexpression vectors for wild type and mutant proteins

To enable expression of SRP54 and SRP19 with an N-terminal histidine tag, *srp54* gene (*saci_1310*) and *srp19* gene (*saci_0759*) was amplified by PCR from genomic DNA of *S. acidocaldarius* DSM639 using primers listed in Table 2.2, digested, and ligated into pET Duet1 vector yielding plasmid pAG3 and pAG13 for SRP54 and SRP19 respectively. For expression analysis, the required vector was transformed into *Escherichia coli* BL21 (DE3) cells containing the RIL Cam^r plasmid (Stratagene). All the strains, primers, and constructs used for cloning wild-type SRP54 and SRP19 are listed in Tables 2.1.1, 2.1.2, and 2.1.3, respectively. The single point mutations were introduced in the pAG3 backbone, individually, by the site-directed mutagenesis protocol using KOD Hotstart polymerase (Novagen). Primers used for this purpose and the final constructs generated are listed in Table 4.1.

Table 3.1 Primers and plasmids used to construct SRP54-G domain mutants

Plasmids	Primers	Relevant characteristics	Reference
pAG45	158	5′-AAGCCAGGATGAGGGCAATAGCAAAAG-3′ Forward primer for SRP54^{R400A}	Present study
	159	5′-CAGCTCCTTTTGCTATTGCCCTCATC-3′ Reverse primer for SRP54^{R400A}	Present study
pAG56	438	5′-ATGAATTCAATGGCATATAAAG-3′ Forward primer for SRP54^{S381A}	Present study
	439	5′-AATTCTTTATATGCCATTGAATTC-3′ Reverse primer for SRP54^{S381A}	Present study
pAG57	440	5′-CAATGACATATGCAGAATTAGATAAC-3′ Forward primer for SRP54^{T383A}	Present study
	441	5′-TTATCTAATTCTGCATATGTCATTG-3′ Reverse primer for SRP54^{T383A}	Present study

3.2.2 Expression of recombinant proteins in *E. coli*

A total volume of 10 ml of an overnight culture of *E. coli* BL21(DE3)-RIL cells containing the RIL Cam^r plasmid and pAG3 or pAG13 was used to inoculate 1 L of

Luria–Bertani medium containing ampicillin (100 µg/ml) and chloramphenicol (34 µg/ml). Cells were grown at 37 °C until OD600 of 0.6 was reached when 500 µM IPTG (isopropyl β-D-thiogalactopyranoside) was added. The temperature was reduced to 16 °C, and growth was continued overnight to reduce inclusion body formation. The cells were collected by centrifugation, resuspended in lysis buffer [50mM Tris-Cl (pH 8.0), 150mM KCl, and 10% glycerol] containing the complete EDTA-free protease inhibitor cocktail (1 tablet/50 ml of lysate; Roche), frozen in liquid nitrogen and stored at - 80 °C.

3.2.3 Purification of recombinant SRP54 and SRP19

Before purification, frozen resuspended cell pellets were thawed on ice. One mM lysozyme was added separately to the lysis buffer. After incubation on ice for 30 min, cells were lysed by sonication with Soniprep150 (DJB Labcare, UK). Cell debris was removed by centrifugation at 15000 rpm for 30 min (rotor SA-300; Sorval RC6+ Thermo Scientific). For the purification of histidine-tagged proteins, the supernatant was applied to a Ni^{2+}-NTA affinity column (Qiagen). Bound proteins were washed gradually with lysis buffer containing 10 mM and 20 mM imidazole, respectively. The bound protein fraction was eluted in a lysis buffer containing 100 mM of imidazole. The eluted fraction was monitored by running reducing SDS-PAGE. The fraction containing the desired protein was dialyzed overnight in a lysis buffer.

3.2.4 Cloning, transcription, and purification of SRP RNA

The full-length 7S RNA (*saci_0095*) and the S domain of 7S RNA (7S.S) were cloned from the *S. acidocaldarius* DSM639 genomic DNA using primers and vectors listed in Table 2.2 and 2.3. RNA was synthesized using *in vitro* transcription (Thermo Scientific) with T7 RNA polymerase (see 2.2.8.1). The synthesized product was purified using the solvent-separation protocol (see 2.2.8.3).

3.2.5 Homology modeling and docking

The three-dimensional structure of SRP54 and SRP19 was homology modeled using the RNA-bound structure of SRP54 and SRP19 from *Sulfolobus solfataricus* (1QZW and 3KTW, respectively) as the template. Swiss-Model webserver (Guex et al., 2009;

Waterhouse et al., 2018; Studer et al., 2020) was used to perform the homology modeling. Molecular docking was performed with HADDOCK (**H**igh **A**mbiguity **D**riven protein-protein **DOCK**ing) webserver (van Zundert et al., 2015; Honorato et al., 2021) using the homology modeled structure of *Saci*SRP54, *Saci*SRP RNA, and *Saci*SRP19 as the macromolecular templates. HADDOCK encodes information from identified or predicted protein interfaces in ambiguous interaction restraints (AIRs) to drive the docking process. For water refinement, a solvent shell was built around the complex and, subsequently, a series of short MD simulations were performed according to the default parameters, all atoms except the side-chain atoms at the interface were restrained to their original position. Next, 1250 MD steps were performed at 300 K with position restraints for heavy atoms which are not part of the PPI (residues not involved in intermolecular contacts within 5 Å). Finally, the system is cooled down (1000 MD steps at 300, 200, and 100 K) with position restraints on the backbone atoms of the protein complex, excluding the interface atoms. The result was obtained in multiple clusters based on the FCC method with a cut-off of 0.6 for complex clustering. Only the model showing the closest resemblance (lowest RMSD) with the crystal structure and the lowest energy was selected in each case.

3.2.6 Secondary structure prediction of SRP RNA

The secondary structures of *S. acidocaldarius* 7S RNA and 7S.S RNA were built using MXfold2 webserver using a deep neural network integrated with Turner's nearest-neighbor free energy parameters (Sato et al., 2021). The model is trained using the max-margin framework with thermodynamic regularization to ensure that folding scores and the calculated free energy are as close as possible.

3.2.7 GTP hydrolysis assay and kinetic analysis

For estimating GTPase activity, the proteins were maintained in the binding buffer [50 mM Tris (pH 8.0), 150 mM KCl and 10% glycerol]. The same composition was used for the assay buffer with 5 mM $MgCl_2$. Fixed concentrations (2 μM) of proteins were pre-incubated for 5 mins and then incubated with 100 μM GTP at 75 °C for 15 min. The reaction was stopped by freezing in liquid nitrogen. To determine the

activity of SRP54 as a function of temperature, pH, nucleotides, and divalent cations, the assay was performed at different temperatures, in different buffers [50 mM citrate (pH 3.0–5.5), MES (pH 6.0–6.5), HEPES (pH 7.0–7.5) or Tris/HCl (pH 8.0–9.5)], with different NTPs (5 mM of ATP, GTP, CTP or UTP), and in the absence of or with different divalent cations (5 mM of Na-EDTA, $NiCl_2$, $MgCl_2$, $MnCl_2$ or $CaCl_2$,) respectively (Ghosh et al., 2011). For the Michaelis-Menten kinetic analyses, 0.05-2 mM of GTP was used as the substrate and 2 μM of SRP54 was assayed for the GTPase activity for 20 mins, in the presence and/or absence of 7S RNA. An aliquot of 20 μl from each sample was mixed with 200 μl of Malachite Green reagent and the absorbance was measured at 620 nm spectrophotometrically (Ghosh et al., 2011). The data were corrected for non-enzymatic GTP hydrolysis. The amount of GTP hydrolyzed per minute per μmoles of SRP54 was determined as a function of substrate concentration, and the resulting data were fitted to the following equation:

$$V_0 = V_{max} \times \frac{[GTP]}{K_M + [GTP]}$$

where V_0 is the observed reaction rate at a specific substrate concentration, V_{max} is the maximal rate with saturating substrate, and K_M is the substrate (GTP) concentration that provides half the maximal velocity.

3.2.8 Electrophoretic mobility shift assay

The protein-SRP RNA complex formation was monitored on native PAGE following standard protocol. Complex formation was induced by mixing radiolabelled 7S RNA (10^4 CPM) with SRP54 (0.005-0.4 μM) or SRP19 (0.01-0.5 μM) in binding buffer [50 mM Tris (pH 8.0), 150 mM KCl] with 5 mM $MgCl_2$ and then incubated at 75 °C for 10 min followed by snap chilling in ice. A competitive reaction mixture was also prepared where the reaction with maximum protein concentration (0.4 μM) was doped with an excess of non-radiolabelled 7S RNA (2 μM). Total reaction mixtures were analyzed on 4% native PAGE at room temperature using 1X TAE buffer. The gel was further dried, and the radiation was measured by Typhoon Phospho-imager (GE Healthcare). The data were analyzed by ImageJ software and the curve fitting was done with the aid of SigmaPlot12.0 software.

3.3 RESULTS

3.3.1 Purification and enzymatic characterization of archaeal SRP proteins

Sulfolobus acidocaldarius is a thermoacidophilic organism that thrives at temperatures as high as 70-80 °C and has an external pH of around 2-3. Due to the exposure to this extreme habitat, the cellular machinery within the organism is adapted to perform in such conditions. This feature has been successfully employed in the purification of recombinant archaeal protein to exclude the load of bacterial protein impurity. The overnight grown, IPTG-induced cells were precipitated and solubilized using lysis buffer (binding buffer + lysozyme) and sonicated to obtain the cellular fraction. This fraction was incubated at 60 °C in a water bath that ensured aggregation of all bacterial proteins (Ghosh et al., 2011). Following centrifugation, the soluble fraction was obtained which primarily contained the recombinant archaeal protein. The lysate was loaded into a Ni-NTA agarose column, and the proteins were eluted using increasing concentrations of imidazole. The computed molecular weights of SRP54 and SRP19 were calculated to be 49.65 kDa and 11 kDa, which were visualized in SDS-PAGE following the migration of 50 kDa and 10 kDa marker, respectively.

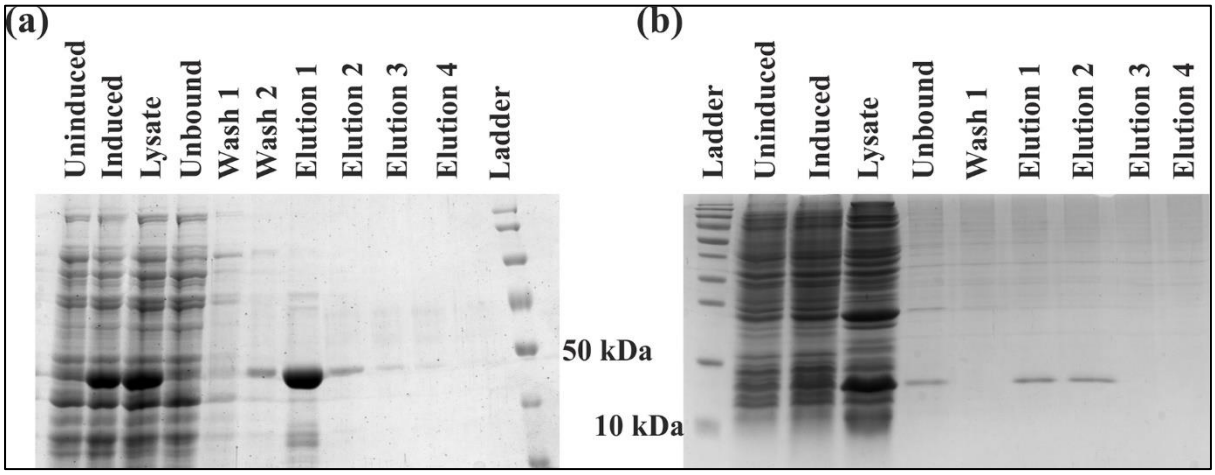

Figure 3.1. Purification of recombinant SRP proteins. Proteins were purified using affinity chromatography and the column was washed with 10 mM imidazole (Wash 1) and 20 mM imidazole (Wash 2), and the proteins were eluted using 100-400 mM imidazole (Elution 1-4). SRP54 migrated below 50 kDa marker (a) and SRP19 migrated above 11 kDa (b). Both proteins were eluted at a 100 mM imidazole fraction.

SRP GTPases (SRP54 and FtsY) belong to the SIMIBI class of GTP hydrolyzing enzymes that contain the classical P-loop GTPase motifs (G1-G5) which provide a binding pocket for the nucleotide and Mg^{2+} ion (Leipe et al., 2002). Additionally, the SRP-G domain contains an insertion loop inside the IBD that probably represents the switch II region found in Ras-like GTPases (Freymann et al., 1997; Montoya et al., 1997). A unique GY dipeptide sequence is found in this region inside the crenarchaeal SRP54 (Montoya et al., 2000; Rosendal et al., 2003). The IBD motif is supposed to stabilize the nucleotide-free protein as there is no known guanine nucleotide exchange factor present for SRP GTPases. The enzymatic ability of SRP54 has been investigated in bacteria as well as in higher eukaryotes and both were found to have a weak basal hydrolyzing activity (Connolly & Gilmore, 1993; Dong et al., 2006). Although crenarchaeal SRP54 structure has been analyzed to point out key residues possibly involved in its GTP hydrolyzing ability, no concrete biochemical characterization has ever been attempted. In the present study, recombinant SRP54, purified from *S. acidocaldarius* (*Saci*SRP54) was analyzed for its ability for optimal GTP hydrolysis (Supplementary Material, Gupta et al., 2021). Surprisingly, *Saci*SRP54 showed a similar affinity toward CTP and GTP, when tested for its nucleotide specificity (Fig. 2a). It showed a considerable, yet lower, specificity toward ATP but could not hydrolyze UTP at all. Different divalent cations were used to measure the specificity of the protein for its cofactor. Structural data suggest that SRP54 binds GTP in an Mg^{2+}-dependent manner and the biochemical evidence corroborated that fact. The highest GTPase activity was recorded in presence of Mg^{2+} and almost similar activity was also found in presence of another divalent cation, Mn^{2+} (Fig. 2b). For the maximal GTP hydrolysis, the optimum pH was found to be between 6 and 7 and the optimum temperature was around 80 °C, which were in direct agreement with the natural environment of *S. acidocaldarius* which maintains the cellular pH at around 6.5 and thrives at 75-80 °C (Fig. 2c-d).

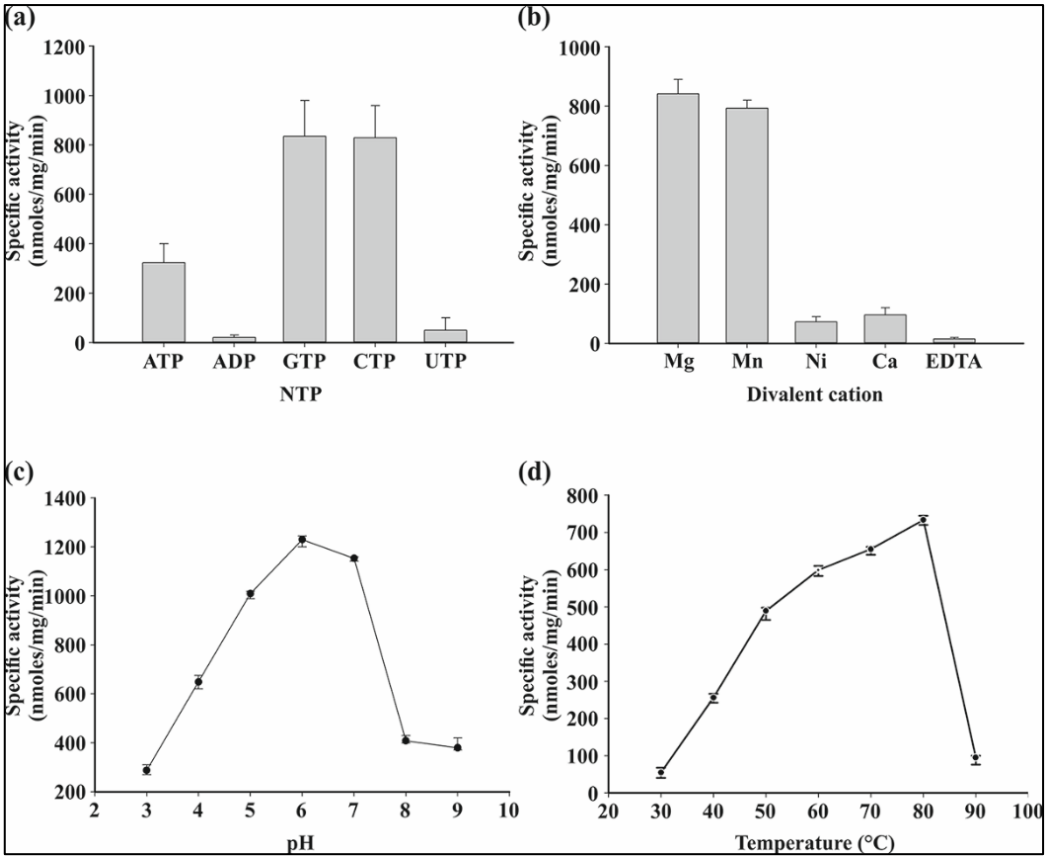

Figure 3.2. GTPase activity of SRP54 under different optimal conditions. The specific activity of the enzyme was calculated as nanomoles of inorganic phosphate produced per minute per milligram of protein. Total Pi released upon GTP (NTP) hydrolysis was measured using the Malachite Green assay. (a) Analysis of optimal substrate for hydrolysis. NTPs were added to a final concentration of 5 mM. (b) Preference for optimal divalent metal ion as a cofactor in GTPase activity. The final concentration of SRP54 used in the assays was 1 µM and the final concentration of metal ions was 5mM. (c) Influence of pH on SRP54 GTPase activity. (d) Influence of temperature on SRP54 GTPase activity (Supplementary Material, Gupta et al., 2021).

3.3.2 RNA-protein interaction within the archaeal SRP ensemble

Inside the ribonucleoprotein complex, SRP, the 7S RNA binds SRP19 and SRP54 via its larger S domain. SRP19 contacts the major groove of helix 6 tetraloop and the minor groove of helix 8 tetraloop via its L1 and L2 loop regions. The interaction widens the major groove of the RNA at helix 8 which facilitates the binding of SRP54 (Gupta et al., 2016). The RNA-protein interaction has been studied extensively in bacterial SRP systems, where Ffh from *Mycobacterium tuberculosis* was shown to associate specifically with the 4.5S SRP RNA (Palaniyandi et al., 2012). In the archaeal community, 7S RNA from *Sulfolobus solfataricus* was found to be recognized

by SRP54 from *Acidianus ambivalens* (Moll et al., 1999) which shows that the residues involved in the interaction are conserved among organisms.

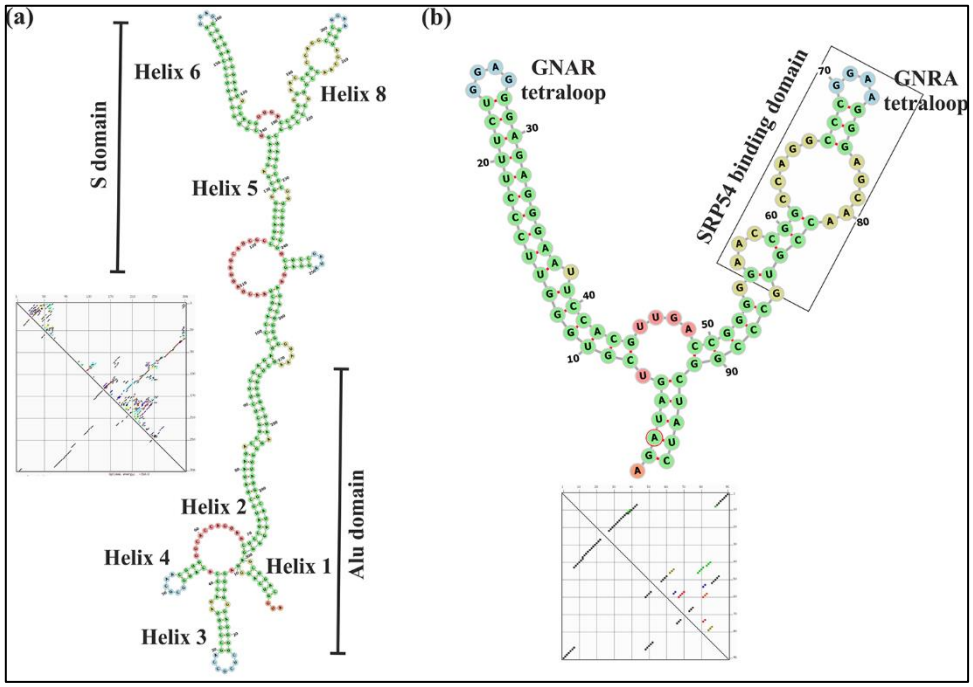

Figure 3.3. Secondary structure prediction for RNA. SRP RNA from *Sulfolobus acidocaldarius* was modeled for a probable secondary structure with standard thermodynamic constraints used by MXfold2. The structure of full-length 7S RNA (a) and 7S.S RNA (b) are marked by structural motifs; loops, bulges, helices, and tips are colored by brown, pink, green, and blue respectively. The energy dot plots for all the possible predictions are shown in the inset. The final ΔG for the shown structures of 7S and 7S.S RNA were -144.93 and -44.6, respectively.

The S domain of SRP RNA (7S.S) from *Archaeoglobus fulgidus* bound full-length SRP54 and its M-domain with an intrinsic high affinity. The *Afu*SRP19 was also found to bind the SRP RNA with similar affinity (Diener & Wilson, 2000). Another study by Christian Zwieb (1994) showed that a similar association exists between human 7S RNA and SRP19 through base-specific interactions. To assess the structural motifs and interactive domains of 7S RNA in *S. acidocaldarius*, a sequence-based secondary structure was predicted using an MXfold2 webserver that builds secondary structures of non-coding RNAs from scratch, using thermodynamic energy calculations. Figure 3.3a depicts the predicted secondary structure of *Saci*7S RNA with the highest free energy (ΔG = -144.93) where all the structural motifs, specific to archaeal 7S RNA, have been addressed. Helix 1 is unique to archaea that

are formed upon pairing of the 5′ and 3′ termini of the RNA. There are two loops in the stem of helix 8 right below the apical tetraloop region – the asymmetric and the symmetric loops. The symmetric loop has four non-Watson-Crick base pairing (GA, GG, AC, CA) that is conserved among archaea, bacteria, and humans (Nagai et al., 2003). When the SRP54-M domain contacts the symmetric loop, the asymmetric loop becomes well-ordered and the bases of the ACC trinucleotide present in that loop become continuously stacked to form a platform for SRP54 interaction. The apical tetraloop region of helix 8 contains the consensus sequence GNRA instead of GNAR in the tetraloop of helix 6. A part of the S domain of the RNA has been mapped using the same constraints (Fig. 3.3b, ΔG = -44.6) where the helices 6 and 8 are prominent. This is the smallest functional domain of eukaryotic and archaeal SRP RNA that has been employed in several biophysical and biochemical analyses.

Next, the 7S RNA was synthesized in vitro in presence of α^{32}P-UTP, and the purified product was used in the protein binding assay. The mixture of cognate protein and the RNA was incubated at 70 °C and then loaded into native polyacrylamide gel. A range of increasing concentration of SRP54 (5-400 nM) and SRP19 (10-500 nM) was visualized by the shift in the mobility of the RNA-protein complex (Fig. 3.4a-b); the last lane in the RNA-SRP54 binding reaction contained an excess of unlabelled RNA which competitively bound to the protein, replacing the labeled RNA (Fig. 3.4a). The gel image was analyzed using ImageJ software to calculate the relative density of the radiation spots. A comparative analysis between the free RNA and the bound RNA spots resulted in a percentage of the bound fraction that was plotted against the concentration of the protein. The resulting graph was fitted using the protein-ligand binding equation and the K_d of the association was determined in each case. SRP19 bound the RNA with a stronger affinity (Fig. 3.4d) as denoted by the K_d of 139.62 ± 18 nM, whereas the RNA-SRP54 binding was characterized by a K_d value of 39.32 ± 7 nM (Table 3.2). This was in agreement with the available structural data which implies that SRP19 binds the SRP RNA via base-specific interactions at both helices (6 and 8) but SRP54 contacts the RNA only at helix 8. The stronger RNA-binding property of SRP19 may have conferred to it the ability to stack two helices closer for an effective reorientation that favors SRP54 binding.

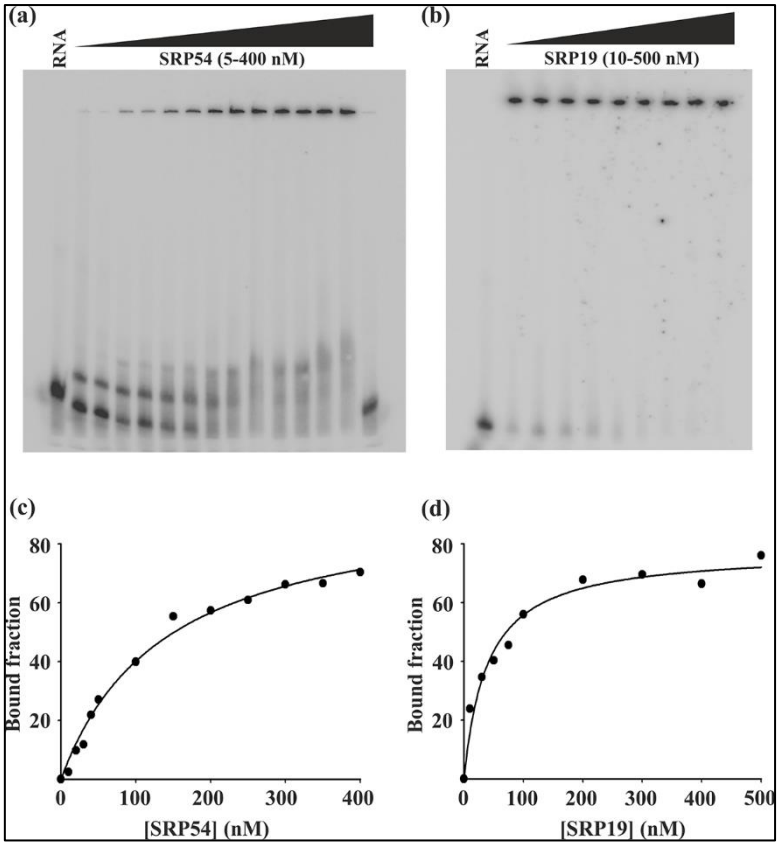

Figure 3.4. RNA-protein interaction among archaeal SRP components. The EMSA for 7S RNA-SRP54 (a) and 7S RNA-SRP19 (b) binding were run using a 4% native PAGE in 1X TAE buffer. For the SRP54 binding assay, the last lane was supplemented with excess unlabelled 7S RNA which competitively replaced the bound labeled RNA. The densitometric calculations were plotted using the protein-ligand function and the apparent K_d was calculated to be 139.62 ± 18 nM for SRP54 (c) and 39.32 ± 7 nM for SRP19 (d).

3.3.3 Role of SRP RNA in the GTPase activity of SRP54

SRP RNA has been implicated to induce important conformational reorientations in SRP54, both in bacteria and archaea (Rosendal et al., 2003; Hainzl et al., 2005). In *E. coli*, the presence of 4.5S RNA was shown to be a key factor for faster association between Ffh and FsY (Peluso et al., 2000). Also, the Ffh-4.5S-FtsY complex was found to dissociate at a much faster rate compared to the Ffh-FtsY complex (Peluso et al., 2000) which revealed that the SRP RNA may have stabilized a transition state for the binding reaction, lowering the energy barrier separating free and complexed components. Since the two SRP GTPases reciprocally activate each other, their enhanced association directly translates into better enzymatic hydrolysis of the bound GTP (Shen et al., 2013). Although bacterial SRP RNA has been shown to exert

little effect on the basal GTPase activity of Ffh (Peluso et al., 2001; Zhang et al., 2008), the overall catalytic role of the RNA has been quite evident. Presently in this study, the *Saci*SRP54 has been investigated for its enzymatic efficiency and whether the association of the 7S RNA moiety has any significant role in it. To address these questions, hydrolytic activity of SRP54 was measured, with or without 7S RNA, in presence of varying concentrations of GTP (0.05-2 μM). The amount of inorganic phosphate released was measured spectrophotometrically by Malachite-Molybdate reagent and the specific activity was calculated as the total nanomoles of phosphate released per minute per μmoles of protein used. This was plotted against the increasing concentrations of GTP and the resulting graph was fitted using the classical Michaelis-Menten kinetic equation to obtain an understanding of the enzymatic efficiency. The affinity of SRP54 for the nucleotide substrate was reflected in the apparent K_M, calculated as the substrate concentration required to attend half the maximum velocity (V_{max}). Though the overall V_{max} of the reaction was only slightly increased in presence of 7S RNA (Fig. 3.5b) than in the absence of it (Fig. 3.5a), the affinity for GTP remained almost unchanged (Table 3.2).

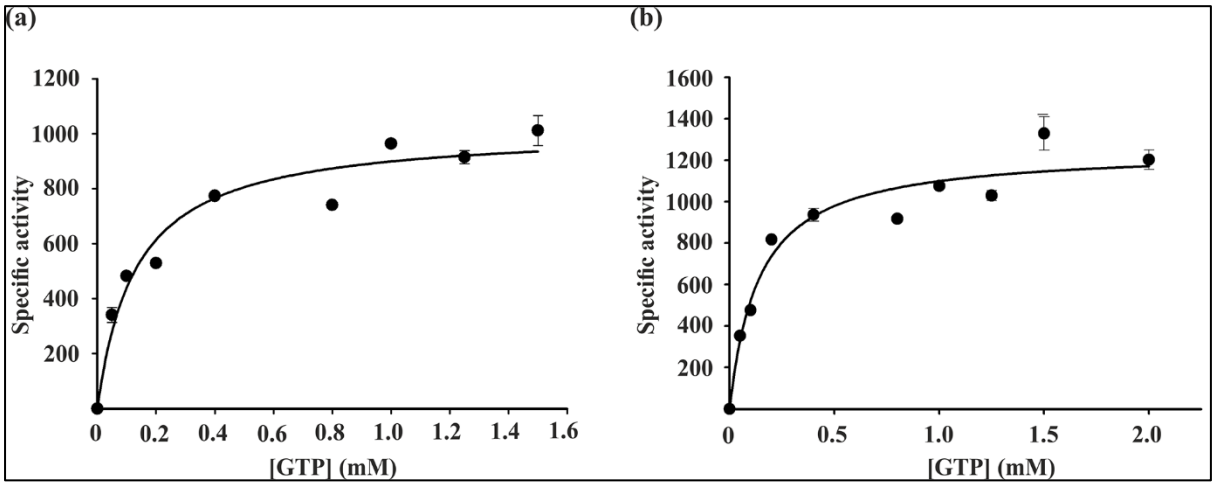

Figure 3.5. Effect of 7S RNA on the basal enzymatic activity of SRP54. The Amount of GTP hydrolyzed by the protein was measured using the Malachite-Molybdate reagent. The specific activity of SRP54 was calculated as nmoles of phosphate released minute^{-1} μmole^{-1} of protein used. The reaction was carried out with (a) SRP54 alone and (b) in complex with 7S RNA, and the affinity for GTP was found to be 131 μM (a) and 139 μM (b) respectively.

Table 3.2. Kinetic features of SRP-GTPase and RNA-binding activity

Sample	V_{max}	K_m	K_d
SRP54	102 nmoles min^{-1} $\mu mole^{-1}$	131 μM	-
SRP54+7S RNA	125 nmoles min^{-1} $\mu mole^{-1}$	139 μM	-
SRP54-7S RNA	-	-	139.62 ± 18 nM
SRP19-7S RNA	-	-	39.32 ± 7 nM

The measured nucleotide affinity of SRP54 depicts that the effect of SRP RNA upon the basal enzymatic activity of the protein is not significant. This perfectly corroborates with the data available from studies in the bacterial SRP system.

3.3.4 Computational analysis of structural features of SRP components

To date, many structural analyses regarding the ribonucleoprotein complex of SRP have been performed across all the domains of life. Few have addressed the SRP19-RNA interactions in humans as well as in archaea (Oubridge et al., 2002; Wild et al., 2009), whereas some have investigated the nature of the interaction between Ffh/SRP54 and SRP RNA (Batey et al., 2000; Kuglstatter et al., 2002; Rosendal et al., 2003). Overall, SRP19 is said to induce the side-by-side alignment of the two helices of the S domain of SRP RNA, which in turn favors the conformational changes in the asymmetric loop of the helix 8 necessary to bind SRP54. Though, reports are confirming tight binding of RNA by SRP54 even in the absence of SRP19 (Maeshima et al., 2001; Tozik et al., 2002) which hint at the possible key role of the apical tetraloops of the two RNA helices, rather than SRP19 itself. The asymmetric and the symmetric loop of helix 8 contact the M domain of SRP54 and such binding induces a compact rearrangement around the IBD of the G domain (Rosendal et al., 2003; Nagai et al., 2003). Crystal structures of SRP54 alone or in combination with helix 8 and that of SRP19 complexed with 7S.S RNA have been solved in *S. solfataricus, A. ambivalens,* and *M. jannaschii* (Montoya et al., 2000; Rosendal et al., 2003; Hainzl et al., 2007) but such detailed structural information is absent in *S. acidocaldarius*. Therefore, the present work sought to identify the protein-RNA interaction interface and the important residues involved by computational designing and homology modeling.

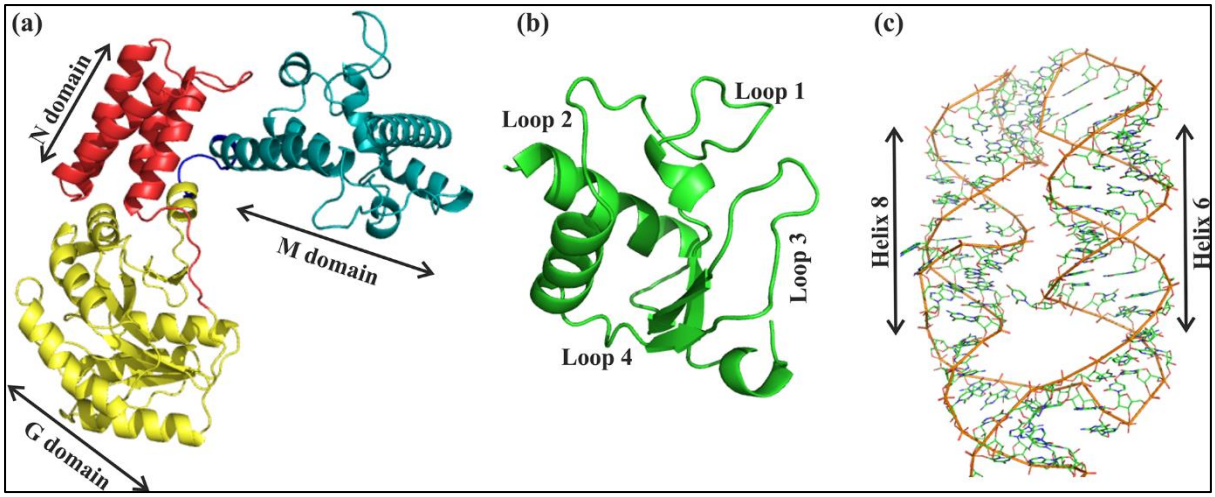

Figure 3.6. Structure prediction by sequence-based homology modeling. The structure of (a) SRP54 and (b) SRP19 from *S. acidocaldarius* was modeled using the solved crystal structures of homologous proteins in *S. solfataricus* (1QZW, 3KTW respectively). The different domains of SRP54 have been marked as – red for N domain, yellow for G domain, teal for M domain, and blue for G-M linker. The structure of the S domain of SRP RNA (c) from *S. acidocaldarius* was modeled using 3KTW (C and D chains) as the template.

The tertiary structures of the proteins were generated using the SWISS-MODEL web server and that of the 7S.S RNA was built by using the 3dRNA webserver. The characteristic domain arrangements of SRP54/Ffh were observed in the modeled structure as well. It consisted of the N-terminal N domain, closely followed by the G domain. Together they build the catalytic NG domain which binds and hydrolyses GTP and interacts with the NG domain of FtsY. The C-terminal M domain is linked to the G domain via a flexible linker region with consensus sequence 'RXLGXGD', present in *S. acidocaldarius* as 'RLLGLGD' (Fig. 3.6a, blue region). The conserved glycine residues in this region may allow possible conformational rearrangements within SRP54 upon binding with RNA or signal sequence. Figure 3.6b shows the structure of SRP19 with its four characteristic loops. The L1 is a rigid, well-defined region that acts as the primary surface for the protein-RNA interaction (Hainzl et al., 2005). The L2 region remains relatively disordered in free protein but refolds upon contacting the SRP RNA (Wild et al., 2010) and establishes base-specific hydrogen bonds with the RNA backbone. The tertiary structure of the S domain of 7S RNA clearly shows the helices 6 and 8 (Fig. 3.6c), generated by the 3dRNA webserver that built the RNA model based on its secondary structure alignment with experimental

templates (Wang et al., 2019). In case of non-availability of the template, a distance-geometry-based loop building method is used to build segments of the secondary structure and the final model is optimized by the Simulated Annealing Monte Carlo method. The resulting structure aligned considerably well (RMSD = 3.792) with the available structure of *Sulfolobus* 7S.S RNA (3KTW). The asymmetric loop in the helix 8 was reoriented in the model which can be observed upon SRP54 binding. In *Methanococcus jannaschii*, free 7S.S RNA has its ACC trinucleotide (195-197) of the asymmetric loop pointing toward the interior of the RNA helix. These bases become stably stacked, upon contacting the SRP54-M domain, causing an upward movement of the bulged backbone that brings both the symmetryic and symmetric loops closer (Hainzl et al., 2007). An effective RNA-protein interaction similarly induces the M domain to undergo conformational rearrangements that favor signal sequence binding. Here, a structural model of *Saci*SRP54 was created using a novel machine learning approach called AlphaFold2 (Jumper et al., 2021). The AlphaFold network takes advantage of the primary amino acid sequence and aligned sequences of homologs as inputs to directly predict the 3D coordinates of all heavy atoms for a given protein. The prediction is viewed as a graph interface in three-dimensional space where the edges are defined by the proximal residues. The predicted accuracy of these network-based models is represented as a per-residue confidence score (pLDDT) that ranges between 0 to 100. The structure of *Saci*SRP54 predicted by AlphaFold showed an overall confident scoring (90 > pLDDT > 70) with some areas, comprising part of the catalytic domain and the RNA-binding residues of M domain, showing very high confidence (pLDDT > 90) and few unstructured or loop region residues scoring low (pLDDT < 70). When the AlphaFold predicted structure was aligned with the sequence-homology-driven structure of *Saci*SRP54, a marked difference in conformation was observed around the M domain (Fig. 3.7a). The M domain has a unique all-helical conformation that consists of seven alpha helices – αML, αM1, αM1b and αM2-αM5 (Gupta et al., 2016). A detailed observation into the aligned M domains from the two predictions provided an important insight – within the AlphaFold prediction, the overall orientation of the M domain has been shifted to the other side of a rotational axis placed at the G-M linker region. Interestingly,

the most prominent stretch to score the lowest confidence (67 > pLDDT > 54) in the AlphaFold prediction comprises a short helical turn (Gln349-Val360) which forms part of the signal sequence binding finger-loop groove in homology driven model (Pro352-Leu367) as well as in *Ssol*SRP54 crystal structure. The finger-loop is located between αM1b and αM2 and the formation is lined by αM1, αM2, and αM5 (Rosendal et al., 2003) before being induced by SRP RNA. The αM5 and the primary RNA-binding helix αM4 were shifted by approximately 25 Å in the AlphaFold prediction from their respective positions in the homology-driven model (Fig. 3.7b).

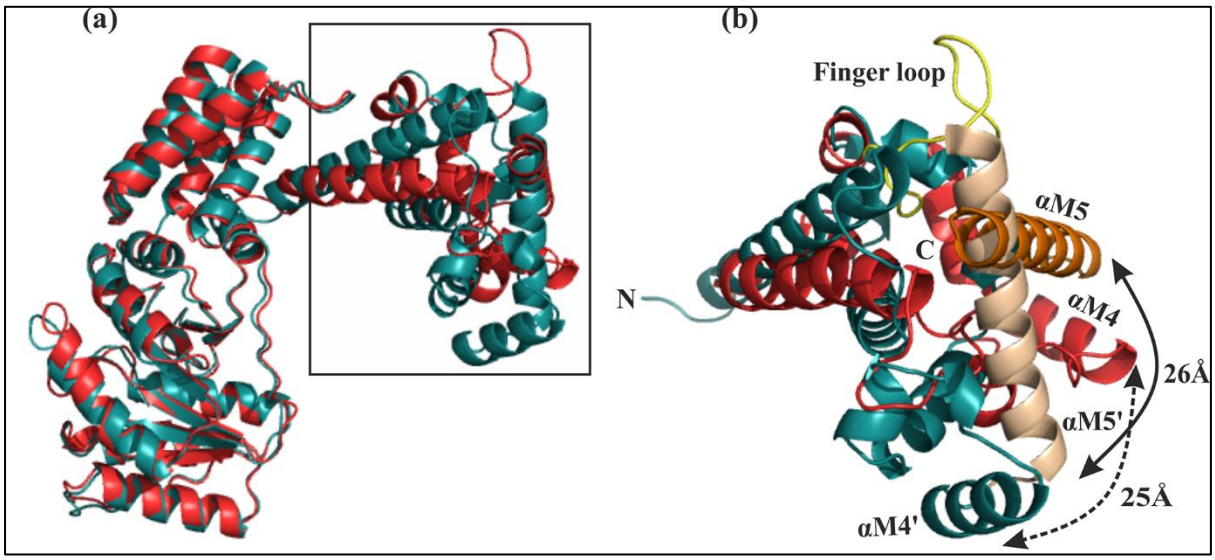

Figure 3.7. Structural alignment of predicted models of SRP54. The overall structures of SRP54 were aligned using PyMOL; the AlphaFold predicted model is shown in teal blue and the homology driven model is shown in red (a). M domains from respective models were aligned along a fixed rotational axis (b) and regions of interest were marked. The prominent finger loop region (yellow) belonged to the homology-driven model. The terminal helices αM4′ and αM5′ in AlphaFold prediction were found to be 25 Å and 26 Å apart from the respective helices αM4 and αM5 in homology driven model.

Such observations strongly suggest that in presence of SRP RNA, the M domain of SRP54 reorients its constituting alpha-helices to fit the minor groove of the helix 8. In doing so, the short unstructured region between the αM1b and αM2 takes a conformation favorable to accommodate signal peptides. AlphaFold derives the structure of a given protein by sequence and pairwise alignment and then trains the network with the produced feed. In absence of any nucleic acid partner, the network delivered the conformation best attained by the protein in its native state.

3.3.5 Contact analysis in the RNA-protein interaction

The association of 7S RNA with either SRP54 or SRP19 is driven by strong, residue-specific interactions. The residues involved in RNA binding in *Ssol*SRP54 were found to be distributed among αM2, αM3, and αM4 helices (Rosendal et al., 2003) whereas, in *Mjan*SRP19, the RNA-binding amino acids could be located in the L1 and L2 loops (Oubridge et al., 2002; Hainzl et al., 2002). To address the issue in the *Sulfolobus acidocaldarius* SRP system, the predicted structural model of SRP RNA was docked with SRP54 and SRP19, separately, using HADDOCK, and the most probable residues involved in the interaction were mapped across the RNA and the protein backbone, based on their permissible proximity for bond formation (Table 3.3).

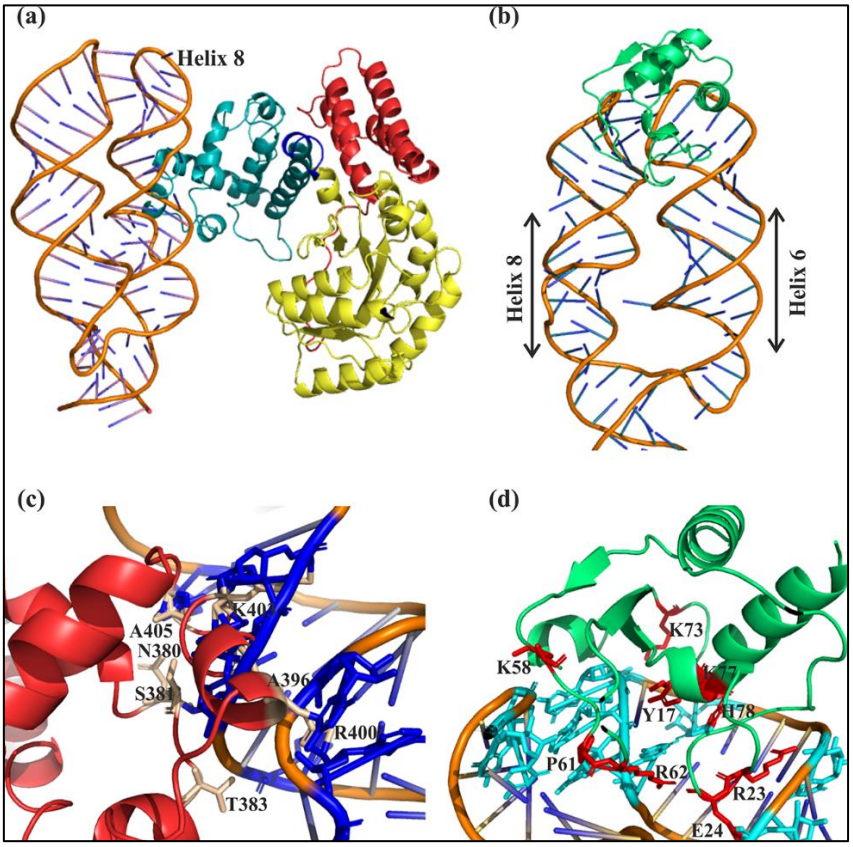

Figure 3.8. Residues involved in the base-specific interaction with 7S RNA. The 3dRNA derived structure of *Saci*SRP RNA was used to dock the *Saci*SRP54 (a) and *Saci*SRP19 (b). The color codes were maintained as in Fig. 3.6 and the interacting helices have been marked. A detailed observational analysis of the protein-RNA contact surface identified amino acid residues of SRP54 (c) and SRP19 (d) that were involved in direct interaction with either the bases or the backbone of the RNA shown in blue (c) or cyan (d).

Table 3.3 Residues involved in the RNA-protein interaction

SRP54	7S RNA	Distance	SRP19	7S RNA	Distance
Gln380	A220	3.0 Å	Tyr17	G166	3.7 Å
Ser381	A219	2.6 Å	Arg23	U158	3.2 Å
Thr383	C222	3.2 Å	Glu24	C156	1.6 Å
Ala396	C197	2.7 Å	Lys58	G209	3.6 Å
Arg400	A195	1.8 Å	Pro61	C207	4.2 Å
Lys403	C218	1.6 Å	Arg62	G167	2.6 Å
Ala405	A203	2.5 Å	Lys73	G164	2.6 Å
			Lys77	A165	2.7 Å
			His78	U162	0.6 Å

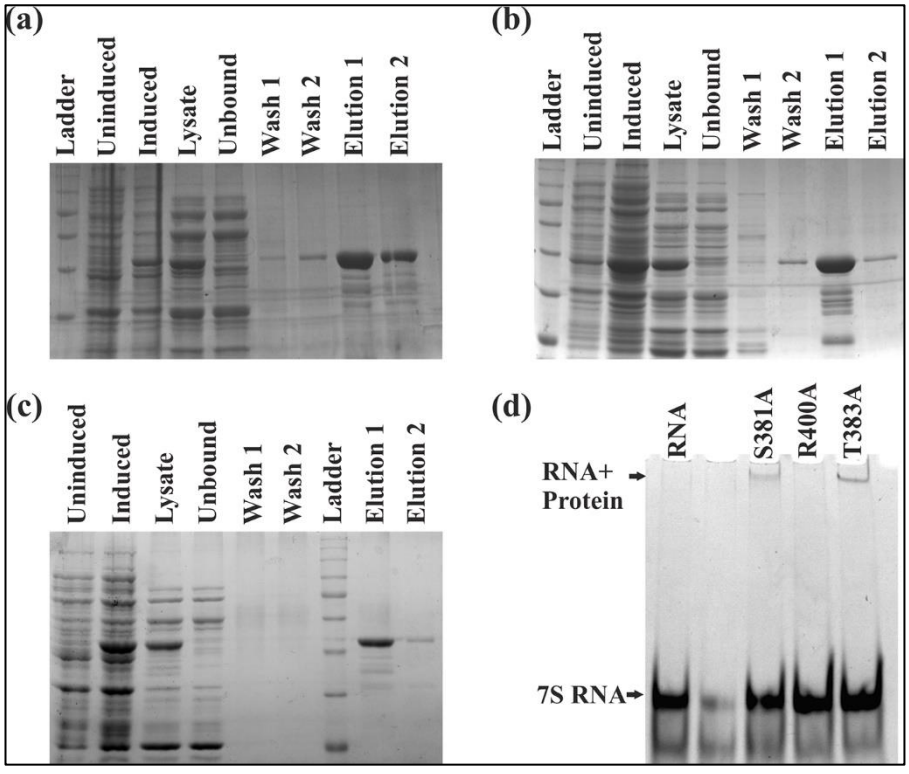

Figure 3.9. Purification and characterization of SRP54 mutants. Proteins were overexpressed using IPTG and purified via affinity chromatography and loaded on different polyacrylamide gels to obtain specific separation for (a) SRP54^{S381A}, (b) SRP54^{T383A}, and (c) SRP54^{R400A}. Radiolabelled 7S RNA was incubated with 1 μM of each of the mutant proteins and separated via native-PAGE.

The selected residues from the SRP54-M domain showed probable extensive pairing with the bases in both the symmetric and the asymmetric loops of the helix 8. Three residues, Ser381, Thr383, and Arg400, were selected for biochemical characterization for their possible role in the interaction with the RNA. The resultant mutant proteins were successfully purified (Fig. 3.9a-c) and tested for their RNA binding ability (Fig. 3.9d). RNA binding was found to be completely abrogated in SRP54^{R400A} but retained in residual strength by SRP54^{S381A} and SRP54^{T383A}. The selected serine and threonine residues lie close to adenine and cytosine at 219th and 222nd position respectively in the widened helix 8 minor groove. The arginine at 400th position, on the other hand, possibly makes a contact with the 195th base adenine, lying in the asymmetric loop. Since SRP54 contacts 7S RNA at the minor groove of its helix 8, Ser381 and Thr383 probably establish a strong contact with the RNA. The A195 in the asymmetric loop is highly conserved and therefore its interacting partner in the protein, Arg400, may be important for RNA binding to a large extent. These data indicate the importance of the predicted residues in maintaining the necessary RNA-protein interaction in the SRP ribonucleoprotein system.

3.4 DISCUSSION

Signal recognition particle in archaea consists of SRP19, SRP54, and 7S RNA where the RNA acts as a scaffold for the proteins to optimally rearrange their conformation. Several structural studies have elucidated the possible role of SRP RNA in facilitating a stable conformational intermediate of the trimolecular complex. Biochemical characterization of bacterial Ffh or mammalian SRP54 GTPase activity has been pivotal to map the thermodynamic as well cell biological understanding of the system, whereas such evidence in the archaeal domain has been scarce. SRP54 from *A. ambivalens*, showed an optimal GTP hydrolysis at 81 °C at neutral pH, with an affinity for the nucleotide measuring 13.7 μM (Moll et al., 1999) and bound the 7S RNA from *S. solfataricus* with high affinity. On the other hand, SRP54 from both *A. fulgidus* and *M. jannaschii* bound 7S RNA with high affinity which was enhanced in the presence of SRP19 (Diener & Wilson, 2000; Hainzl et al., 2005). The present study

investigated specific enzymatic and RNA-binding features of *Saci*SRP54 and SRP19 which enlightened the basic understanding of the ribonucleoprotein complex adjusting the protein targeting process.

SRP54 from *S. acidocaldarius* was found to be enzymatically most active at 75-80 °C and a near-neutral pH in an Mg^{2+} ion-dependent way, with an almost equal affinity for both GTP and CTP. The optimal temperature and pH of the enzymatic property of SRP54 correspond to the natural habitat ecology of *S. acidocaldarius*. SRP54 and SRP19 both bound the 7S RNA with considerable affinity but the binding between SRP19 and RNA seemed stronger as reflected by the corresponding K_d values (Table 3.2). Rosendal et al. (2003) and Hainzl et al. (2007) depicted the conformational changes brought by the SRP RNA upon the SRP54-M domain, mostly regarding the signal sequence binding. Signal peptides are recognized by SRP54 using its finger-loop region and our computational data strongly corroborate the idea that such a fold is induced by the binding of 7S RNA. It was evident from the model predicted by AlphaFold2 that the addition of RNA completely reorients the SRP54-M domain that possibly brings a shift of ~25 Å in the corresponding arrangement of M domain helices, contrary to the observed 10 Å shift in *Ssol*SRP54 crystal structure (Rosendal et al., 2003). RNA-M domain interaction also favors an association between the RNA and the catalytic NG domain of SRP54 (Hainzl et al., 2007) which strongly affects the GTPase activity of the protein. This was further substantiated by the data obtained from the Michaelis-Menten kinetics of *Saci*SRP54 GTPase which showed a clear improvement in the affinity toward the substrate in presence of 7S RNA (Table 3.2). Thus, the importance of SRP RNA in the active crenarchaeal SRP assembly can be established beyond just being a mere scaffold. The possible catalytic role of 7S RNA fuelled the quest for unraveling the molecular players involved in the RNA-protein interaction. Docking experiment between homology driven models of SRP54/SRP19 and 7S RNA revealed a battery of important residues on both sides, involved in specific interaction In SRP54, these residues are distributed across the αM3 and αM4 helices. Three such residues – Ser381, Thr383, and Arg400 – were selected for mutational substitution with alanine. Subsequent mutant proteins – $SRP54^{S381A}$, $SRP54^{T383A,}$ and $SRP54^{R400A}$ – were purified and checked for their ability to bind 7S

RNA. SRP54^{R400A} was found to have severely impaired RNA-binding function, whereas the other two mutations resulted in reduced binding compared to the wild type. These residues, therefore, serve as binding hotspots that can be manipulated to gain further insights into the mechanistic detail of the interaction.

3.5 CONCLUSION

Taken together, the results established the first critical characterization of the SRP components in the thermoacidophilic crenarchaeal system. The molecular adaptations corresponding to the natural habitat of the organism were substantiated through analyses of the enzymatic ability of *Saci*SRP54. Furthermore, the binding of 7S RNA to both SRP54 and SRP19 was characterized to the molecular extent and the nature of a heterotrimeric assembly was investigated by the computational and mutational study. The results give a holistic projection of this trimolecular interaction as depicted below –

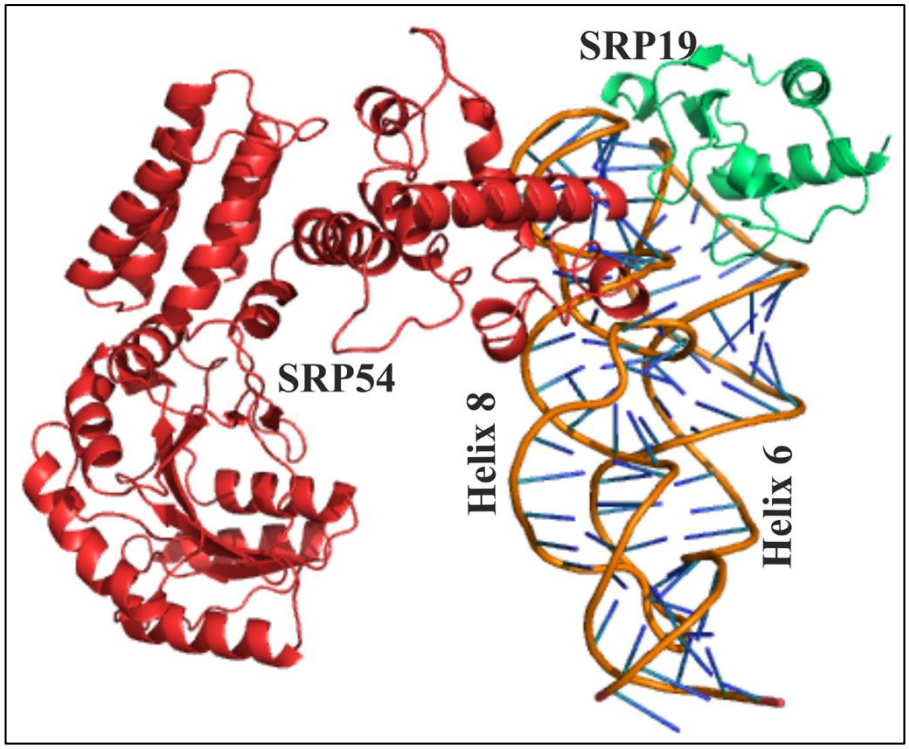

Figure 3.10. Structural depiction of the active SRP ribonucleoprotein assembly in *S. acidocaldarius*.

3.6 BIBLIOGRAPHY

Akopian, D., Shen, K., Zhang, X., & Shan, S. (2013). Signal recognition particle: an essential protein-targeting machine. In *Annual review of biochemistry* (Vol. 82).

Batey, R. T., Rambo, R. P., Lucast, L., Rha, B., & Doudna, J. A. (2000). Crystal structure of the ribonucleoprotein core of the signal recognition particle. *Science*, *287*(5456), 1232–1239.

Batey, R. T., Rambo, R. P., Lucast, L., Rha, B., & Doudna, J. A. (2000). Crystal structure of the ribonucleoprotein core of the signal recognition particle. *Science*, *287*(5456), 1232–1239.

Connolly, T., & Gilmore, R. (1993). GTP hydrolysis by complexes of the signal recognition particle and the signal recognition particle receptor. *Journal of Cell Biology*, *123*(4), 799–807.

Diener, J. L., & Wilson, C. (2000). Role of SRP19 in assembly of the Archaeoglobus fulgidus signal recognition particle. *Biochemistry*, *39*, 12862–12874.

Dong, H. J., Tao, S. M., Li, Y. Q., Chan, S. H., Shen, X. L., Wang, C. X., & Guan, W. J. (2006). Analysis of the GTPase activity and active sites of the NG domains of FtsY and Ffh from Streptomyces coelicolor. *Acta Biochimica et Biophysica Sinica*, *38*(7), 467–476.

Freymann, D. M., Keenan, R. J., Stroud, R. M., & Walter, P. (1997). Structure of the conserved GTPase domain of the signal recognition particle. *Nature*, *385*(6614), 361–364.

Ghosh, A., Hartung, S., Van Der Does, C., Tainer, J. A., & Albers, S. V. (2011). Archaeal flagellar ATPase motor shows ATP-dependent hexameric assembly and activity stimulation by specific lipid binding. *Biochemical Journal*, *437*(1), 43–52.

Grudnik, P., Bange, G., & Sinning, I. (2009). Protein targeting by the signal recognition particle. *Biological Chemistry*, *390*(8), 775–782.

Guex, N., Peitsch, M.C., Schwede, T. (2009). Automated comparative protein structure modeling with SWISS-MODEL and Swiss-PdbViewer: A historical perspective. *Electrophoresis, 30*, S162-S173.

Gupta, S, Roy, M., & Ghosh, A. (2016). The Archaeal Signal Recognition Particle: Present Understanding and Future Perspective. *Current Microbiology*, *74*(2), 284–297.

Gupta, Sayandeep, Roy, M., Dey, D., Bhakta, K., Bhowmick, A., Chattopadhyay, D., & Ghosh, A. (2021). Archaeal SRP RNA and SRP19 facilitate the assembly of SRP54-FtsY targeting complex. *Biochemical and Biophysical Research Communications*, *566*, 53–58.

Hainzl, T., & Elisabeth Sauer-Eriksson, A. (2015). Signal-sequence induced conformational changes in the signal recognition particle. *Nature Communications*, *6*, 1–7.

Hainzl, T., Huang, S., & Sauer-Eriksson, A. E. (2002). Structure of the SRP19 RNA complex and implications for signal recognition particle assembly. *Nature*, *417*, 767–771.

Hainzl, T., Huang, S., & Sauer-Eriksson, A. E. (2005). Structural insights into SRP RNA: An induced fit mechanism for SRP assembly. *Rna*, *11*(7), 1043–1050.

Hainzl, T., Huang, S., & Sauer-Eriksson, A. E. (2007). Interaction of signal-recognition particle 54 GTPase domain and signal-recognition particle RNA in the free signal-recognition particle. *Proceedings of the National Academy of Sciences of the United States of America*, *104*(38), 14911–14916.

Hainzl, T., Huang, S., Meriläinen, G., Brännström, K., & Sauer-Eriksson, A. E. (2011). Structural basis of signal-sequence recognition by the signal recognition particle. *Nature Structural and Molecular Biology*, *18*(3), 389–391.

Halic, M., Blau, M., Becker, T., Mielke, T., Pool, M. R., Wild, K., Sinning, I., & Beckmann, R. (2006). Following the signal sequence from ribosomal tunnel exit to signal recognition particle. *Nature*, *444*(7118), 507–511.

Honorato, R. V., Koukos, P. I., Jiménez-García, B., Tsaregorodtsev, A., Verlato, M., Giachetti, A., Rosato, A., & Bonvin, A. M. J. J. (2021). Structural Biology in the Clouds: The WeNMR-EOSC Ecosystem. *Frontiers in Molecular Biosciences*, *8*, 708.

Janda, C. Y., Li, J., Oubridge, C., Hernández, H., Robinson, C. V., & Nagai, K. (2010). Recognition of a signal peptide by the signal recognition particle. *Nature*, *465*(7297), 507–510.

Keenan, R. J., Freymann, D. M., Stroud, R. M., & Walter, P. (2001). The signal recognition particle. *Annual Review of Biochemistry*, *70*, 755–775.

Kempf, G., Wild, K., Sinning, I. (2014). Structure of the complete bacterial SRP Alu domain. *Nucleic Acids Research, 42*(19):12284–12294.

Kuglstatter, A., Oubridge, C., & Nagai, K. (2002). Induced structural changes of 7SL RNA during the assembly of human signal recognition particle. *Nature Structural Biology*, *9*(10), 740–744.

Leipe, D. D., Wolf, Y. I., Koonin, E. V., & Aravind, L. (2002). Classification and evolution of P-loop GTPases and related ATPases. *Journal of Molecular Biology*, *317*(1), 41–72.

Maeshima, H., Okuno, E., Aimi, T., Morinaga, T., & Itoh, T. (2001). An archaeal protein homologous to mammalian SRP54 and bacterial Ffh recognizes a highly conserved region of SRP RNA. *FEBS Letters*, *507*(3), 336–340.

Moll, R., Schmidtke, S., & Schäfer, G. (1999). Domain structure, GTP-hydrolyzing activity and 7S RNA binding of Acidianus ambivalens ffh-homologous protein suggest an SRP-like complex in archaea. *European Journal of Biochemistry / FEBS*, *259*(1–2), 441–448.

Moll, R., Schmidtke, S., Petersen, A., & Schäfer, G. (1997). The signal recognition particle receptor a subunit of the hyperthermophilic archaeon Acidianus ambivalens exhibits an intrinsic GTP-hydrolyzing activity. *Biochimica et Biophysica Acta - General Subjects*, *1335*(1–2), 218–230.

Montoya, G., Svensson, C., Luirink, J., & Sinning, I. (1997). Crystal structure of the NG domain from the signal-recognition particle receptor FtsY. *Nature*, *385*(6614), 365–368.

Montoya, G., Te Kaat, K., Moll, R., Schäfer, G., & Sinning, I. (2000). The crystal structure of the conserved GTPase of SRP54 from the archaeon Acidianus ambivalens and its comparison with related structures suggests a model for the SRP-SRP receptor complex. *Structure*, *8*(5), 515–525.

Nagai, K., Oubridge, C., Kuglstatter, A., Menichelli, E., Isel, C., & Jovine, L. (2003). Structure, function and evolution of the signal recognition particle. *EMBO Journal*, *22*(14), 3479–3485.

Oubridge, C., Kuglstatter, A., Jovine, L., & Nagai, K. (2002). Crystal structure of SRP19 in complex with the S domain of SRP RNA and its implication for the assembly of the signal recognition particle. *Molecular Cell*, *9*(6), 1251–1261.

Palaniyandi, K., Veerasamy, M., & Narayanan, S. (2012). Characterization of Ffh of Mycobacterium tuberculosis and its interaction with 4.5S RNA. *Microbiological Research*, *167*(9), 520–525.

Peluso, P., Shan, S. O., Nock, S., Herschlag, D., & Walter, P. (2001). Role of SRP RNA in the GTPase cycles of Ffh and FtsY. *Biochemistry*, *40*(50), 15224–15233.

Peluso, Paul, Herschlag, D., Nock, S., Freymann, D. M., Johnson, A. E., & Walter, P. (2000). Role of 4.5S RNA in assembly of the bacterial signal recognition particle with its receptor. *Science*, *288*(5471), 1640–1643.

Pohlschröder, M., Dilks, K., Hand, N. J., & Rose, R. W. (2004). Translocation of proteins across archaeal cytoplasmic membranes. *FEMS Microbiology Reviews*, *28*(1), 3–24.

Poritz, M. A., Bernstein, H. D., Strub, K., Zopf, D., Wilhelm, H., & Walter, P. (1990). An E. coli Ribonucleoprotein Containing 4.5S RNA Resembles Mammalian Signal Recognition Particle. *Science*, *250*(494), 1111–1117.

Powers, T., & Walter, P. (1995). Reciprocal stimulation of GTP hydrolysis by two directly interacting GTPases. *Science*, *269*(5229), 1422–1424.

Rosendal, K. R., Wild, K., Montoya, G., & Sinning, I. (2003). Crystal structure of the complete core of archaeal signal recognition particle and implications for interdomain communication. *Proceedings of the National Academy of Sciences of the United States of America*, *100*(25), 14701–14706.

Sato, K., Akiyama, M., & Sakakibara, Y. (2021). RNA secondary structure prediction using deep learning with thermodynamic integration. *Nature Communications*, *12*(1), 941.

Shen, K., Wang, Y., Hwang Fu, Y. H., Zhang, Q., Feigon, J., & Shan, S. O. (2013). Molecular Mechanism of GTPase Activation at the Signal Recognition Particle (SRP) RNA Distal End. *Journal of Biological Chemistry*, *288*(51), 36385–36397.

Studer, G., Rempfer, C., Waterhouse, A.M., Gumienny, G., Haas, J., Schwede, T. (2020). QMEANDisCo - distance constraints applied on model quality estimation. *Bioinformatics, 36*, 1765-1771.

Tozik, I., Huang, Q., Zwieb, C., & Eichler, J. (2002). Reconstitution of the signal recognition particle of the halophilic archaeon Haloferax volcanii. *Nucleic Acids Research*, *30*(19), 4166–4175.

Van Zundert, G. C. P., Rodrigues, J. P. G. L. M., Trellet, M., Schmitz, C., Kastritis, P. L., Karaca, E., Melquiond, A. S. J., Van Dijk, M., De Vries, S. J., & Bonvin, A. M. J. J. (2016). The HADDOCK2.2 Web Server: User-Friendly Integrative Modeling of Biomolecular Complexes. *Journal of Molecular Biology*, *428*(4), 720–725.

Voigts-hoffmann, F., Schmitz, N., Shen, K., Shan, S., Ataide, S. F., & Ban, N. (2013). Article The Structural Basis of FtsY Recruitment and GTPase Activation by SRP RNA. *Molecular Cell*, *52*(5), 643–654.

Wang, C. Y., & Miller, T. F. (2014). Allosteric response and substrate sensitivity in peptide binding of the signal recognition particle. *Journal of Biological Chemistry*, *289*(44), 30868–30879.

Waterhouse, A., Bertoni, M., Bienert, S., Studer, G., Tauriello, G., Gumienny, R., Heer, F.T., de Beer, T.A.P., Rempfer, C., Bordoli, L., Lepore, R., Schwede, T. (2018). SWISS-MODEL: homology modelling of protein structures and complexes. *Nucleic Acids Research, 46*(W1), W296-W303.

Wild, Klemens, Bange, G., Bozkurt, G., Segnitz, B., Hendricks, A., & Sinning, I. (2010). Structural insights into the assembly of the human and archaeal signal recognition particles. *Acta Crystallographica Section D: Biological Crystallography*, *66*(3), 295–303.

Zhang, X., Kung, S., & Shan, S. (2008). *Demonstration of a Multistep Mechanism for Assembly of the SRP · SRP Receptor Complex : Implications for the Catalytic Role of SRP RNA*. *54*, 581–593.

Zwieb, Christian. (1994). *Identification of the nucleotides in helix 8 required for interaction with protein SRP19*. *890*, 885–890.

CHAPTER 4

Characterization of the functional targeting complex in archaea and the role of SRP components in facilitating the event at high temperature

4.1 INTRODUCTION

The signal recognition particle (SRP) and its receptor constitute essential cellular machinery required to execute co-translational translocation of nascent polypeptides across the membranes in all three domains of life. The signal sequence at the N-terminus of the nascent polypeptide chain is recognized and bound by SRP. After that, it forms a complex with a cognate receptor (SR, in eukaryotes; FtsY, in prokaryotes) located on the target membrane. Such interaction is followed by a series of conformational rearrangements in the SRP-FtsY complex that leads to the delivery of the ribosome-nascent chain complex (RNC) to the nearby translocon (SecYEG). Once the RNC is released, the SRP-FtsY complex dissociates through concomitant GTP hydrolysis by both the proteins (Gupta et al., 2016). The SRP shares its structural and functional similarities across different domains of life. Mammalian SRP consists of six proteins (SRP54, SRP19, SRP68, SRP72, SRP9, and SRP14) and a 7S RNA (Keenan et al., 2001), whereas the bacterial counterpart consists of only one protein (Ffh, SRP54 homolog) and a 4.5S RNA (Batey et al., 2000; Buskiewicz et al., 2005). The ribonucleoprotein complex's functional core comprises the RNA and SRP54 protein that performs signal recognition, receptor interaction, and GTP hydrolysis (Akopian et al., 2013). Archaea, being a true mosaic of eukaryotic and prokaryotic features, shares the similarities of mammalian SRP54, SRP19, and 7S RNA and the bacterial SRP receptor (Zwieb & Eichler, 2002; Grudnik et al., 2009). The 7S RNA and GTP, the key regulators in the evolutionarily conserved targeting process, are bound by the M domain and NG domain in SRP54, respectively. The catalytic NG domain is also the interacting domain for both SRP54 and FtsY, and the G domain shares the motifs of the classic P-loop GTPases (Leipe et al., 2002; Gupta et al., 2021). The classical GTPase motifs I-IV (Bourne et al., 1991) are present in both SRP GTPases along with four additional elements, the I-box domain, the closing loop, the DARGG motif, and the ALLEADV motif for essential function (Keenan et al., 2001). Contrary to the classical GTPases, SRP GTPases interact directly to stimulate concomitant hydrolysis of GTP and do not require a guanine nucleotide exchange factor for nucleotide release (Powers & Walter, 1995; Jagath et al., 2000). SRP19 contacts the helices 6 and 8 of the 7S RNA and induce the side-by-side

alignment of these two helices, which supposedly favors the conformational rearrangements in the asymmetric loop of helix 8 necessary for SRP54 binding (Rose & Pohlschroder, 2002; Hainzl et al., 2005; Hainzl et al., 2007). However, SRP19-independent SRP54-7S RNA binding has been shown in *Haloferax volcanii,* where the cells could grow normally even after the deletion of the *SRP19* gene implying the dispensable nature of SRP19 (Yurist et al., 2007).

SRP RNA is crucial to signal sequence recognition and binding as it provides the conformational scaffold for the effective positioning of the SRP54-M domain and induces the finger-loop formation that accepts the signal peptide (Keenan et al., 1998; Rosendal et al., 2003). The M domain of the SRP54 is connected to the catalytic NG domain via a flexible linker region (Rosendal et al., 2003), and signal peptide binding influences the repositioning of this domain so that it binds the GTP more effectively (Hainzl et al., 2007; Janda et al., 2010). Since the two SRP GTPases, SRP54 and SRP receptor (SR/FtsY), interact via their NG domains, the SRP RNA plays a vital role in the interaction of the two GTPases in bacteria evidently (Shen & Shan, 2009; Voights-Hoffmann et al., 2013). Kinetic analyses have shown that bacterial 4.5S RNA does not affect the basal GTPase activity of Ffh but is required for a successful association with FtsY (Powers & Walter, 1995; Peluso et al., 2001). Though the stable assembly of the two proteins is GTP-dependent, it is initiated by an early GTP-independent complex which is significantly stabilized by 4.5S RNA (Zhang et al., 2008). The rate of the Ffh-FtsY association is accelerated by almost 400-folds in the presence of 4.5S RNA (Stroud & Walter, 1999; Peluso et al., 2000), which probably provides a longer lifetime to the transient intermediate required to rearrange to the stable final assembly. On the contrary, GTP hydrolysis by the active targeting complex is enhanced only by 8-fold in the presence of SRP RNA (Peluso et al., 2001). Mutational analyses have shown that blocking GTPase activation, but not the SRP-FtsY assembly, severely compromises translocation of the nascent polypeptide (Shan et al., 2007). Thus, a series of discrete conformational changes happen during SRP-SR association in bacteria that culminate in their reciprocal GTP hydrolysis, ultimately driving the cargo unloading and successful translocation (Shan et al., 2007; Zhang et al., 2009).

Interestingly, the role of archaeal SRP RNA towards the stable association and GTPase activities of SRP54 and FtsY remains elusive. It remains unclear whether the archaeal 7S RNA contributes to the stable complexation of SRP54 and FtsY. Several crystal structures of the individual components of SRP-mediated protein translocation in archaea are available from *Sulfolobus solfataricus*, *Pyrococcus furiosus, Methanococcus jannaschii,* and *Archaeoglobus fulgidus* (Hainzl et al., 2002; Pakhomova et al., 2002; Rosendal et al., 2003; Egea et al., 2008). However, the mechanistic details of the involvement of 7S RNA in SRP54 and FtsY interaction have been largely unexplored.

Here we have characterized the interaction between the two SRP GTPases, SRP54 and FtsY, and established the role of archaeal 7S RNA in the stable *in vitro* SRP54-FtsY assembly in a thermoacidophilic crenarchaeon *Sulfolobus acidocaldarius*. Our results show that archaeal 7S RNA does not influence the GTPase activity of SRP54 alone or in combination with FtsY, but it enhances the association between the two proteins in a GTP-dependent manner. To further investigate the catalytic contribution of the P-loop motifs, we identified key residues in the SRP54-G domain and their contribution to the GTP-binding ability of the wild-type protein. The presence of archaeal SRP19, on the other hand, increases the overall reaction rate of GTP hydrolysis, particularly in combination with the S domain of SRP RNA.

4.2 MATERIALS AND METHODS

4.2.1 Construction of overexpression vectors

Construction of pAG3 and pAG13, expressing wild type SRP54 and SRP19 respectively, were achieved following the protocol listed in 3.2.1. The single point mutations were introduced in the pAG3 backbone, individually, by the site-directed mutagenesis protocol using KOD Hotstart polymerase (Novagen). Primers used for this purpose and the final constructs generated are listed in Table 4.1. To enable expression of FtsY with a C-terminal histidine tag, the *ftsy* gene (*saci_1462*) was amplified by PCR from genomic DNA of *S. acidocaldarius* DSM639 using primers listed in Table 2.2, digested, and ligated into pET28a vector yielding plasmid

pAG351. For expression analysis, the required vector was transformed into *Escherichia coli* BL21 (DE3) cells containing the RIL Cam^r plasmid (Stratagene). All the strains used in the present study are listed in Table 2.1.1. The primers and constructs used for the expression of wild-type proteins are listed in Table 2.1.2 and 2.1.3, respectively.

Table 4.1 Primers and plasmids used to construct SRP54-G domain mutants

Primers, plasmids	Relevant characteristics	Reference
374	5′-ACAGGGAAGTGGTGCGACTACAAC-3′ Forward primer for SRP54^{K108A}	Present study
375	5′-TGCCAGAAGTTGTAGTCGCACCACTTCC-3′ Reverse primer for SRP54^{K108A}	Present study
376	5′-CAGGGAAGTGGTAAGGCTACAAC-3′ Forward primer for SRP54^{T109A}	Present study
377	5′-TGCCAGAAGTTGTAGCCTTACCACTTCC-3′ Reverse primer for SRP54^{T109A}	Present study
378	5′-TAAAGTAGGTTTAGTTGCTGCTGCTATATATCG-3′ Forward primer for SRP54^{D132A}	Present study
379	5′-ATGCAGCAGGACGATATATAGCAGCAGCAACT AAAC-3′ Reverse primer for SRP54^{D132A}	Present study
380	5′-TTGCTGCTGATATATATGCTCCTGCTGCATATG-3′ Forward primer for SRP54^{R135A}	Present study
381	5′-GCTCATATGCAGCAGGAGCATATATATCAG-3′ Reverse primer for SRP54^{R135A}	Present study
384	5′-GTAATAATTGACACAGCCAAAAGGCACGGTT AC-3′ Forward primer for SRP54^{G187K}	Present study
385	5′-CCCCGTAACCGTGCCTTTTGGCTGTG-3′ Reverse primer for SRP54^{G187K}	Present study
386	5′-GGTTCATTAATAGTGTCAGCGATGGACG-3′ Forward primer for SRP54^{K245A}	Present study

387	5′-TTCGCTGTTCCGTCCATCGCTGACAC-3′ Reverse primer for SRP54^{K245A}	Present study
388	5′-AATAGTGTCAAAGATGGCCGGAACAG-3′ Forward primer for SRP54^{D247A}	Present study
389	5′-CTCCTCCTTTCGCTGTTCCGGCCATC-3′ Reverse primer for SRP54^{D247A}	Present study
390	5′-CTCAGATAAAGTTCATAGGTGCAGGAG-3′ Forward primer for SRP54^{T271A}	Present study
391	5′-CATCCAATTTTTCTCCTGCACCTATG-3′ Reverse primer for SRP54^{T271A}	Present study
392	5′-AAAGTTCATAGGTACAGGAGCAAAATTGG-3′ Forward primer for SRP54^{E273A}	Present study
393	5′-CTTCCAATTCATCCAATTTTGCTCCTGTACC-3′ Reverse primer for SRP54^{E273A}	Present study
394	5′-GCTGCTGATATATATCGTGCTGCTGCATATG-3′ Forward primer for SRP54^{P136A}	Present study
395	5′-GCTCATATGCAGCAGCACGATATATATCAG-3′ Reverse primer for SRP54^{P136A}	Present study
pAG61	pETDuet1 carrying N terminal His-tagged *Saci_1310* (SRP54) with K108A substitution	Present study
pAG62	pETDuet1 carrying N terminal His-tagged *Saci_1310* (SRP54) with T109A substitution	Present study
pAG63	pETDuet1 carrying N terminal His-tagged *Saci_1310* (SRP54) with D132A substitution	Present study
pAG64	pETDuet1 carrying N terminal His-tagged *Saci_1310* (SRP54) with R135A substitution	Present study
pAG66	pETDuet1 carrying N terminal His-tagged *Saci_1310* (SRP54) with G187K substitution	Present study
pAG67	pETDuet1 carrying N terminal His-tagged *Saci_1310* (SRP54) with K245A substitution	Present study

pAG68	pETDuet1 carrying N terminal His-tagged (SRP54) with D247A substitution	*Saci_1310*	Present study
pAG69	pETDuet1 carrying N terminal His-tagged (SRP54) with T271A substitution	*Saci_1310*	Present study
pAG70	pETDuet1 carrying N terminal His-tagged (SRP54) with D273A substitution	*Saci_1310*	Present study
pAG71	pETDuet1 carrying N terminal His-tagged (SRP54) with P136A substitution	*Saci_1310*	Present study

4.2.2 Expression of recombinant proteins in *E. coli*

A total volume of 10 ml of an overnight culture of *E. coli* BL21(DE3)-RIL cells containing the RIL Cam^r plasmid, and the recombinant plasmid were used to inoculate 1 L of Luria–Bertani medium containing kanamycin (50 µg/ml) (for pAG351) or ampicillin (for pAG61-71) and chloramphenicol (34 µg/ml). Cells were grown at 37 °C until OD600 of 0.6 was reached when 500 µM IPTG (isopropyl β-D-thiogalactopyranoside) was added. The temperature was reduced to 16 °C, and growth was continued overnight to reduce inclusion body formation. The cells were collected by centrifugation, resuspended in lysis buffer [50mM Tris-Cl (pH 8.0), 150mM KCl, and 10% glycerol] containing the complete EDTA-free protease inhibitor cocktail (1 tablet/50 ml of lysate; Roche), frozen in liquid nitrogen and stored at - 80 °C.

4.2.3 Purification of recombinant proteins

Before purification, frozen resuspended cell pellets were thawed on ice. One mM lysozyme was added separately to the lysis buffer. After incubation on ice for 30 min, cells were lysed by sonication with Soniprep150 (DJB Labcare, UK). Cell debris was removed by centrifugation at 15000 rpm for 30 min (rotor SA-300; Sorval RC6+ Thermo Scientific). For the purification of histidine-tagged proteins, the supernatant was applied to a Ni^{2+}-NTA affinity column (Qiagen). Bound proteins were washed gradually with lysis buffer containing 10 mM and 20 mM imidazole, respectively. The bound protein fraction was eluted in a lysis buffer containing 100 mM of

imidazole. The eluted fraction was monitored by running reducing SDS-PAGE. The fraction containing the desired protein was dialyzed overnight in a lysis buffer.

4.2.4 GTPase assay and kinetic analyses

For estimating GTPase activity, the proteins were first dialyzed into a Tris-Cl buffer [50 mM Tris (pH 8.0), 150 mM KCl and 10% glycerol]. The same composition was used for the assay buffer with 5 mM $MgCl_2$. Fixed concentrations (2 µM) of proteins were pre-incubated for 5 mins and then incubated with 100 µM GTP at 75 °C for 15 min. The reaction was stopped by freezing in liquid nitrogen. To determine the activity of SRP54 as a function of temperature, pH, nucleotides, and divalent cations, the assay was performed at different temperatures, in different buffers [50 mM citrate (pH 3.0–5.5), MES (pH 6.0–6.5), HEPES (pH 7.0–7.5) or Tris/HCl (pH 8.0–9.5)], with different NTPs (5 mM of ATP, GTP, CTP or UTP), and in the absence of or with different divalent cations (5 mM of Na-EDTA, $NiCl_2$, $MgCl_2$, $MnCl_2$ or $CaCl_2$,) respectively (Ghosh et al., 2011). For the kinetic analyses, 1-10 µM of protein was assayed for the GTPase activity over a range of 5-30 mins. An aliquot of 20 µl from each sample was mixed with 200 µl of Malachite Green reagent and the absorbance was measured at 620 nm spectrophotometrically. The data were corrected for non-enzymatic GTP hydrolysis. The amount of GTP hydrolyzed by individual concentrations of the protein was determined as a function of time, and the resulting data were fitted to the following equation:

$$[GTP]hydrolysed = A \times (1 - e^{-kt})$$

where t is the time (min) of incubation, A is the amount of GTP hydrolyzed at each turnover (µM), and k is the reaction rate, measured in min^{-1}.

The affinity of the proteins for GTP can be calculated from the dependence of the observed reaction rate on protein concentration using the following equation:

$$k_{obsd} = k_{cat} \times \frac{[Protein]}{K_m + [Protein]}$$

where k_{obsd} is the observed rate constant at a specific protein concentration, k_{cat} is the maximal rate constant with saturating protein, and K_m is the protein concentration that provides half the maximal rate.

4.2.5 Tagging of proteins with fluorescent probes

Purified recombinant SRP54 and FtsY were conjugated with FITC and TRITC fluorescent probes, respectively, as described by the manufacturer (Sigma-Aldrich, USA). Briefly, SRP54 (50 μM) and FtsY (75 μM) in 50 mM Na-Phosphate buffer supplemented with 100 mM Sodium Bicarbonate (pH 9.0) were mixed either with FITC or TRITC fluorescent probes. A stock solution of FITC or TRITC was prepared in anhydrous DMSO at 600 μg/ml concentration. For labeling protein samples, 50 μl of FITC or TRITC fluorescent probe was taken from the stock solution and added very slowly to 1 ml of the protein with gentle and continuous stirring of the protein sample for 2 h at room temperature. Bio-Gel A column was used to separate the labeled protein from the free probe. The fraction, which contained the labeled SRP54 or FtsY, was collected and dialyzed against 50 mM phosphate buffer (pH 7.2) for 24 h at room temperature. The amount of protein labeled with FITC or TRITC was estimated by measuring the absorbance at 280 nm and 495 nm (for FITC) or 542 nm (for TRITC) of the proteins and respective fluorescence probes. Finally, tagging of the protein was assessed by running an SDS PAGE followed by scanning in a Typhoon scanner (GE Healthcare, Sweden).

4.2.6 Fluorescence resonance energy transfer (FRET)

The fluorescence resonance energy transfer (FRET) technique was used to determine the interaction between the two proteins, SRP54 and FtsY. The donor FITC-labelled SRP54 (100 nM) was incubated for 15 min at 60°C in 50 mM phosphate buffer (pH 7.2) with or without 100 μM of non-hydrolyzable GTP analog (GppNHp) and with or without 7S RNA (100 nM) and then sequentially titrated with TRITC-labelled FtsY (25-400 nM). The reaction mixture was excited at 495 nm and the fluorescence emission spectra were taken from 505-625 nm at 60°C using a Hitachi f-700 spectrophotometer (Hitachi, Japan). The emission intensity of FITC at 520 nm was measured separately at different titration and was used to calculate the dissociation rate constant (K_d) from the following equation:

$$\frac{F_0 - F_t}{F_0} = B \times \frac{[FtsY]}{K_d + [FtsY]}$$

where F_t is the fluorescence intensity at 520 nm at different FtsY concentrations, and F_0 is the fluorescent intensity at [FtsY] = 0; K_d is the dissociation rate constant, B is the maximum intensity achieved at saturation of binding.

4.2.7 Preparation of archaeosome

The archaeal membrane was used to prepare archaeosome to test the interaction of SRP54-FtsY complex with membrane lipids. To make an archaeosome, *S. acidocaldarius* cells were grown aerobically in Brock medium at a pH of 3 and 76°C, and the membranes were isolated following the Bligh-Dyer method. Initially, the solvent for extraction was prepared by mixing chloroform with methanol (2:1). 3.75 ml of this extraction solvent was then added to 1 ml of cell suspension, followed by mixing in a vortex for 10 mins. Further, 1.25 ml of chloroform was added to it followed by mixing by vortex again for 1 min. Finally, 1.25 ml of water was added to the mixture and centrifuged at 1000 rpm for 10 mins. The organic layer was collected, and the chloroform was evaporated in a Turbovap LV concentration evaporator (Biotage, Sweden) under nitrogen gas pressure at 65°C. The membrane was then resuspended in 50 mM phosphate buffer (pH 8.0) preheated at 60°C. The resuspended membrane was then snap-frozen in liquid N_2 followed by thawing in a water bath at 60°C. Archaeosome was prepared from isolated membranes by sonicating the solution in a Soniprep 150 sonicator for 5 min (10 cycles x 30 sec). Stewart assay was used to quantify lipid concentration in the archaeosome preparation which was found to be 1.32 mg/ml.

4.2.8 Homology based modeling and docking

The three-dimensional structure of SRP54 was homology modeled using the RNA-bound structure of SRP54 from *Sulfolobus solfataricus* (1QZW) as the template. Swiss-Model webserver (Guex et al., 2009; Waterhouse et al., 2018; Studer et al., 2020) was used to perform the homology modeling. Molecular docking was performed with Autodock Vina (Trott & Olson, 2010) using the homology modeled structure of Saci_Srp54 as the protein template. The 3D structure of GTP was generated using Corina (Sadowski et al., 1994) and used for docking after energy minimization.

4.3 RESULTS

4.3.1 Purification and enzymatic characterization of archaeal FtsY

The wild-type SRP receptor of *S. acidocaldarius*, FtsY, and the G-domain mutants of SRP54 was purified following the same protocol as described earlier (3.3.1). On separation in SDS-PAGE, FtsY migrated at 48 kDa and the mutants migrated at 49.65 kDa, as same as the wild type SRP54 (Fig. 4.1).

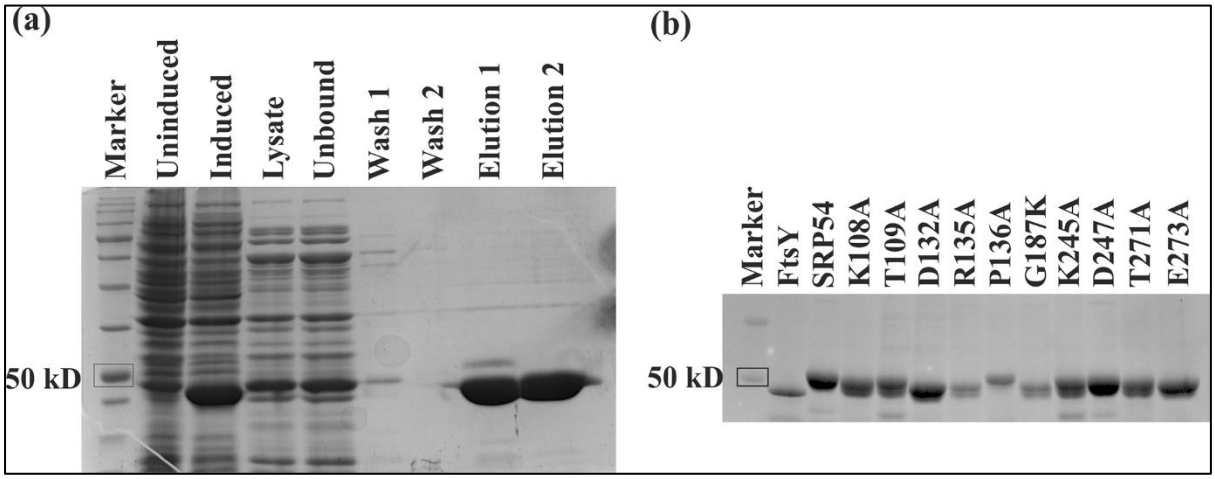

Figure 4.1. Purification of FtsY and mutant-SRP54 proteins. Proteins were purified using affinity chromatography and the column was washed with 10 mM imidazole (Wash 1) and 20 mM imidazole (Wash 2), and the proteins were eluted using 100-200 mM imidazole (Elution 1-2). FtsY migrated below 50 kDa marker (a); purified fractions of wild-type and mutant proteins were run separately (b). All mutant proteins were eluted at 100 mM imidazole fraction.

SRP receptors (SR/FtsY) belong to the SIMIBI class of GTP hydrolyzing enzymes containing the classical P-loop GTPase motifs (G1-G5), as same as found in SRP54 (Leipe et al., 2002). Additionally, the presence of an insertion box domain (IBD) within the SR-G domain probably represents the switch II region found in Ras-like GTPases (Freymann et al., 1997; Montoya et al., 1997). The IBD motif is supposed to stabilize the nucleotide-free protein as there is no known guanine nucleotide exchange factor present for SRP GTPases. The enzymatic ability of FtsY has been investigated in bacteria and found to have a weak basal hydrolyzing activity (Powers & Walter, 1995; Peluso et al., 2000). Although crenarchaeal FtsY structure has been analyzed to point out key residues possibly involved in its GTP hydrolyzing ability (Wild et al., 2016), no concrete biochemical characterization has

ever been attempted. In the present study, recombinant FtsY, purified from *S. acidocaldarius* (*Saci*FtsY) was first analyzed for its GTP hydrolyzing ability in a concentration-dependent manner. Since the two SRP-GTPases undergo reciprocal activation of their enzymatic ability (Powers & Walter, 1995; Gupta et al., 2021), the effect of SRP54-FtsY association on GTP hydrolysis was also tested. Finally, the addition of 7S RNA was found to exert a positive effect on this combinatorial activity (Fig. 4.2a). FtsY alone showed a very weak basal GTPase activity even in comparison with SRP54. Activity at the lowest concentration of SRP54 did not differ much, whether tested alone or in combination with FtsY and/or 7S RNA. Whereas the highest concentration of the protein showed an almost two-fold increase in the activity of SRP54-RNA-FtsY complex than that of SRP54 alone. The presence of the SRP RNA surely increased the overall GTPase activity to a significant extent in all conditions.

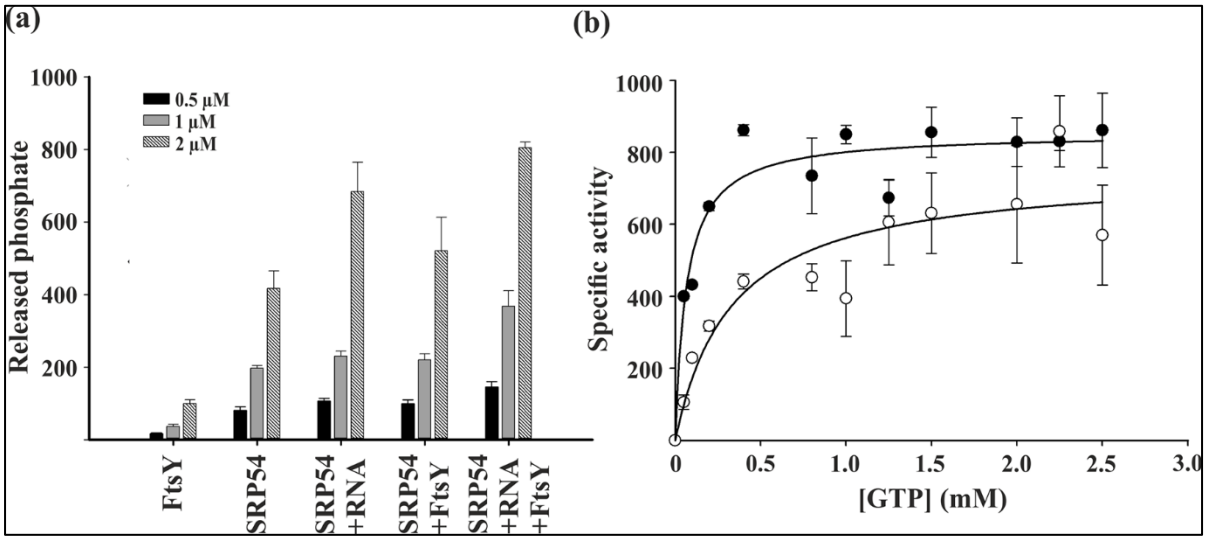

Figure 4.2. Comparative GTP hydrolysis by SRP and SR GTPase. (a) Proteins were used in three consecutive concentrations, 0.5, 1, and 2 µM, and 7S RNA was administered at 250 nM concentration. The combinatorial activity of SRP54-RNA-FTsY at the highest concentration gave the maximum hydrolytic output. (b) The increasing concentration of GTP was plotted against specific activities of FtsY (open circle) and SRP54-FtsY (closed circle). All reactions were incubated for 15 minutes at 70 °C and then measured by Malachite-Molybdate reagent.

To investigate the effect of SRP54 upon the nucleotide-binding affinity of FtsY, the specific activity of the protein was measured alone or in combination with SRP54, in presence of an increasing concentration of GTP (0.5-2.5 mM). The resultant graph

was fit using the standard Michaelis-Menten equation for enzyme kinetics (Fig. 4.2b) and the respective V_{max} and K_m were calculated accordingly (Table 4.2). The weaker basal GTPase activity of FtsY could be attributed to a much lower affinity toward GTP, explained from the higher value of K_m as compared to SRP54 (table 3.1). the complex of FtsY-SRP54, on the other hand, showed the highest affinity toward the nucleotide substrate. Such findings directly hint at the reciprocal activation of GTP hydrolysis, evident from the structural and biochemical studies in bacteria (Gupta et al, 2016).

Table 4.2 Kinetic features of GTP hydrolysis by FtsY

Sample	V_{max}	K_m
FtsY	750 ± 82.3 nmoles min^{-1} $\mu mole^{-1}$	333 ± 144 μM
FtsY-SRP54	853 ± 28.6 nmoles min^{-1} $\mu mole^{-1}$	66 ± 15 μM

4.3.2 Role of RNA and guanine nucleotide in SRP54-FtsY association

The SRP and SR GTPases associate together through a nucleotide-independent early intermediate and the GTP-bound stable complex. After successful cargo transfer, they dissociate following a concomitant GTP hydrolysis (Lichi et al., 2004; Shen & Shan 2009). The bacterial 4.5S RNA was shown to facilitate the early GTP-independent intermediate formed by Ffh and FtsY, where the association of the two proteins was found to accelerate by 400 folds (Peluso et al., 2001). In archaea, the effect of 7S RNA on the complexation between SRP54 and FtsY remains unknown. The present study demonstrated that the archaeal 7S RNA facilitates the formation of the core of the targeting complex (TC) (Table 4.3). The fluorescence resonance energy transfer between differentially labeled SRP54 and FtsY was measured for each of the conditions listed in Table 4.3. In the absence of any of the listed effectors, the association between the two GTPases was the weakest (K_d = 146.8 ± 37.2 nM) (Fig. 4.3a). The addition of both non-hydrolyzable GTP analog (GppNHp) and 7S RNA accelerated the association by almost four folds (K_d = 40.5 ± 10.8 nM) (Fig. 4.3c). Such an observation further supports the idea that the SRP RNA facilitates the

complex formation between the two GTPases. On the other hand, GppNHp alone reduced the dissociation constant by two folds, up to 84.4 ± 15.6 nM (Fig. 4.3b).

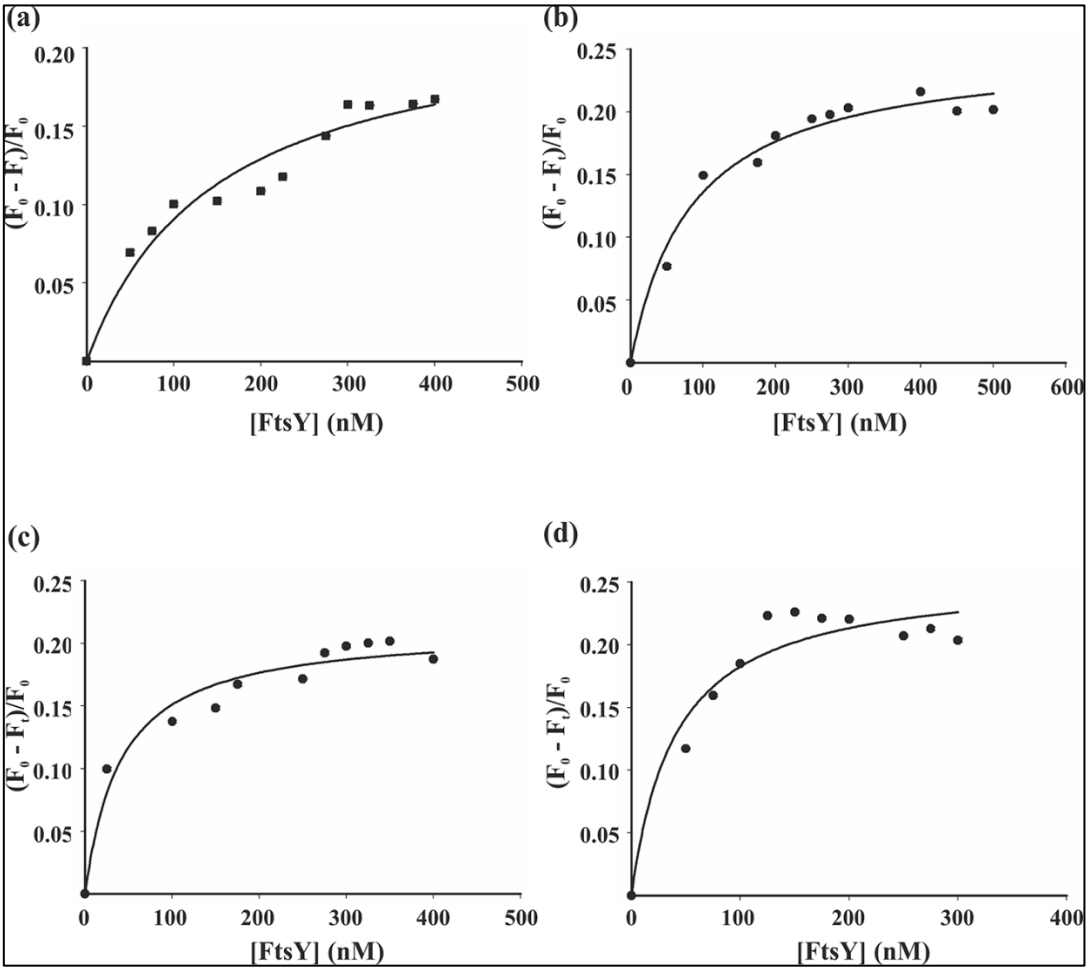

Figure 4.3. SRP54-FtsY complex formation is affected by the 7S RNA and nucleotide. FRET between FITC-tagged SRP54 (100 nM) and TRITC-tagged FtsY (50-400 nM) in absence of any RNA and nucleotide (a), in presence of 100 μM GppNHp alone (b), in presence of both 100 μM GppNHp and 0.5 μM 7S RNA (c) and presence of 100 μM GppNHp, 1 μM 7S RNA and archaeosome fraction (d). The reaction was carried out at λ_{Ex} = 495 nm and data were recorded at λ_{Em} = 520 nm.

Table 4.3. The measure of the SRPP54-FtsY association under different conditions

GMPPNP	RNA	Archaeosome	K_d
-	-	-	146.8 ± 37.2 nM
+	-	-	84.4 ± 15.6 nM
+	+	-	40.5 ± 10.8 nM
+	+	+	40.5 ± 13.7 nM

Unlike GTP, GppNHp allows capturing the stable targeting complex that would not dissociate following the nucleotide's hydrolysis. Since FtsY is membrane-associated, a proper biochemical investigation was needed to know whether archaeal membrane lipid can influence the association process. In bacteria, the positive charges at the N-terminal A domain of the FtsY facilitate the binding of FtsY to the anionic phospholipid of the plasma membrane (Moll R.G., 2003). Archaeal liposome (archaeosome) was prepared from *S. acidocaldarius* by the Bligh-Dyer method (Roy et al., 2018) and incubated the reaction mixture with the liposomal fraction before the fluorescence titration experiment. However, it did not confer any additional advantage to the complex formation event since the K_d (~ 40.5 ± 13.7 nM) remained the same for the association without the archaeosome (Fig. 4.3d). To this end, our results from the FRET analyses suggested that membrane lipids do not affect the association of SRP54 and FtsY in *S. acidocaldarius*. However, the affinity of the targeting complex toward membrane lipids is yet to be investigated.

4.3.3 Effect of RNA on the basal GTP hydrolysis following SRP-FtsY complexation

Multiple studies have established SRP RNA's role in the GTPase cycle of the SRP system in bacteria where the 4.5S RNA in *E. coli* was shown to enhance the combined GTPase activity of Ffh and FtsY (Peluso et al., 2001; Zhang et al., 2008). The RNA tetraloop facilitates the initial binding between the two GTPases and re-localizes the complex to its distal end, crucial for efficient GTPase activation and cargo transfer (Shen et al., 2013). In the present study, we evaluated the kinetic parameters of the GTP hydrolyzing activity of *S. acidocaldarius* SRP54 in the presence and absence of 7S RNA. The basal GTP hydrolyses by SRP54 and FtsY were measured, individually or in combination, for a temporal range of 0-30 minutes and in a concentration range of 1-10 μM. The observed rate constant, k_{obsd}, for each concentration was plotted and used to calculate kinetic values, thereby providing an insight into the trimolecular interaction between 7S RNA, SRP54, and FtsY (Table 4.4, Fig. 4.4).

While the presence of 7S RNA slightly influenced the basal GTPase rate (k_{cat}) of SRP54, the overall catalytic efficiency (k_{cat}/K_m) of the protein remained unchanged both in the absence and presence of RNA ($0.47 \pm 0.04 \times 10^6$ M^{-1} min^{-1} and 0.43 ± 0.03

× 10^6 M^{-1} min^{-1}, respectively) (Table 4.4, Fig. 4.4a). The affinity of SRP54 for the nucleotide (0.73 ± 0.12 μM), as reflected by K_m, was not affected by the presence of SRP RNA (0.97 ± 0.2 μM), although it was significantly higher than that of FtsY (6.73 ± 0.12 μM) (Table 4.4, Fig. 4.4). Based on similar studies with bacterial SRP (Peluso et al., 2001; Akopian et al., 2013), the slower basal reaction rate and weaker affinity for GTP in both the proteins suggested that the nucleotide hydrolysis, not the binding, is rate-limiting for the entire reaction. Therefore, the maximal rate constant, k_{cat}, equals the GTP hydrolysis rate from the protein-GTP complex, and K_m represents the GTP dissociation constant of the protein. Thus, k_{cat}/K_m equals the association rate constant between SRP54 and FtsY, where the complex formation precedes GTP hydrolysis.

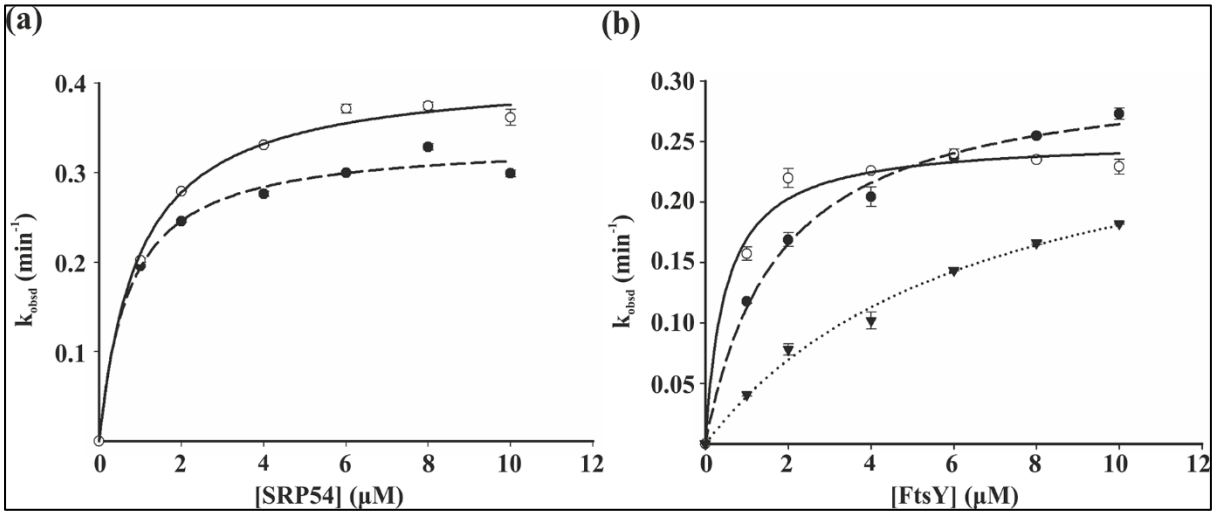

Figure 4.4. Basal GTPase reactions of SRP54 and FtsY were affected by 7S RNA. The reactions were carried out in a series of 0-30 minutes, in the presence of 100 μM GTP. The amount of released phosphate was measured using Malachite-Molybdate reagent and plotted against the time of incubation to generate k_{obsd}. (a) Basal GTP hydrolysis of SRP54 in the presence (-○-) and absence (--●--) of 7S RNA. (b) Basal GTPase activity of FtsY alone (⋯▼⋯) and in combination with SRP54, either in the presence (-○-) or absence (--●--) of 7S RNA.

FtsY showed the slightest affinity for the nucleotide when tested individually (Fig. 4.4b). However, when the concentration dependence of the activity upon complex formation was assessed by measuring the observed rate constants for increasing concentrations (1-10 μM) of FtsY against a fixed concentration (2 μM) of SRP54, the affinity of the association complex for GTP was increased by six-fold (Table 4.4). The

affinity was further increased in the presence of RNA, confirming a possible role of the 7S RNA in the SRP54-FtsY complex formation (Table 4.4, Fig. 4.4b). This was further supported by the association rate constants of the two GTPases, where an increase by three folds from 0.18 × 10^6 M^{-1} min^{-1} to 0.54 × 10^6 M^{-1} min^{-1} was recorded in the presence of the 7S RNA. A previous study in *E. coli* demonstrated that 4.5S RNA directly enhances the rate of GTP hydrolysis by the GTP•Ffh-FtsY•GTP complex (from 0.12 s^{-1} to 0.72 s^{-1}, in the presence of the SRP RNA) (Peluso et al., 2001). Furthermore, the 4.5S RNA facilitates complexation between GTP•Ffh and FtsY•GTP. On the contrary, we observed that archaeal 7S RNA doesn't influence the combined GTP hydrolysis rate by the targeting complex but facilitates the formation of the targeting complex comprising SRP54 and FtsY.

Table 4.4. Summary of catalytic rate constants in dual GTPase cycle

Protein	**7S RNA**	**k_{cat} (min^{-1})**	**K_m (μM)**	**k_{cat}/K_m (10^6 M^{-1} min^{-1})**
SRP54	-	0.34 ± 0.01	0.73 ± 0.12	0.47 ± 0.04
SRP54	+	0.413 ± 0.02	0.97 ± 0.2	0.43 ± 0.03
FtsY	-	0.3 ± 0.02	6.73 ± 0.12	0.045 ± 0.001
SRP54-FtsY	-	0.31 ± 0.01	1.76 ± 0.2	0.18 ± 0.01
SRP54-FtsY	+	0.25 ± 0.01	0.48 ± 0.12	0.54 ± 0.07
SRP54-SRP19	+	0.32 ± 0.01	0.45 ± 0.16	0.77 ± 0.15
SRP54-SRP19	+7S.S	1.25 ± 0.05	0.42 ± 0.12	3.13 ± 0.46
SRP54-SRP19-FtsY	+	0.49 ± 0.02	0.37 ± 0.12	1.42 ± 0.25
SRP54-SRP19-FtsY	+7S.S	0.28 ± 0.002	0.27 ± 0.02	1.04 ± 0.04
$SRP54^{K108A}$-FtsY	+	0.3 ± 0.04	5.12 ± 1.5	0.06 ± 0.006
$SRP54^{G187K}$-FtsY	+	0.05 ± 0.002	2.7 ± 0.23	0.02 ± 0.001

4.3.4 Role of SRP19 and 7S RNA in the concomitant GTP hydrolysis by GTP•SRP54-FtsY•GTP complex

Unlike bacteria, the archaeal SRP complex contains an SRP19 homolog along with SRP54 and 7S RNA. Archaeal SRP19 is reminiscent of its eukaryotic counterpart. It binds the 7S RNA at the helices 6 and 8 in the S domain (Diener et al., 2000; Wild et al., 2010). Interestingly, SRP19 was reported to be a dispensable SRP component in halophilic euryarchaeon *H. volcanii* (Yurist et al., 2007). We, therefore, sought to investigate the importance of SRP19 of thermoacidophilic crenarchaeon *S. acidocaldarius* on concomitant GTP hydrolysis by GTP•SRP54-FtsY•GTP complex in the presence of full-length and S domain of SRP RNA. The S domain of archaeal 7S RNA (7S.S RNA), the smallest functional unit, comprises helices 6 and 8 and part of helix 5 and ensures correct binding of all the proteins. Various concentrations of SRP54 were incubated with small, fixed concentrations of 7S or 7S.S RNA and SRP19 before the addition of GTP. Subsequent hydrolysis rate constants were plotted against the protein concentrations to obtain the maximal rate constants 0.32 ± 0.01 min^{-1} and 1.25 ± 0.05 min^{-1}, in the presence of 7S RNA and 7S.S RNA, respectively (Fig. 4.5a). The result indicated that the S domain could increase the basal GTPase rate of SRP54 by four-fold, but its affinity for the nucleotide remained unchanged (0.45 ± 0.16 μM and 0.42 ± 0.12 μM) (Table 4.4).

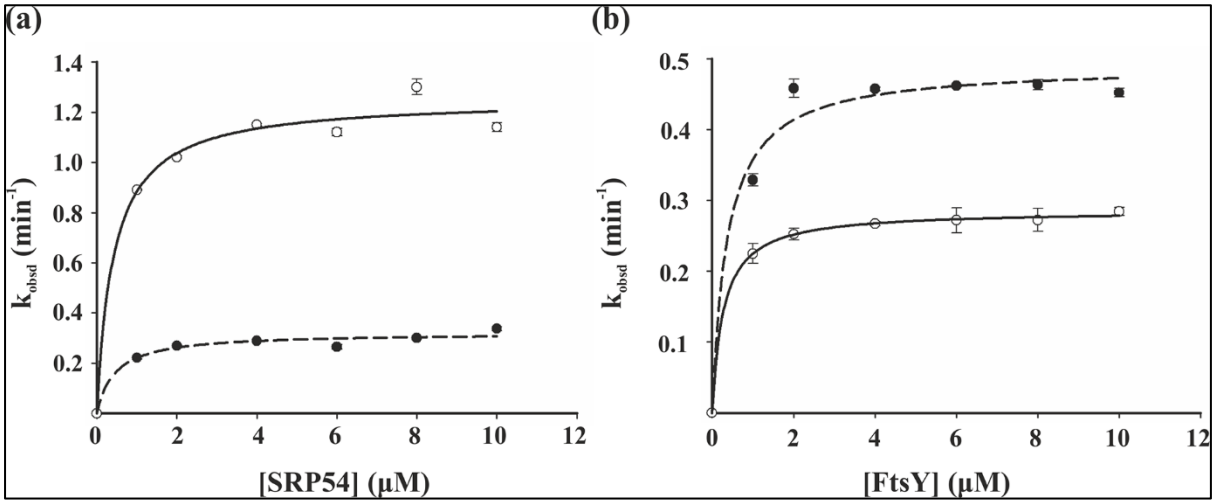

Figure 4.5. Basal GTPase reactions of SRP54 and FtsY were affected by SRP19. (a) Basal GTPase activity of SRP19-SRP54 complex in presence of 7S.S RNA (-○-) and 7S RNA (--●--). (b) Basal GTP hydrolysis of SRP9-SRP54-FtsY complex in presence of 7S.S RNA (-○-) and 7S RNA (--●--).

In the following experiment, the role of SRP19 and SRP RNA in the concomitant GTP hydrolysis by the GTP•SRP54-FtsY•GTP complex was estimated. Surprisingly, a higher k_{cat} value was obtained upon the addition of full-length SRP RNA/SRP19 (0.49 ± 0.02 min^{-1}) than in the presence of 7S.S RNA/SRP19 (0.28 ± 0.002 min^{-1}) (Table 4.5). However, the equilibrium affinity was not affected to a significant extent (0.37 ± 0.12 μM and 0.27 ± 0.02 μM) (Fig. 4.5b). Such an observation strongly suggests that in the presence of SRP19 and 7S RNA, conformational rearrangement stabilizes the complex formation between the two GTPases. Together, we believe that the full-length SRP RNA and SRP19 facilitate concomitant GTP hydrolysis by stabilizing the TC complex.

4.3.5 SRP54-G domain is essential for GTPase function

The G domain of the SRP GTPase comprises classical G elements and specific sequence motifs. The five distinct G elements contain all the residues necessary for the GTP binding and hydrolyzing function. These residues, along with the SRP GTPase specific "ALLEADV," "DARGG," "RILGMGD," and I-box motifs, are highly conserved across all three domains of life (Gupta et al., 2016; Wild et al., 2016). We have generated a homology-based model of the *Saci*SRP54 bound to GTP, taking the cue from the published *Ssol*SRP54 crystal structures (PDB 5L3S and 5L3V) (Wild et al., 2016). The aligned amino acid sequences of SRP54 from *S. solfataricus* and *S. acidocaldarius* revealed maximum homology, where the (n)-th residue of the former is corresponded by the (n-1)-th residue from the latter. Based on these structural and sequence-based details, we identified residues potentially involved in the nucleotide interaction and possible targets for generating a battery of mutants (Table 4.5). The residues were selected in a manner so that the mutations would cover all the classical and SRP-specific motifs present in the G domain of SRP54 (Fig. 4.6). These mutations include K108A and T109A in G1, D132A, and R135A in G2, P136A as part of the IBD, G187K within G3, K245A and D247A within G4 and T271A and E273A within G5 element (Table 4.5). All these mutants were expressed and purified from *E. coli* (Fig. 4.1b).

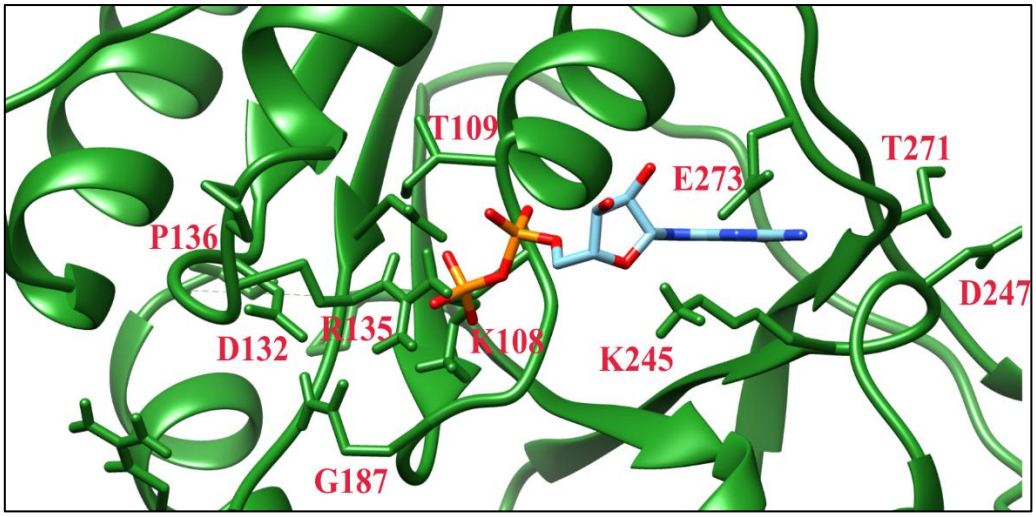

Figure 4.6. Homology-based model of SRP54•GTP complex in *S. acidocaldarius*, generated using Chimera 2.0 and Autodock Vina. Important amino acid residues from all the classical G-domain motifs were selected for mutational analysis, as marked throughout the structure.

Table 4.5. Summary of mutations in the SRP54-G domain

G domain motifs	Conserved sequence	SRP54 mutations	Probable function
G1	GVQGSGKT	K108A	Mg^{2+} ion coordination
		T109A	Mg^{2+} ion coordination
G2	DIYR	D132A	Mg^{2+} ion coordination
		R135A	Binding γ-phosphate of GTP
IBD	DIYRP	P136A	Loop stabilization
G3	DTAGR	G187K	GTP dependent hinge formation
G4	SKMD	K245A	GTP binding pocket
		D247A	Specificity for guanine nucleotide
G5	GTGE	T271A	GTP binding pocket
		E273A	GTP binding pocket

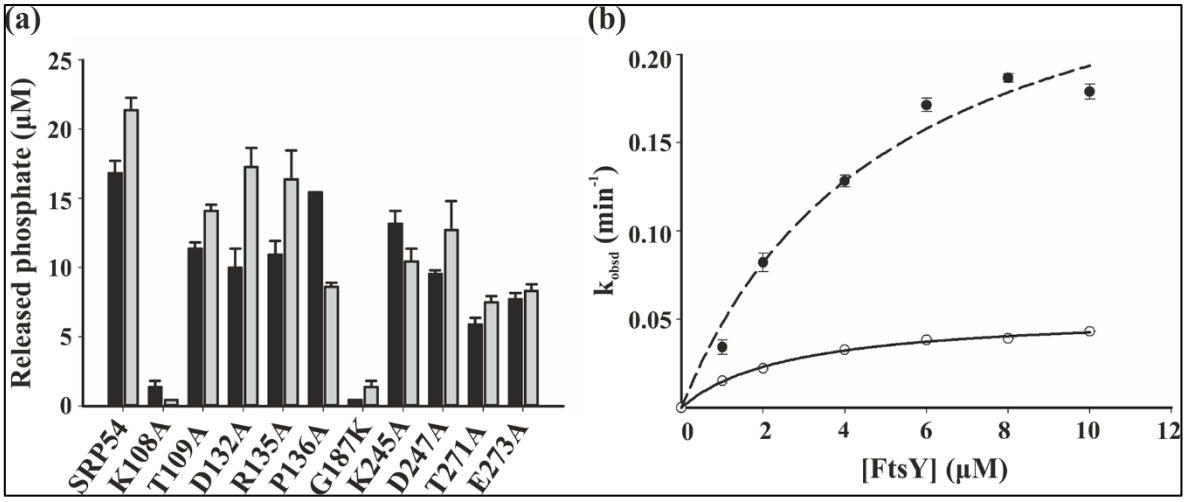

Figure 4.7. Kinetic analysis of G-domain mutants of SRP54. (a) The measure of GTP hydrolysis by wild-type SRP54 and mutants in the presence (grey) and absence (black) of 7S RNA. Each reaction contained 1 µM of protein and was incubated for 15 minutes at 70 °C. (b) Basal GTPase activity of the SRP54^{K108A}-FtsY (--●--) and SRP54^{G187K}-FtsY (-○-) complexes.

The purified wild-type SRP54 of *S. acidocaldarius* showed a basal GTPase activity (Fig. 4.4a), which was mildly augmented by 7S RNA (Fig. 4.4a and 4.5b). All the G-element mutants of SRP54 showed reduced activity compared to the wild type (Fig. 4.7a) and two G-element mutants, SRP54^{K108A} and SRP54^{G187K}, were completely inactive (Fig. 4.6b). These results identified several residues essential for the GTPase activity of *Saci*SRP54, of which K108 and G187 seemed to be the most crucial. Subsequently, we were interested in finding out if GTP hydrolysis by both participating SRP GTPases is necessary for an effective targeting complex (TC). GTP hydrolysis rates of SRP54^{K108A} and SRP54^{G187K} were measured in the presence of increasing concentrations of FtsY which gave estimated k_{cat} values of 0.3 ± 0.04 min^{-1} and 0.05 ± 0.002 min^{-1}, respectively (Table 4.4, Fig. 4.7b). Interestingly, introducing a mutation at G187 residue resulted in a considerable reduction of enzymatic activity rate compared with the wild-type targeting complex (0.25 ± 0.01 min^{-1}). Such an observation further confirms the importance of this residue in forming the nucleotide-dependent hinge to facilitate effective GTP hydrolysis (Wild et al., 2016). The corresponding high K_m values (5.12 ± 1.5 µM and 2.7 ± 0.23 µM) indicate weaker affinities towards GTP for both the mutants (Table 4.4). The K108A mutation did not affect the basal GTPase rate, but the affinity towards GTP was nevertheless weakened. Together, our results confirmed a considerable reduction in GTP affinity

for mutants K108A and G187K of *Saci*SRP54. We further believe that these residues are essential for the necessary nucleotide-dependent conformational rearrangements required in the formation of TC.

4.4 DISCUSSION

In co-translational protein targeting, an interaction between the signal-recognition particle (SRP) and its receptor (SR) plays an essential role by forming the targeting complex (TC) (Grudnik et al., 2009). SRP and SR interact through their core GTPase domains and four-helix bundles at the N-terminus (Grudnik et al., 2009). In bacteria, SRP RNA has been shown to stimulate complexation between bacterial Ffh and FtsY to form the targeting complex (TC) (Akopian et al., 2013). However, a thorough biochemical investigation on the role of SRP RNA in the formation of a core of the targeting complex (TC) between SRP54 and FtsY/SR remains elusive in the other two domains of life. The present work sought to characterize these structural elements biochemically and bridge the gap in understanding the role of SRP RNA and SRP19 in protein translocation in archaea.

SRP RNA has been extensively shown to enhance the association between Ffh and FtsY in *E. coli* which leads to an overall increment in the GTPase rate of the targeting complex (Zhang et al., 2008). The 4.5S RNA speeds both the association and disassociation of the Ffh-FtsY complex by around 200 folds (Walter et al., 2000). The initial assembly of the two GTPases is facilitated by the RNA tetraloop and the targeting complex successfully relocalizes to the distal end of the SRP RNA (Shen et al., 2013). This conformational reorientation is crucial for enzymatic activation and cargo transfer. Mutations in the conserved IBD region of Ffh and FtsY completely blocked the process of translocation (Shan et al., 2007), which was indicative of the importance of the G-domain in cargo unload. In the present study, 7S RNA from *Sulfolobus acidocaldarius* was found to facilitate the formation of the SRP54-FtsY targeting complex and accelerate their reciprocal GTPase activity. The addition of SRP RNA and GTP lowered the K_d of the associating complex from 146.8 ± 37.2 nM to 40.5 ± 10.8 nM (Table 4.3). A previous study with *Acidianus ambivalens* SRP54 and

FtsY showed that the two proteins have an intrinsic affinity towards the tetraether lipids (Moll R.G., 2003; Lichi et al., 2004). This coordinated affinity was proposed to be responsible for pulling the targeting complex to the archaeal plasma membrane. Interestingly, both the bacterial and archaeal FtsY share structural similarities with the eukaryotic SRα subunit, but the integral membrane binding SRβ is not present in any of them. Such absence of membrane-spanning domain in archaeal FtsY corroborates well with its intrinsic affinity towards tetraether lipids. The FRET analyses investigating the targeting complex association found no effect of the archaeosome extracted from *S. acidocaldarius* (Table 4.3, Fig. 4.3d). Subsequently, the catalytic rate and the affinity to nucleotide for FtsY was found to be enhanced greatly in presence of SRP54, by Michaelis constant (Table 4.2, Fig. 4.2b) and catalytic rate constant (Table 4.4, Fig. 4.4b) respectively, which corroborated with the reciprocal nature of activation of SRP-GTPases.

In the previous chapter, computational evidence pointed to a substantial role of SRP19 in the SRP54-7S RNA association, which has been investigated biochemically in detail in this section. In *M. jannaschii*, the presence of SRP19 was shown to strengthen the SRP54-SRP RNA binding (Hainzl et al., 2005) and various crystallographic studies in archaeal SRP system have predicted the possible role of SRP19 in reorienting the asymmetric loop in helix 8 of 7S RNA so that the binding of SRP54-M domain is favored (Hainzl et al., 2002; Rosendal et al., 2003; Wild et al., 2010). *Saci*SRP19 showed a profound effect on the catalytic efficiency of SRP54-GTPase as well as SRP54-FtsY dual GTPase (Table 4.4, Fig. 4.5). Interestingly, the addition of 7S.S RNA augmented the catalytic efficiency but decreased the mutual affinity between the components of the targeting complex. This implies that the full-length 7S RNA may induce conformational reorientation in SRP54 that facilitates its association with FtsY.

The crystal structure of the targeting complex of *Sulfolobus solfataricus* provided a clear understanding of the conformational arrangement of the two archaeal GTPases in their GTP-bound heterodimeric form (de Leeuw et al., 2000). On a general note, the composite active site in a TC, shaped by the two half-sites consisting of

corresponding G elements, holds two GTP molecules arranged in a 'head-to-tail manner (Wild et al., 2016). The G1 element (GxXGxGKT, where x is any amino acid and X is any of a few conserved amino acids) is the classical Walker-A motif (Leipe et al., 2002) that forms an anion hole for the β-phosphate, the G2 element (DTΦR, where Φ is any aromatic amino acid) assists in magnesium ion coordination and also marks the start of the IBD, the G3 (DTAGR) completes the IBD along with forming a GTP-dependent hinge, the G4 (TKxD) establishes the specificity for guanine nucleotides and the final element, G5 (GxGE), creates the GTP binding pocket. We, therefore, sought to investigate key residues with each of these domains that contribute to the G-domain functionality. The site-directed mutagenesis approach generated a battery of mutant SRP54, of which many were non-functional in terms of catalytic activity. In *S. solfataricus*, amino acid residue G188 has been shown to form a hinge for efficient nucleotide-binding (Wild et al., 2016). Mutation in the corresponding amino acid residue G187 (G187K) in *Saci*SRP54 resulted in the complete inactivation of the GTPase. Such an observation further suggests its critical role in forming the hinge region and, thereby, in the nucleotide-dependent conformational rearrangement. As evident from the homology-based model, residues K108, T109, and D132 in the G1 and G2 motifs of the *Saci*SRP54 probably coordinate with the cofactor Mg^{2+} of SRP54 (Fig. 3a). Among these residues, a mutation in K108 (K108A) resulted in a complete loss of activity. Since the G1 element comprises the classical Walker A motif (Leipe et al., 2002), we propose that a change in this highly conserved GTPase motif is critical for its GTP hydrolyzing activity. Together, these results provide an insight into factors governing the formation of an active archaeal TC.

4.5 CONCLUSION

In the present study, mechanistic analyses of the effects of 7S RNA on the GTPase cycle and the association of the SRP-SR complex have elucidated the role of SRP RNA in the SRP-mediated targeting process. The kinetic measurements of the rate-limiting hydrolysis step in a multi-turnover reaction have provided valuable

information to establish SRP RNA as a critical regulatory factor in the association between SRP54•GTP and FtsY•GTP. The mutations introduced in the SRP54-G domain help us to find out residues crucial for successful hydrolytic function. The crystal structure of the SRP54-FtsY and SRP54-7S RNA complex in archaea provided a basic framework of the checkpoints of their interaction. This study also provides the first biochemical insight into the role of SRP19 and SRP RNA in stable TC formation and concomitant GTP hydrolysis in the archaeal SRP system which can be culminated into a simple diagrammatic model as below -

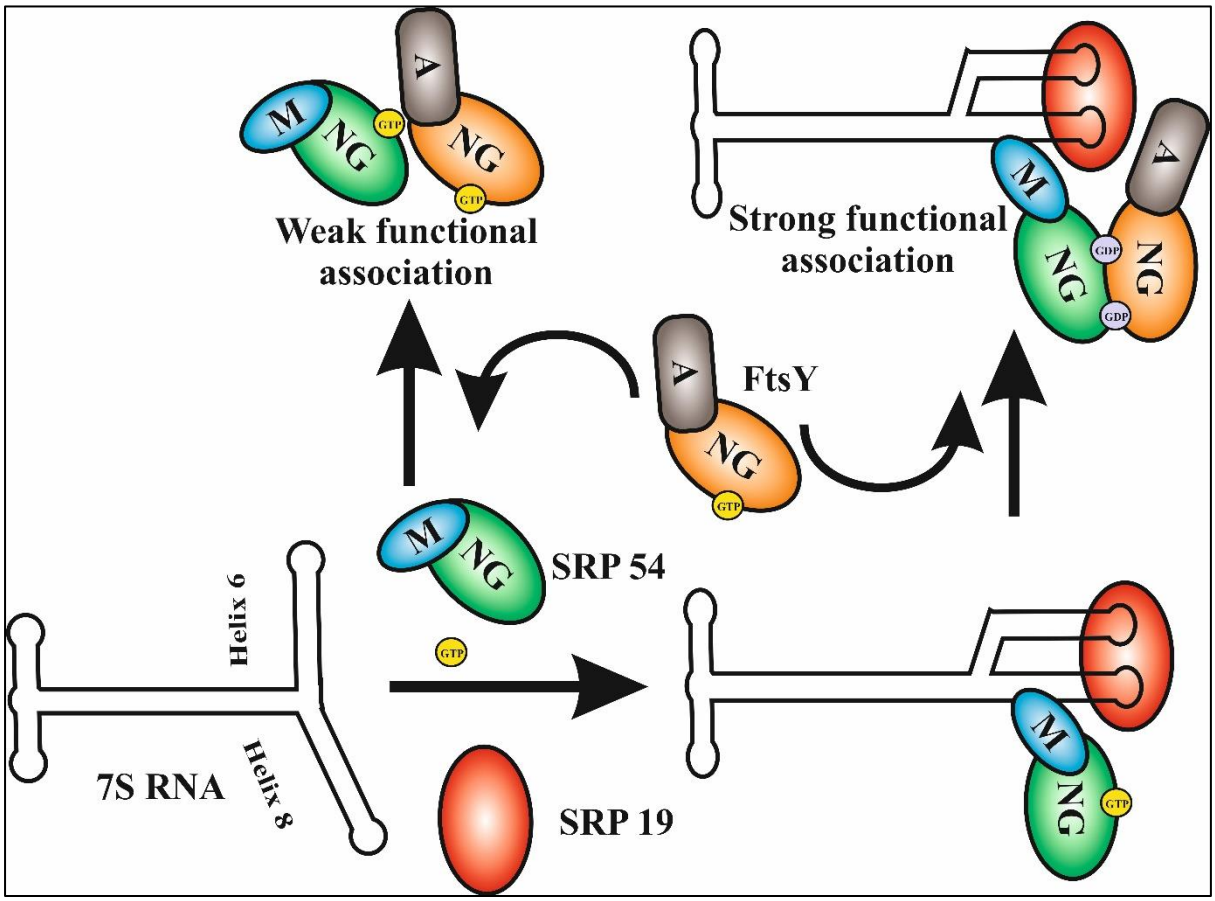

Figure 4.8. Schematic representation of active TC formation catalyzed by SRP RNA in crenarchaea.

4.6 BIBLIOGRAPHY

Akopian, D., Dalal, K., Shen, K., Duong, F., & Shan, S. O. (2013). SecYEG activates GTPases to drive the completion of cotranslational protein targeting. *Journal of Cell Biology*, *200*(4), 397–405.

Akopian, D., Shen, K., Zhang, X., & Shan, S. (2013). Signal recognition particle: an essential protein-targeting machine. In *Annual review of biochemistry* (Vol. 82).

Batey, R. T., Rambo, R. P., Lucast, L., Rha, B., & Doudna, J. A. (2000). Crystal structure of the ribonucleoprotein core of the signal recognition particle. *Science*, *287*(5456), 1232–1239.

Bourne, H. R., Sanders, D. A., & McCormick, F. (1991). The GTPase superfamily: conserved structure and molecular mechanism. *Nature*, *349*(6305), 117–127.

Buskiewicz, I., Kubarenko, A., Peske, F., Rodnina, M. V., & Wintermeyer, W. (2005). Domain rearrangement of SRP protein Ffh upon binding 4.5S RNA and the SRP receptor FtsY. *Rna*, *11*(6), 947–957.

Buskiewicz, I., Peske, F., Wieden, H. J., Gryczynski, I., Rodnina, M. V., & Wintermeyer, W. (2005). Conformations of the signal recognition particle protein Ffh from Escherichia coli as determined by FRET. *Journal of Molecular Biology*, *351*(2), 417–430.

De Leeuw, Erik, Poland, D., Mol, O., Sinning, I., Ten Hagen-Jongman, C. M., Oudega, B., & Luirink, J. (1997). Membrane association of FtsY, the E. coli SRP receptor. *FEBS Letters*, *416*(3), 225–229.

Diener, J. L., & Wilson, C. (2000). Role of SRP19 in assembly of the Archaeoglobus fulgidus signal recognition particle. *Biochemistry*, *39*, 12862–12874.

Egea, P. F., Tsuruta, H., de Leon, G. P., Napetschnig, J., Walter, P., & Stroud, R. M. (2008). Structures of the signal recognition particle receptor from the archaeon Pyrococcus furiosus: implications for the targeting step at the membrane. *PloS One*, *3*, e3619.

Freymann, D. M., Keenan, R. J., Stroud, R. M., & Walter, P. (1997). Structure of the conserved GTPase domain of the signal recognition particle. *Nature*, *385*(6614), 361–364.

Ghosh, A., Hartung, S., Van Der Does, C., Tainer, J. A., & Albers, S. V. (2011). Archaeal flagellar ATPase motor shows ATP-dependent hexameric assembly and activity stimulation by specific lipid binding. *Biochemical Journal*, *437*(1), 43–52.

Grudnik, P., Bange, G., & Sinning, I. (2009). Protein targeting by the signal recognition particle. *Biological Chemistry*, *390*(8), 775–782.

Guex, N., Peitsch, M.C., Schwede, T. (2009). Automated comparative protein structure modeling with SWISS-MODEL and Swiss-PdbViewer: A historical perspective. *Electrophoresis, 30*, S162-S173.

Gupta, S, Roy, M., & Ghosh, A. (2017). The Archaeal Signal Recognition Particle: Present Understanding and Future Perspective. *Current Microbiology*, *74*(2), 284–297.

Gupta, Sayandeep, Roy, M., Dey, D., Bhakta, K., Bhowmick, A., Chattopadhyay, D., & Ghosh, A. (2021). Archaeal SRP RNA and SRP19 facilitate the assembly of SRP54-FtsY targeting complex. *Biochemical and Biophysical Research Communications*, *566*, 53–58.

Hainzl, T., Huang, S., & Sauer-Eriksson, A. E. (2002). Structure of the SRP19 RNA complex and implications for signal recognition particle assembly. *Nature*, *417*, 767–771.

Hainzl, T., Huang, S., & Sauer-Eriksson, A. E. (2005). Structural insights into SRP RNA: An induced fit mechanism for SRP assembly. *Rna*, *11*(7), 1043–1050.

Hainzl, T., Huang, S., & Sauer-Eriksson, A. E. (2007). Interaction of signal-recognition particle 54 GTPase domain and signal-recognition particle RNA in the free signal-recognition particle. *Proceedings of the National Academy of Sciences of the United States of America*, *104*(38), 14911–14916.

Jagath, J. R., Rodnina, M. V, & Wintermeyer, W. (2000). Conformational changes in the bacterial SRP receptor FtsY upon binding of guanine nucleotides and SRP. *Journal of Molecular Biology*, *295*, 745–753.

Janda, C. Y., Li, J., Oubridge, C., Hernández, H., Robinson, C. V., & Nagai, K. (2010). Recognition of a signal peptide by the signal recognition particle. *Nature*, *465*(7297), 507–510.

Keenan, R. J., Freymann, D. M., Stroud, R. M., & Walter, P. (2001). The signal recognition particle. *Annual Review of Biochemistry*, *70*, 755–775.

Keenan, Robert J., Freymann, D. M., Walter, P., & Stroud, R. M. (1998). Crystal structure of the signal sequence binding subunit of the signal recognition particle. *Cell*, *94*(2), 181–191.

Leipe, D. D., Wolf, Y. I., Koonin, E. V., & Aravind, L. (2002). Classification and evolution of P-loop GTPases and related ATPases. *Journal of Molecular Biology*, *317*(1), 41–72.

Lichi, T., Ring, G., & Eichler, J. (2004). Membrane binding of SRP pathway components in the halophilic archaea Haloferax volcanii. *European Journal of Biochemistry / FEBS*, *271*, 1382–1390.

Moll, R. G. (2003). Protein-protein, protein-RNA and protein-lipid interactions of signal-recognition particle components in the hyperthermoacidophilic archaeon Acidianus ambivalens. *Biochem. J*, *374*, 247–254.

Montoya, G., Svensson, C., Luirink, J., & Sinning, I. (1997). Crystal structure of the NG domain from the signal-recognition particle receptor FtsY. *Nature*, *385*(6614), 365–368.

Pakhomova, O. N., Deep, S., Huang, Q., Zwieb, C., & Hinck, A. P. (2002). Solution structure of protein SRP19 of Archaeoglobus fulgidus signal recognition particle. *Journal of Molecular Biology*, *317*(1), 145–158.

Peluso, P., Shan, S. O., Nock, S., Herschlag, D., & Walter, P. (2001). Role of SRP RNA in the GTPase cycles of Ffh and FtsY. *Biochemistry*, *40*(50), 15224–15233.

Peluso, Paul, Herschlag, D., Nock, S., Freymann, D. M., Johnson, A. E., & Walter, P. (2000). Role of 4.5S RNA in assembly of the bacterial signal recognition particle with its receptor. *Science*, *288*(5471), 1640–1643.

Powers, T., & Walter, P. (1995). Reciprocal stimulation of GTP hydrolysis by two directly interacting GTPases. *Science*, *269*(5229), 1422–1424.

Rose, R. W., & Pohlschröder, M. (2002). In vivo analysis of an essential archaeal signal recognition particle in its native host. *Journal of Bacteriology*, *184*(12), 3260–3267.

Rosendal, K. R., Wild, K., Montoya, G., & Sinning, I. (2003). Crystal structure of the complete core of archaeal signal recognition particle and implications for interdomain communication. *Proceedings of the National Academy of Sciences of the United States of America*, *100*(25), 14701–14706.

Roy, M., Gupta, S., Patranabis, S., & Ghosh, A. (2018). The oligomeric plasticity of Hsp20 of Sulfolobus acidocaldarius protects environment-induced protein aggregation and membrane destabilization. *Biochimica et Biophysica Acta - Biomembranes*, *1860*(12), 2549–2565.

Sadowski, J., Gasteiger, J., & Klebe, G. (1994). Comparison of Automatic Three-Dimensional Model Builders Using 639 X-ray Structures. *Journal of Chemical Information and Computer Sciences*, *34*(4), 1000–1008.

Shan, S., Chandrasekar, S., & Walter, P. (2007). Conformational changes in the GTPase modules of the signal reception particle and its receptor drive initiation of protein translocation. *Journal of Cell Biology*, *178*(4), 611–620.

Shen, K., & Shan, S. O. (2010). Transient tether between the SRP RNA and SRP receptor ensures efficient cargo delivery during cotranslational protein targeting. *Proceedings of the National Academy of Sciences of the United States of America*, *107*(17), 7698–7703.

Shen, K., Wang, Y., Hwang Fu, Y. H., Zhang, Q., Feigon, J., & Shan, S. O. (2013). Molecular Mechanism of GTPase Activation at the Signal Recognition Particle (SRP) RNA Distal End. *Journal of Biological Chemistry*, *288*(51), 36385–36397.

Stroud, R. M., & Walter, P. (1999). Signal sequence recognition and protein targeting. *Current Opinion in Structural Biology*, *9*(6), 754–759.

Studer, G., Rempfer, C., Waterhouse, A.M., Gumienny, G., Haas, J., Schwede, T. (2020). QMEANDisCo - distance constraints applied on model quality estimation. *Bioinformatics, 36*, 1765-1771.

Trott, O., & Olson, A. J. (2010). AutoDock Vina: improving the speed and accuracy of docking with a new scoring function, efficient optimization and multithreading. *Journal of Computational Chemistry*, *31*(2), 455.

Voigts-hoffmann, F., Schmitz, N., Shen, K., Shan, S., Ataide, S. F., & Ban, N. (2013). Article The Structural Basis of FtsY Recruitment and GTPase Activation by SRP RNA. *Molecular Cell*, *52*(5), 643–654.

Walter, P., & Johnson, A. E. (1994). Signal sequence recognition and protein targeting to the endoplasmic reticulum membrane. *Annual Review of Cell Biology*, *10*, 87–119.

Waterhouse, A., Bertoni, M., Bienert, S., Studer, G., Tauriello, G., Gumienny, R., Heer, F.T., de Beer, T.A.P., Rempfer, C., Bordoli, L., Lepore, R., Schwede, T. (2018). SWISS-MODEL: homology modelling of protein structures and complexes. *Nucleic Acids Research, 46*(W1), W296-W303.

Wild, Klemens, Bange, G., Bozkurt, G., Segnitz, B., Hendricks, A., & Sinning, I. (2010). Structural insights into the assembly of the human and archaeal signal recognition particles. *Acta Crystallographica Section D: Biological Crystallography*, *66*(3), 295–303.

Wild, Klemens, Bange, G., Motiejunas, D., Kribelbauer, J., Hendricks, A., Segnitz, B., Wade, R. C., & Sinning, I. (2016). Structural Basis for Conserved Regulation and Adaptation of the Signal Recognition Particle Targeting Complex. *Journal of Molecular Biology*, *428*(14), 2880–2897.

Yurist, S., Dahan, I., & Eichler, J. (2007). SRP19 is a dispensable component of the signal recognition particle in Archaea. *Journal of Bacteriology*, *189*(1), 276–279.

Zhang, X., Kung, S., & Shan, S. (2008). Demonstration of a Multistep Mechanism for Assembly of the SRP ·SRP Receptor Complex : Implications for the Catalytic Role of SRP RNA. *Journal of Molecular Biology, 54*, 581–593.

Zhang, X., Schaffitzel, C., Ban, N., & Shan, S. O. (2009). Multiple conformational switches in a GTPase complex control co-translational protein targeting. *Proceedings of the National Academy of Sciences of the United States of America*, *106*(6), 1754–1759.

Zwieb, Christian, & Eichler, J. (2002). Getting on target: The archaeal signal recognition particle. *Archaea*, *1*(1), 27–34.

CHAPTER 5

Role of archaeal membrane and the structural domains of the SRP receptor in the activity of targeting complex at high temperature

5.1 INTRODUCTION

Archaeal SRP receptor shares structural similarity with the bacterial counterpart, FtsY, which itself is a homolog of the alpha subunit of eukaryotic SRP receptor (SRα) (Miller et al., 1994). It has an N-terminal A domain consisting of acidic (negatively charged) residues, followed by a conserved NG domain, the same as the one shared by SRP54 (Gupta et al., 2016). The classical GTPase motifs (I-V) are also shared by the two SRP GTPases, along with the IBD and other signature motifs (Keenan et al., 2001; Leipe et al., 2002) but contrary to the classical P-loop GTPases, they do not employ a guanine nucleotide exchange factor and directly interact with each other to stimulate the concomitant hydrolysis of GTP (Powers & Walter, 1995; Jagath et al., 2000). Membrane targeting by the RNC-SRP complex is facilitated via multiple conformational changes brought about by the dynamic interaction between NG domains of the SRP GTPases (Shan et al., 2007; Zhang et al., 2009). This interaction was found to be strengthened by the helix 8 tetraloop of the SRP RNA where the SRP•GTP-GTP•SR complex initially assembles and then relocalizes to the distal end where the GTP hydrolysis is stimulated (Ataide et al., 2011; Shen et al., 2012; Shen et al., 2013). The "twinned" hydrolyses of the bound GTPs promote the dissociation of the Ffh-FtsY targeting complex and thus the cargo is unloaded upon the translocon (Egea et al., 2004; Shan et al., 2004).

Structural analyses of the Ffh-FtsY complex have established the contribution of NG domains of the two proteins in their mutual interaction. The heterodimeric complex from *Thermus aquaticus* revealed that the primary interactive interface exists between the G domains, accompanied by the interaction between N domains, comprising extensively of hydrogen bonds and van der Waals contacts (Egea et al., 2004). Individual mutagenesis of the residues along the interaction surface of FtsY in *E. coli* severely depleted the reciprocally stimulated GTP hydrolysis by Ffh-FtsY but the basal GTPase activity of FtsY was unaffected (Egea et al., 2004). The association of the targeting complex and its dual GTPase activity depended extensively on the full-length SRP RNA both in bacteria and in archaea (Zhang et al., 2008; Gupta et al., 2021). Crystal structure of the bacterial TC showed profound domain rearrangement

of Ffh upon binding the 4.5S RNA at the tetraloop region via the M domain leading to the movement of the NG domain to the distal region of helix 5 (Ataide et al., 2011). This was further substantiated by the binding analyses between NG and M domains of Ffh and FtsY in the presence or absence of SRP RNA (Buskiewicz et al., 2005). The binding of FtsY-NG with the SRP54/Ffh-NG is facilitated due to this positional reorientation in the latter and enhanced greatly by the presence of GTP (Jagath et al., 2000; Gupta et al., 2021). Together, the two reoriented NG domains form a composite active center of the TC that binds and hydrolyses GTP, and finally, the activated TC complexed with the RNC interacts with the membrane-bound translocon SecYEG via FtsY (Draycheva et al., 2016).

Although the Ffh-associating NG domain of FtsY is quite conserved, the unstructured A domain varies among different homologs of the prokaryotic SRP receptor (Bibi et al., 2001). The eukaryotic homolog SRα, which carries out similar functions as FtsY, remains associated with its integral membrane-bound component SRβ (Walter & Johnson, 1994). The absence of such membrane-spanning counterpart and the evidence of FtsY being distributed between the cytoplasm and the membrane have confirmed the soluble nature of the receptor in bacteria (Luirink et al., 1994). Therefore, it was suggested that the A domain may have a role in membrane association (Powers & Walter, 1997; Zelazny et al., 1997), though both A and NG domains of bacterial FtsY have been shown to have an affinity toward membrane phospholipid (de Leeuw et al., 2000). However, the A domain in *E. coli* was shown to be necessary for targeting the NG domain to the membrane and carrying out efficient translocation (Powers & Walter, 1997). Functional replacement of this domain with an unrelated integral membrane polypeptide proved the importance of the acidic domain in membrane association (Zelazny et al., 1997). Surprisingly, deletion of the A domain (1-195 residues) from *Ecoli*FtsY, termed NG+1, did not affect its cellular functions significantly, but deletion of a single residue (Phe196) lead to a completely inactive NG construct (Bahari et al., 2007; Draycheva et al., 2016). FtsY-NG retained its *in vitro* basal GTPase and Ffh-binding activities and accumulated in the plasma membrane along with SRP-RNC, indicating that release of the complex from the membrane was indeed defective (Bahari et al.,

2007). This led the researchers to believe that the interaction with lipid is not essential for either membrane targeting or receptor docking, rather for efficient release of the complex upon cargo unloading. This was further confirmed by the finding that anionic phospholipid induced conformational changes in FtsY which stimulated its basal GTPase activity (de Leeuw et al., 2000; Lam et al., 2010) and facilitated the formation of the GTP dependent intermediate of TC (Lam et al., 2010). The N-terminal alpha-helices in both proteins play major roles in complex assembly and function, in fact, deletion of αN1 of FtsY greatly enhanced the complex formation and the basal GTPase activity as seen in the presence of phospholipid (Stjepanovic et al., 2011). Thus, phospholipid may induce the conformational change in the αN1 helix that is part of the proposed membrane targeting sequence (MTS).

In the haloarchaeal SRP system, the *in vivo* functionality of the FtsY was found to be similar both in the presence and absence of the A domain (Haddad et al., 2005). Structural studies involving the FtsY from *Pyrococcus furiosus* (Egea et al., 2008) and *Sulfolobus acidocaldarius* (Wild et al., 2016) have contributed considerably to the otherwise scarce pool of knowledge about archaeal SRP receptors. The *Pfu*FtsY showed an elongated αN1 helix instead of the unfolded A domain commonly found in bacteria whereas *Saci*FtsY had a shorter αN1 and the contacting residues between SRP54 and FtsY were mapped along the αN1-N3 helices. Interestingly, the crystal structure did not employ the initial 20 amino acids at the N-terminus into account – a region rich in negatively charged residues. Such observation led us to investigate the contribution of each of the three participating helices (αN1-3) in terms of membrane association and functional TC formation. Lack of proper biochemical evidence and an in-depth understanding of the minimal functional MTS and its mechanism of membrane targeting in archaea have been the major driving factor for this work. By utilizing a vast array of biophysical techniques such as fluorescence resonance energy transfer, circular dichroism, anisotropy, and biochemical characterization of the reciprocal GTPase activity, we sought to elucidate the protein-protein and lipid-protein interactions controlling the archaeal TC assembly.

5.2 MATERIALS & METHODS

5.2.1 Construction of overexpression vectors

Construction of pAG3 and pAG351, expressing wild type SRP54 and FtsY respectively, was achieved following the protocol listed in 3.2.1. The deletion mutants were generated using the pAG351 backbone (Section 4.2.1). Primers used for this purpose and the final constructs generated are listed in Table 5.1. For expression analysis, the required vector was transformed into *Escherichia coli* BL21 (DE3) cells containing the RIL Cam^r plasmid (Stratagene). All the strains used in the present study are listed in Table 2.1.1. The primers and constructs used for the expression of wild-type proteins are listed in Table 2.1.2 and 2.1.3, respectively.

Table 5.1 Primers and plasmids used to construct FtsYΔαN mutants

Plasmids	Primers	Relevant characteristics	Reference
pAG352	535	5′-CCATGGGCTATAAAACGATAAAAGAG-3′ Forward primer for FtsYΔαN1	Present study
pAG353	536	5′-CCATGGGCTCTGATGTATCTTATGAAG-3′ Forward primer for FtsYΔαN2	Present study
pAG354	537	5′-CCATGGGCATGCTGAAGAAAAATAAC-3′ Forward primer for FtsYΔαN3	Present study
	165	5′-CTCGAGACTACTGAATATCCTTTCTAC-3′ Reverse primer for FtsY	Present study

5.2.2 Expression of recombinant proteins in *E. coli*

A total volume of 10 ml of an overnight culture of *E. coli* BL21(DE3)-RIL cells containing the RIL Cam^r plasmid, and the recombinant plasmid were used to inoculate 1 L of Luria–Bertani medium containing kanamycin (50 µg/ml) (for pAG351) or ampicillin (for pAG61-71) and chloramphenicol (34 µg/ml). Cells were grown at 37 °C until OD600 of 0.6 was reached when 500 µM IPTG (isopropyl β-D-thiogalactopyranoside) was added. The temperature was reduced to 16 °C, and growth was continued overnight to reduce inclusion body formation. The cells were collected by centrifugation, resuspended in lysis buffer [50mM Tris-Cl (pH 8.0), 150mM KCl, and 10% glycerol] containing the complete EDTA-free protease inhibitor cocktail (1 tablet/50 ml of lysate; Roche), frozen in liquid nitrogen and stored at - 80 °C.

5.2.3 Purification of recombinant proteins

Before purification, frozen resuspended cell pellets were thawed on ice. One mM lysozyme was added separately to the lysis buffer. After incubation on ice for 30 min, cells were lysed by sonication with Soniprep150 (DJB Labcare, UK). Cell debris was removed by centrifugation at 15000 rpm for 30 min (rotor SA-300; Sorval RC6+ Thermo Scientific). For the purification of histidine-tagged proteins, the supernatant was applied to a Ni^{2+}-NTA affinity column (Qiagen). Bound proteins were washed gradually with lysis buffer containing 10 mM and 20 mM imidazole, respectively. The bound protein fraction was eluted in lysis buffer containing 100 mM and 200 mM of imidazole. The eluted fraction was monitored by running reducing SDS-PAGE. The fraction containing the desired protein was dialyzed overnight in a lysis buffer.

5.2.4 Preparation of archaeosome

Archaeosome preparation from *Sulfolobus acidocaldarius* was carried out by the previously described protocol (Section 4.2.7).

5.2.5 GTPase assay and kinetic analyses

The basal GTPase activity and the kinetics of dual GTP hydrolysis were measured following the protocol discussed in Section 4.2.4.

5.2.6 Tagging of proteins with fluorescent probes

Tagging the proteins with fluorescent probes was achieved by the protocol listed in Section 4.2.5. SRP54 (50 µM) was tagged with FITC and the FtsYΔαN constructs were tagged with TRITC.

5.2.7 Fluorescence resonance energy transfer (FRET)

Fluorescent titration experiments were designed following the protocol described in Section 4.2.6. All the reactions were carried out in presence of 100 nM 7S RNA and 100 µM GMPPNP (non-hydrolyzable GTP analog).

5.2.8 Membrane fluidity measurement

Membrane fluidity was monitored by the fluorescence anisotropy assay established in the laboratory (Roy et al., 2018). Briefly, a 10 mM solution of DPH (1,6-Diphenyl-1,3,5-hexatriene) (Sigma) was prepared in DMSO. It was then added to a 100-fold diluted sample of archaeosome with the final DPH concentration being 3 µM. This was followed by incubation at 16 °C for 10 min. Anisotropy of DPH was then measured in a JASCO fluorimeter (Jasco, Japan) at 35°C. Changes in anisotropy of DPH were monitored with archaeosome mixed either with 10 µM of wildtype and

mutant FtsY with or without 10 µM of SRP54. Anisotropy percentage was calculated by considering the anisotropy of the archaeosome as 100% and plotted against each of the additions using Sigma plot 12.0.

5.2.9 Protein secondary structure analysis

Far-UV Circular dichroism spectra of wild-type FtsY and its deletion mutants were collected from 200 to 250 nm using a quartz cell with a 1 mm path length in a CD-spectropolarimeter (JASCO, Japan). Data were collected with a pitch of 1 nm and a scan rate of 50 nm/s. The far-UV spectra were recorded after incubating FtsY or FtsYΔαN1 or FtsYΔαN2 either in presence of archaeosome or SRP54 and archaeosome. The reported spectra for far-UV are the mean of three scans.

5.2.10 Small-angle X-ray scattering

Purified FtsY was analyzed on SAXS (BM29- ESRF, Grenoble). A concentration series (0.5-3 mg/ml) was used for their scattering behavior. Individual scattering curves were normalized to the incident beam intensity, corrected for background, and radially averaged. R_g (radius of gyration) was calculated from the small-angle scattering data using the Guinier equation –

$$\ln I(q) = \ln\ I_0 \times \frac{-q^2 R_g^2}{3}$$

where, I_0 is the zero-angle scattering, determined by protein concentration and molecular weight, and q is the scattering vector for a scattering angle of 2θ. The equation defines the quality of the sample, and no aggregation of the particle was observed in the merged scattering intensities at low angles. Theoretical scattering of the crystal structure (PDB: 5L3W) was fitted to the solution scattering using Crysol. The P(r) intensities are plotted against the diameter of the scattering vectors and the maximum dimension of the macromolecule, D_{max}, was calculated from the plot. All the data were analyzed using the ATSAS package and the structural model was prepared using PyMol.

5.2.11 Structural modeling

Molecular dynamic simulations have been performed on four *Sulfolobus acidocaldarius* SRP54 bound to FtsY receptor protein complexes; (i) the wild-type variant: full-length FtsY receptor in complex with full-length SRP54, (ii) the N1 variant: Y87-S369 fragment of the FtsY receptor in complex with the full-length SRP54, (iii) the N2 variant: S109-S369 fragment of the FtsY receptor in complex with the full-length SRP54, and (iv) the N3 variant: G129-S369 fragment of the FtsY receptor in complex with the full-length SRP54. Due to the unavailability of experimentally reported structures, ColabFold notebook (Mirdita et al., 2022) has

been used to take advantage of the AlphaFold-Multimer model for the building of the initial complexes. The predicted models are in good agreement with the experimentally reported archaeal complex of SRP54-FtsY (PDB: 5L3S). The estimated RMSDs considering the common domains of the built complexes with the archaeal complex are ~1.75 Å for wild type model, ~1.21 Å for the N1 variant, ~1.75 Å for N2 variant, and ~1.9 Å for the N3 variant. In the experimentally reported complex structure, though the FtsY receptor was obtained from *Sulfolobus acidocaldarius*, it was missing the initial M1-L85 fragment. In the AlphoFold predicted wild-type complex, the FtsY unit displayed an RMSD of ~1.44 Å from the experimentally solved FtsY receptor. All the systems were then solvated in a water box of OPC water models (Izadi et al., 2014) where on each side of the protein complex padding of at least ~12 Å of water is maintained. The overall charges of the systems were further neutralized by the addition of an adequate number of Na^+ ions, and then excess Na^+ and Cl^- ions were added to top-up the salt concentration to 0.15 M.

5.2.12 Molecular dynamic simulation

MD simulations were performed using the Amber ff19SB force field parameters (Tian et al., 2020) for the protein molecules. First, all the systems were subjected to minimization to overcome potential inter-and intra-molecular steric clashes. Then, the systems were equilibrated for 200 ps each while imposing positional restraints of 200 kJ/mol. $Å^2$ on the protein backbone to relax water molecules and ions around the complexes.

Finally, the backbone restraints were removed and each of the four systems was simulated for 30 ns in 3 replicas each, accumulating ~120 ns of total sampling. All simulations were performed under NPT ensemble by keeping the temperature at 300K using the Langevin thermostat,[15] with a collision frequency $\gamma = 1$ ps^{-1}, and pressure at 1 atm using the Monte Carlo barostat (Åqvist et al., 2004). The integration time step of 2 fs has been used after constraining all bonds involving Hydrogen atoms to their equilibrium bond lengths with the SHAKE algorithm (Ryckaert et al., 19770. For all these simulations, short-range nonbonded interactions were calculated using cutoff at 12 Å, whereas the long-range electrostatic interactions were computed using the Particle Mesh Ewald method (Darden et al., 1993). All the simulations were performed using the *Making it Rain* (Arantes et al., 2021) Google Colab framework that utilizes OpenMM toolkit to run simulations (Eastman et al., 2017).

5.2.13 Calculation of Binding Free Energy

For the comparison of binding free energies between the studied complexes, molecular mechanics Poisson-Boltzmann surface area (MM/PBSA) method

(Kollman et al., 2000) has been employed in each of the simulated ensembles. In this post-processing method, representative snapshots or conformations from an ensemble are used to calculate the free energy change between the bound and free states of a receptor and ligand. Free energy changes of complexation are calculated by combining the gas-phase energy contributions as well as the solvation free energy components (electrostatic and hydrophobic contributions) calculated from an implicit solvent model for each of the units undergoing complexation. Here, we have calculated the free energies from the last 2 ns of each of the replicas simulated in this investigation by selecting snapshots at 20 ps intervals. All analyses were performed with the MMPBSA.py script included in the AmberTools package (Miller et al., 2012). Entropic contributions to free energy have not been estimated in the present study because of the significant computational cost involved in such calculation for large systems like ours. So, the results are only comparable on a qualitative aspect between systems of interest.

5.3 RESULTS

5.3.1 Purification and characterization of deletion mutants

The previously solved crystal structure of the crenarchaeal FtsY (5L3W) provided a composite view of the NG domain heterodimer formed by SRP54 and FtsY where the αN1 helix of the receptor was shown to be detached from the core of archaeal TC (Wild et al., 2016). It was found that the extensive electrostatic interaction between the two GTPases is established mostly along the αN2 and αN3 helices (Fig. 5.1a). Surprisingly, when we modeled the TC in *S. acidocaldarius* without any bound nucleotide, with the help of AlphaFold2, the initial Met1-Gln71 region (excluded in the crystal structure) adopted a helix-turn-helix conformation, which was predicted to include an otherwise disordered acidic domain (Fig. 5.1b). This raised a vital question regarding the involvement of the acidic domain as well as the αN1 domain in the formation of TC. We, therefore, sought to resolve the issue by investigating the effect of these domains upon SRP54-FtsY interaction. Three different deletion constructs were designed – FtsYΔαN1 (Tyr87-Ser369), FtsYΔαN2 (Ser109-Ser369), and FtsYΔαN3 (Gly129-Ser369) – which were purified using affinity chromatography and separated in SDS-PAGE following approximate molecular weights 38 kDa, 35 kDa, and 32 kDa, respectively (Fig. 5.1c). Since the αN1 deletion removed a considerable portion from the N-terminus of the protein, we tested the structural integrity of our construct before moving to functional TC analyses.

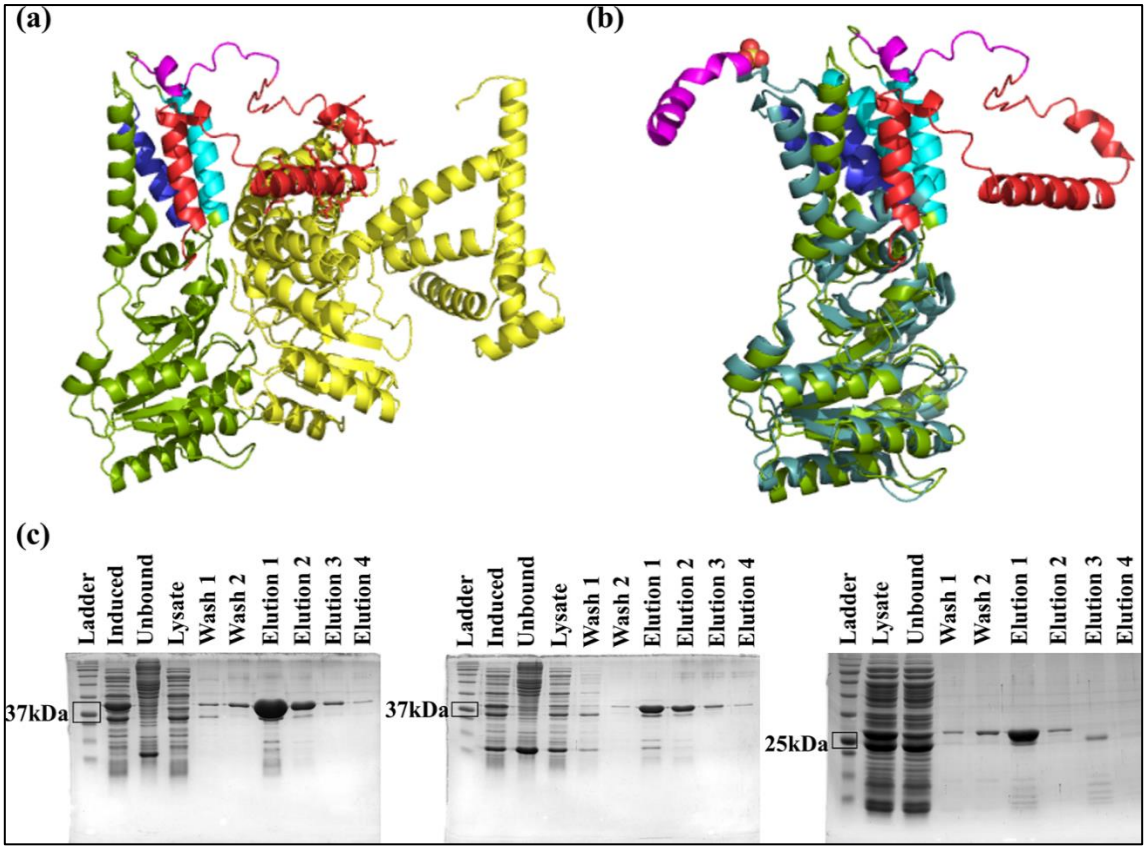

Figure 5.1. Modeling of archaeal FtsY and purification of its variants. (a) The targeting complex in *Sulfolobus acidocaldarius* was modeled using AlphaFold2 Multimer; SRP54 (yellow) and FtsY (green) are shown in the ribbon diagram. N-terminal motifs are marked in FtsY (A domain, red; αN1, magenta; αN2, cyan; αN3, blue). (b) AlphaFold2 prediction of full length FtsY (colour) aligned with 5L3W (colour) (RMSD = 3.299). (c) Purification pattern of αN1, αN2, and αN3 deletion variants, as run on SDS-PAGE.

5.3.2 Conformational analysis of the solution structure of FtsY

Small-angle X-ray scattering (SAXS) was used to study the molecular shape and size of the αN1 deletion variant of the archaeal SRP receptor. A concentration-dependent study of the apparent radius of gyration was done from concentrations ranging from 0.5-3 mg/ml in the small-angle region. No protein aggregation or association was observed in this range. The experimental value for the radius of gyration, R_g = 22.4 ± 0.08 Å, is in good agreement with that calculated from the crystal structure, R_g = 25.02. The chi-square (χ^2) value from Crysol for crystal structure and solution scattering was estimated to be 1.24, which signifies that the protein has similar architecture (no flexibility) in both crystalline and solution states. The D_{max} defines the maximum diameter present in solution which was about 80 ± 5 Å and agreed with the value from the crystal structure, ~ 88.7 Å.

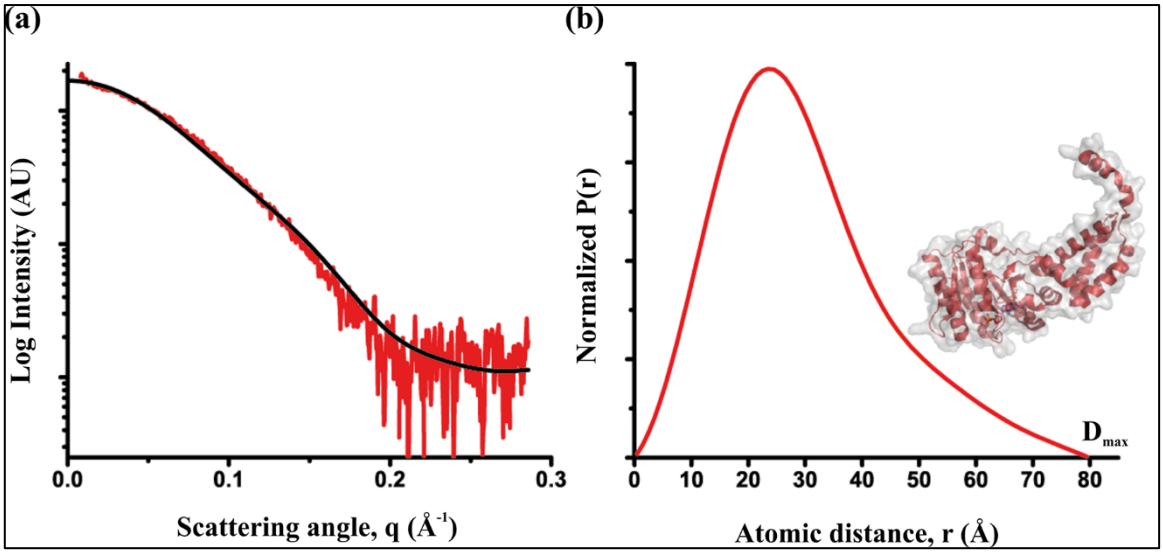

Figure 5.2. Solution structure analysis by SAXS. (a) The cumulative (merged) scattering measured profile (red line) of all scattered intensities, which is plotted in a log Intensity vs scattering angle. (b) P(r) distribution of the 1D merged solution scattering using pair distribution function and GNOM algorithm.

5.3.3 Role of N-terminal alpha-helices in SRP54-FtsY association

Energy transfer due to fluorescence resonance is an important tool that has been employed to assess protein-protein interaction in several assays. The addition of GTP and Ffh was shown to impart an increment and blue shift in the intrinsic tryptophan fluorescence of FtsY (Jagath et al., 2000) which was a direct measure of their association kinetics. Inter-domain interaction, as observed between NG and M domains of Ffh upon FtsY or 4.5S RNA addition, could be followed to saturation using different fluorophore labels (Buskiewicz et al., 2005). The present experiment employed FITC-labelled *Saci*SRP54 and TRITC-labelled variants of FtsY, and it was observed that with each N-terminal alpha-helix deletion, the association between the two proteins was gradually abrogated (Table 5.2). Since twinning of the nucleotide substrate and SRP RNA binding were found to be decisive in a strong interaction between SRP54/Ffh and FtsY (Egea et al., 2004; Zhang et al., 2008), saturating concentrations of archaeal 7S RNA and non-hydrolyzable GTP analog, GMPPNP, were used in all assays. Unlike GTP, GMPPNP allows capturing the stable targeting complex that would not dissociate following the nucleotide's hydrolysis. The bacterial and crenarchaeal targeting complexes were previously found to harbor strong electrostatic interactions across the N-terminal alpha-helices in both participating SRP-GTPases (Egea et al., 2004; Ataide et al., 2011; Wild et al., 2016). Deletion of those helices consequently affected the association between the two proteins. The Association of the wildtype TC in *S. acidocaldarius* was recorded previously by a similar FRET experiment (Gupta et al., 2021) which was found to be 40.5 ± 10.8 nM (Table 4.3, Fig. 4.3c-d). Deletion of 1-72 residues (αN1) augmented the

equilibrium dissociation constant for SRP54-binding by almost two folds (K_d = 75 ± 5.4 nM). Subsequent deletions of 1-86 residues (αN2) and 1-108 residues (αN3) raised the K_d value to 114.14 ± 24.5 nM and 272.18 ± 47.5 nM, respectively. The highly increased value of the equilibrium dissociation constant possibly indicates that the SRP54-FtsYΔαN3 complex may not be a functional association at all, a consideration that needed to be checked in light of the inherent enzymatic activity of the targeting complex.

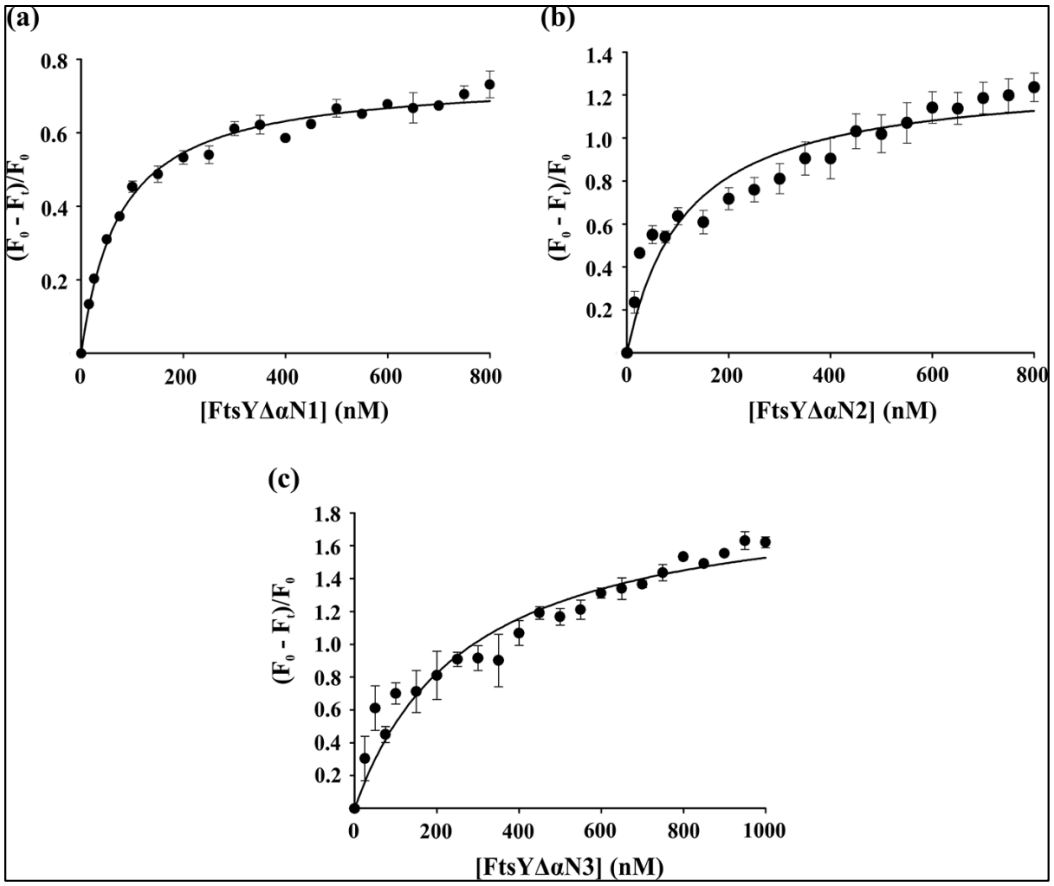

Figure 5.3 Targeting complex association is governed by N-terminal alpha-helices in FtsY. FRET between FITC-tagged SRP54 (100 nM) and TRITC-tagged FtsY variants (50-400 nM) was carried out in presence of both 100 μM GppNHp and 0.5 μM 7S RNA. The reaction was carried out at λ_{Ex} = 495 nm and data were recorded at λ_{Em} = 520 nm for FtsYΔαN1 (a), FtsYΔαN2 (b), and FtsYΔαN3 (c).

Table 5.2 Summary of binding and catalytic constants of TC variants

Targeting complex variant	K_d (nM)	k_{cat} (min^{-1})	K_m (μM)	k_{cat}/K_m (10^6 M^{-1} min^{-1})
SRP54-FtsYΔαN1	75 ± 5.4	0.183 ± 0.005	0.248 ± 0.08	0.79 ± 0.14
SRP54-FtsYΔαN2	114.14 ± 24.5	0.33 ± 0.02	1.43 ± 0.42	0.242 ± 0.03
SRP54-FtsYΔαN3	272.18 ± 47.5	0.082 ± 0.014	0.96 ± 0.01	0.085 ± 0.01

5.3.4 Reciprocal GTPase activity affected by deletion variants of FtsY

The SRP GTPases are known to reciprocally activate the GTP hydrolyzing ability of each other – an event that is catalyzed by SRP RNA and facilitated by the proper association of the two proteins (Shan et al., 2004; Zhang et al., 2008; Gupta et al., 2021). Several structural studies with both bacterial and archaeal SRP systems have shown that dual interaction of SRP54-M domain and NG domain with the proximal and distal helices of SRP RNA, respectively, reorient the SRP54 protein in a certain conformation that favors a functional NG-heterodimeric association between SRP54/Ffh and FtsY (Rosendal et al., 2003; Hainzl et al., 2007; Ataide et al., 2011; Voights-Hoffmann et al., 2013). Considering the abrupt changes in the binding phenomenon of the two GTPases because of N-terminal alpha-helix deletions in FtsY, the present experiment sought to characterize the TC variants for their basal GTPase activity. The reactions were set up following the protocol described earlier (Section 4.2.4) where a fixed concentration (2.5 μM) of SRP54 was combined with varying concentrations (1-15 μM) of FtsY for assessing the rate of GTP hydrolysis through 0-30 minutes. The resultant rate constants were fit in a modified ligand binding equation and the k_{cat} and K_m were calculated accordingly (Table 5.2). The maximum hydrolytic capacity of the SRP54-FtsYΔαN1 complex was calculated to be 0.183 ± 0.005 min^{-1}, which was lower than that of wildtype SRP54-FtsY complex (0.25 ± 0.01 min^{-1}, Table 4.4). But surprisingly, its affinity for the nucleotide (0.248 ± 0.08 μM), as well as the catalytic efficiency (0.79 ± 0.14 × 10^6 M^{-1} min^{-1}) became a little improved compared to the wildtype complex which has a K_m of 0.48 ± 0.12 μM and k_{cat}/K_m of 0.54 ± 0.07 × 10^6 M^{-1} min^{-1} (Table 4.4). The crystal structure of the crenarchaeal FtsY has shown that the αN1 helix is excluded from NG heterodimer in its crystalline state (Wild et al., 2016). This could probably be the reason for the efficient catalytic activity presented by the αN1-deletion variant. The SRP54-FtsYΔαN2 complex showed a lower affinity toward GTP (1.43 ± 0.42 μM) and subsequently a much lower catalytic efficiency (0.242 ± 0.03 × 10^6 M^{-1} min^{-1}) which directly connects to the fact that αN2 helix is directly involved in the interaction between the two GTPases (Wild et al., 2016). The final TC variant, SRP54-FtsYΔαN3, scored the lowest in terms of catalytic activity (0.085 ± 0.01 × 10^6 M^{-1} min^{-1}) though its substrate affinity (0.96 ± 0.01 μM) was comparable to the SRP54-FtsYΔαN2 variant. It was obvious since both αN2 and αN3 helices were deleted in this variant, the overall binding with SRP54 would be largely affected.

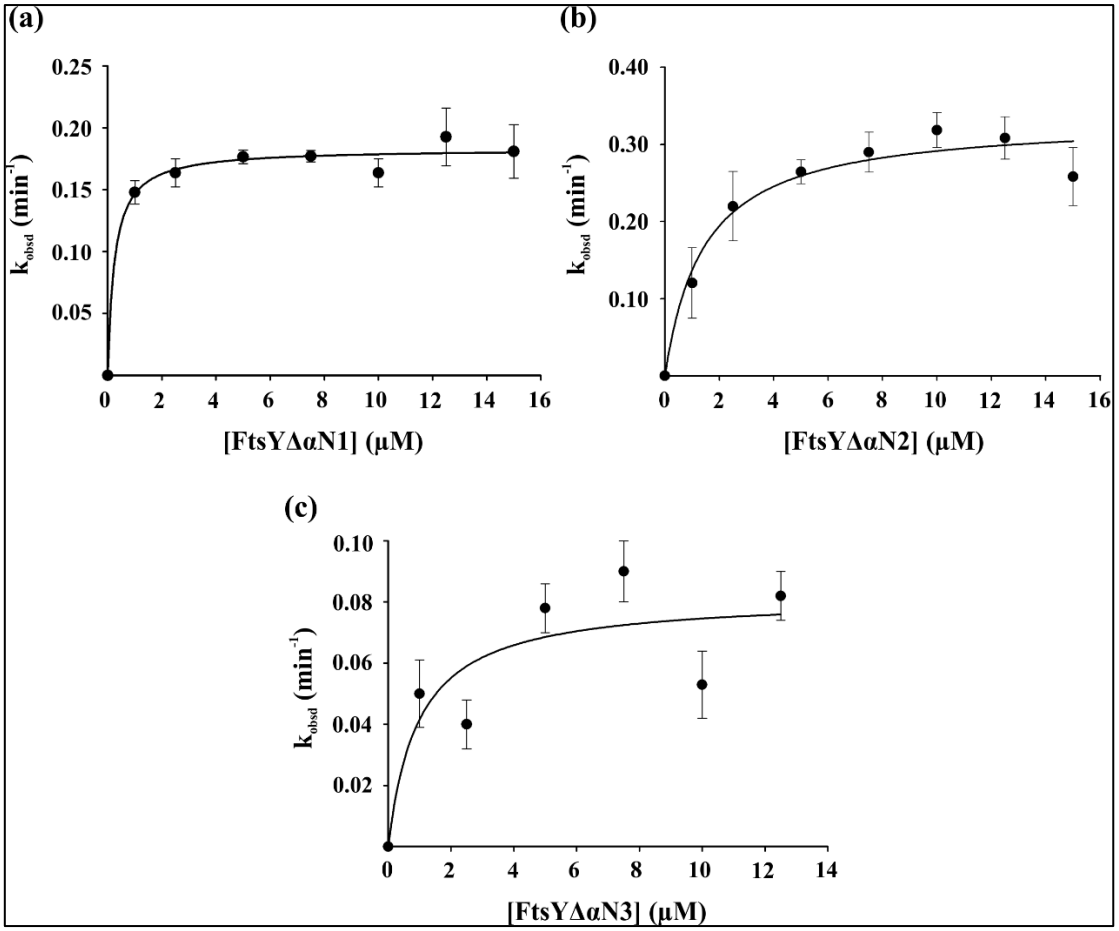

Figure 5.4 Dual GTPase activity of the targeting complex variants. The reactions were carried out in a series of 0-30 minutes, in the presence of 2.5 μM SRP54. The amount of released phosphate was measured using Malachite-Molybdate reagent and plotted against the time of incubation to generate k_{obsd}. Each reaction was carried out through a fixed concentration range (1-15 μM) for FtsYΔαN1 (a), FtsYΔαN2 (b), and FtsYΔαN3 (c).

5.3.5 Thermodynamic stabilization of targeting complex variants

The consecutive experiments assessing the ability of functional targeting complex formation have projected the αN3-deletion mutant as the least functional FtsY variant. It was evident from the facts that the apparent complexation of this variant with SRP54 was hugely affected in a way that the basal GTPase activity of the complex largely deteriorated. To investigate the probable dynamicity of these TC associations *in silico*, molecular dynamics simulation was carried out. The binding free energy of the protein-protein interaction with Amber-ff19SB was calculated using the standard MM/PBSA technique in three independent runs for each system. The experimental binding energy was calculated as $\Delta G = RT\ ln\ K_d$, where K_d is the equilibrium dissociation constant (Table 5.2). It can be noted that the binding energy predicted by the standard MM/PBSA was much stronger than the experimental energy (Fig. 5.5), with the value for ΔαN3 variant being positive (ΔG = 5.62 ± 0.47 kcal/mole). This may be attributed to the exclusion of any entropic contribution

though, however, studies have shown previously that introducing entropy does not guarantee an obvious improvement in prediction (Sun et al., 2018; Wang et al., 2019).

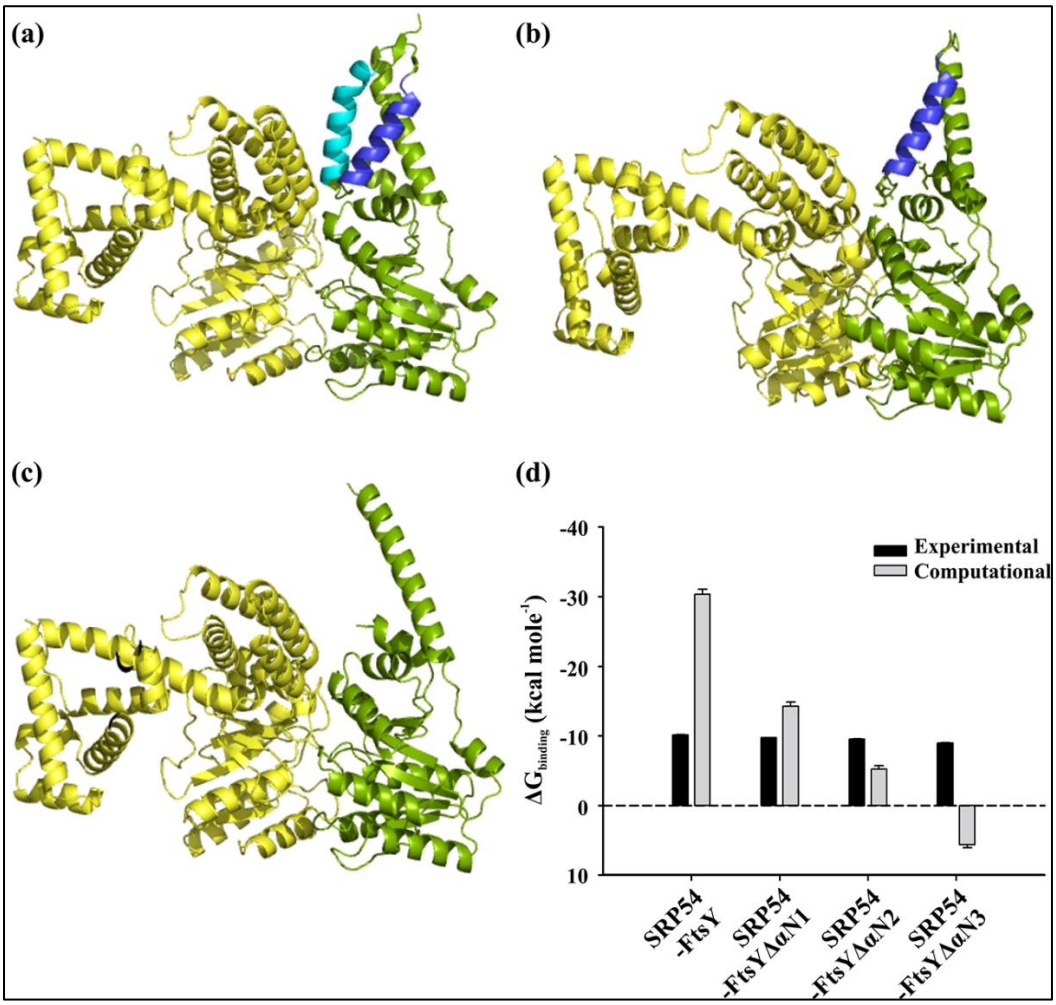

Figure 5.5 Comparison of the binding profile of targeting complex variants. Each variant was modeled using the AlphaFold2-multimer program and simulated under the Amber-ff19SB force field. The resultant models were processed in PyMol as a complex of SRP54 (yellow) with (a) FtsYΔαN1, (b) FtsYΔαN2, and (c) FtsYΔαN3 (all shown in green). The N-terminal helices are marked as indicated in Fig. 5.1. (d) Overall comparison of the binding free energy of wildtype and mutants obtained from experimental (black) and MM/PBSA calculation (grey).

The N-terminal acidic domain of FtsY (Met1-Leu85) that was excluded in the X-ray diffraction analysis (Wild et al., 2016), took a short alpha-helical confirmation following an initial disordered region in the AlphaFold2 model (Fig. 5.1a). Consequently, this full-length FtsY variant, complexed with SRP54, showed huge conformational variability in MD simulation which could have contributed to the much stronger binding free energy, ΔG = -30.34 ± 0.74 kcal mole^{-1}, compared to the experimental estimation of -10.094 ± 0.094 kcal mole^{-1}. Though the experimental energy estimation for ΔαN1 and ΔαN2 variants (-9.716 ± 0.025 and -9.475 ± 0.075 kcal mole^{-1}) lied close to that of the wildtype, their simulated free energy calculations were hugely varying (-14.23 ± 0.62 and -5.22 ± 0.48 kcal mole^{-1}). Deletion of all three

N-terminal helices has been shown to abrogate the formation of a functional targeting complex and thereafter its activity (Fig. 5.2 and 5.3). Thus, positive binding energy possibly hints at the loss of association between SRP54 and FtsYΔαN3 as evident from the much higher K_d value of their binding interaction (Table 5.2). Overall, the simulation experiment suggests that the functional association between SRP54 and FtsY is not permitted beyond the deletion of the αN1 and αN2 helices; also, together the αN1 and the acidic domain may contribute largely to favor the association.

Table 5.3 Summary of the experimental and estimated binding free energy

Targeting complex variant	K_d (nM)	ΔG_{Exp} (kcal/mole)	ΔG_{Est} (kcal/mole)
SRP54-FtsY	40.5 ± 10.8	- 10.094 ± 0.094	- 30.34 ± 0.74
SRP54-FtsYΔαN1	75 ± 5.4	- 9.716 ± 0.025	- 14.23 ± 0.62
SRP54-FtsYΔαN2	114.14 ± 24.5	- 9.475 ± 0.075	- 5.22 ± 0.48
SRP54-FtsYΔαN3	272.18 ± 47.5	- 8.957 ± 0.061	5.62 ± 0.47

5.3.6 Effect of membrane lipid on the conformation of TC variants

Studies in *E. coli* SRP system have shown that the highly charged acidic domain (initial 196 residues) in FtsY is involved in successful membrane targeting (de Leeuw et al., 1997, Zelazny et al., 1997). The otherwise cytosolically distributed bacterial SRP receptor was found to associate strongly with anionic phospholipids, thus proving the importance of negatively charged A domain (de Leeuw et al., 2000; Lam et al., 2010). However, deletion of this domain, but one amino acid, retained most of the functionalities of FtsY in *E. coli* (Stjepanovic et al., 2011; Draycheva et al., 2016). The effect of membrane lipid on the secondary structure of individual peptide segments representing different parts of the membrane targeting sequence (MTS) of bacterial FtsY was assessed by circular dichroism analysis (Stjepanovic et al., 2011) which revealed induction of alpha-helix formation with increasing concentrations of anionic phospholipid. Here, the ΔαN variants of crenarchaeal FtsY were investigated for any change in their apparent secondary structure in presence of archaeosome

isolated from *S. acidocaldarius*. The far-UV CD spectra recorded for the wildtype FtsY and both ΔαN variants, in the presence and absence of SRP54 and archaeosome, were presented as a plot of mean residue ellipticity (MRE) versus wavelength (Fig. 5.6a-c), after subtracting the background signal and the spectrum for SRP54 alone. Based on the previous observations, FtsYΔαN3 was excluded from any further experiment. A decrease in the alpha-helical content of FtsY was evident only after the addition of SRP54 alone or with lipid (Fig. 5.6a), classically depicted by the decrease in the negative value of MRE at 208 nm and 222 nm (Greenfield NJ, 2007). A similar pattern was observed for FtsYΔαN1 after SRP54 and archaeosome addition but to a lower extent, though the MRE was slightly reduced after initial addition of archaeosome alone (Fig. 5.6b). When the MRE at 222 nm (θ_{222}) was plotted against the varying reaction conditions (Fig. 5.6d), FtsYΔαN1 showed a steady decrease in its alpha-helical content, comparable to the pattern found in wildtype receptor. The most dramatic change was observed for FtsYΔαN2 as it underwent a sharp increment in its alpha-helical content upon the addition of SRP54. But an incubation with archaeosome and SRP54 reduced the signal to a value similar to the one found in FtsYΔαN2 and FtsY after the addition of archaeosome alone (Fig. 5.6c-d). Interaction with SRP54 is maintained along the N-terminal alpha-helices, αN2 and αN3, in FtsY. In absence of αN2, αN3 probably attains a more rigid conformation around SRP54 which might result in the apparent increase in the MRE. The exclusion of αN1 from the core NG heterodimer probably attributes to the slight change in its alpha-helical conformation. FtsY, on the other hand, has the full-length A domain along with the αN1 helix. Structural modeling of the wildtype TC showed the αN1 region to be randomly coiled, as opposed to a helix (Fig. 5.1a, magenta region). MD simulation also observed a highly dynamic nature of this region in targeting complex formation, which may include the opening of short helices, leading to the observed decrease in MRE for FtsY.

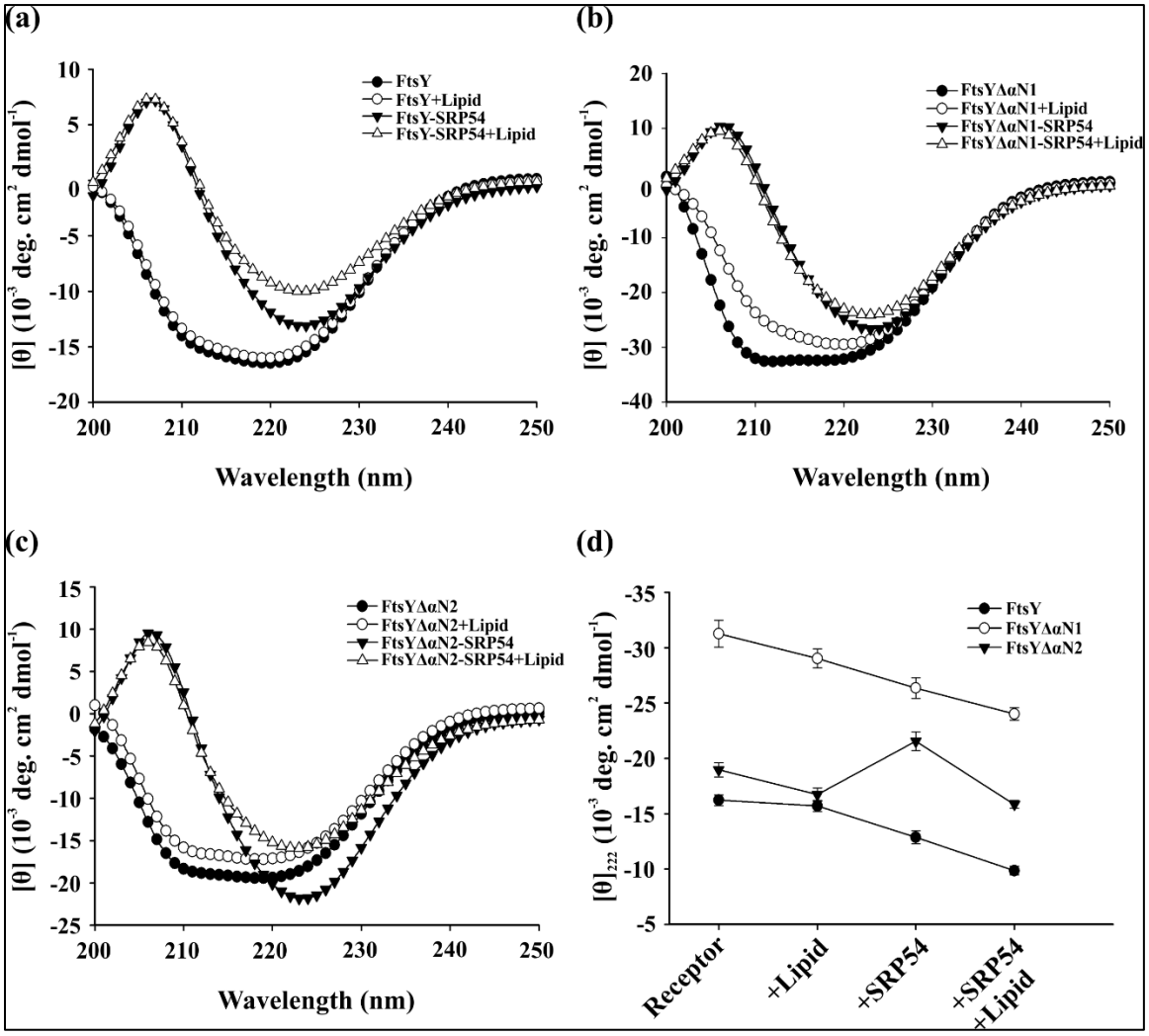

Figure 5.6 Lipids induce change in helical content of the TC variants. The wildtype, ΔαN1, and ΔαN2 variants of FtsY were analyzed in presence of archaeosome, SRP54, and both SRP54 and archaeosome. The spectrum was recorded at 200-250 nm range and 35 °C for FtsY (a), FtsYΔαN1 (b), and FtsYΔαN2 (c) and represented as mean residue ellipticity. (d) The overall transition of the secondary structure for the variants was shown as a function of the reaction conditions.

5.3.7 SRP receptor influences membrane fluidity

A close correlation has been observed between the lipid association of membrane targeting proteins and membrane fluidity (Kremer et al., 2001; Roy et al., 2018). To determine if FtsY interacts with membrane phospholipids via an integral domain, we tested the effect of the receptor and its ΔαN variants on archaeosome formed of lipids extracted from *S. acidocaldarius* cells. To assess membrane fluidity, the lipophilic probe DPH was tagged to the archaeosome preparation. The steady-state fluorescence anisotropy of this probe is inversely related to the fluidity of the

membrane and thus used to monitor the dynamic properties of the membrane. Since DPH attaches to the hydrophobic core of the lipid bilayer, its motional order within the core affects its inherent fluorescence property. The current experiment presents a comparative account of the anisotropy measurement taken in presence of different variants of SRP receptor and the targeting complex (Fig. 5.7). The anisotropy of the labeled archaeosome (R = 0.0598 ± 0.003) was taken as 100% and the rest of the values were normalized accordingly. It showed that the addition of FtsY and SRP54-FtsY complex decreased the anisotropy value by ~25%, whereas any of the ΔαN variants, alone or in complex with SRP54, did not alter the DPH anisotropy to any significant extent. The reduced anisotropy values were measures of increased fluidity of the bilayer in presence of the wildtype receptor and targeting complex, proving that initial N-terminal domains of the A-αN1 region may be critical for membrane association.

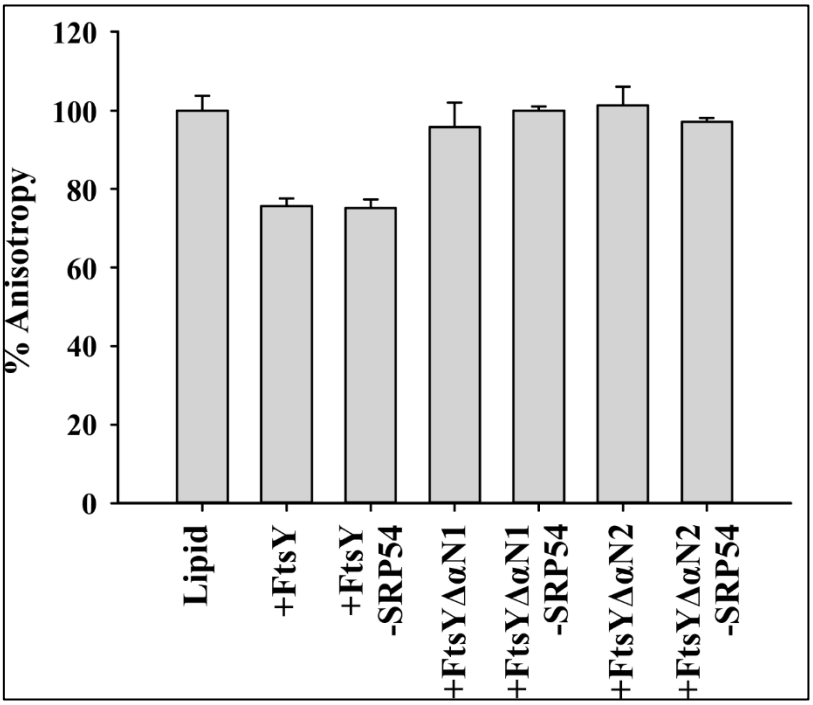

Figure 5.7 Membrane fluidity is affected by functional targeting complex. Changes in the membrane fluidity of isolated archaeosome fraction upon addition of different protein assemblies were evaluated by measuring the alteration in DPH anisotropy. Individual measurements were taken for FtsY, FtsYΔαN1, FtsYΔαN2, SRP54-FtsY, SRP54-FtsYΔαN1 and SRP54-FtsYΔαN2 at λ_{Ex} = 350 nm and λ_{Em} = 430 nm.

5.4 DISCUSSION

The signal recognition particle system across all domains of life employs two special GTPases – SRP54/Ffh and SR/FtsY. Bypassing the need for an external guanine nucleotide exchange factor, these two proteins make use of the unique insertion box domain present in their classical GTPase motifs, that acts as an internal tool to control the exchange of GDP and GTP (Moser et al., 1997), and reciprocally activate each other (Egea et al., 2004; Focia et al., 2004). For a successful turnover of this reciprocal activation, the two GTPases need to associate together to form a functional targeting complex with a composite catalytic core formed by electrostatic interaction between their respective NG domains (Gupta et al., 2016). Studies with crystal structures of SRP receptors in bacterial and archaeal domains have identified the N-terminal alpha-helices in the NG domains of both proteins to be the key players in mediating this extensive interaction (Ataide et al., 2011; Wild et al., 2016), though concrete biochemical evidence is absent in archaeal SRP system. Apart from the C-terminal NG domain, FtsY has a highly acidic N-terminal A domain that has always been hypothesized to be randomly disordered in solution. Although its importance in targeting complex association has not been clear, with some groups reporting proper cellular functioning in absence of A domain (Haddad et al., 2005) while some others showing abrogated SRP activity (Zelazny et al., 1997), the involvement of this domain in membrane targeting has been thoroughly established in bacteria (Lam et al., 2010; Draycheva et al., 2018).

The present work sought to establish the biochemical basis of the structural contribution of the FtsY-N domain motifs in the functional association of the crenarchaeal targeting complex. The three-terminal helices, αN1, αN2, and αN3, were sequentially deleted to construct three subsequent deletion variants - FtsYΔαN1, FtsYΔαN2, and FtsYΔαN3. These three variants were tested for their ability to bind SRP54 and catalyze dual GTP hydrolysis in complex and their probable association with archaeal membrane lipids were also checked to identify the probable membrane-targeting domain in FtsY. The formation of NG heterodimer between SRP and its receptor is thought to reorient the G domains to form a

composite active site at the dimer interface (Shan & Walter, 2005; Egea et al., 2008) that facilitates the reciprocal GTP hydrolysis. Wild et al. (2016) have shown that the αN1 helix of the crenarchaeal FtsY is excluded from the targeting complex association in its crystalline state and the maximum interaction is intensified in the αN2 and αN3 helices. To establish our system to be in total agreement with the already published data, we solved the solution structure of FtsY by small-angle X-ray scattering analysis. SAXS data were fit into the corresponding GNOM plot and the resulting χ^2 value of 1.24 indicated a very well match of the solution and crystal structure data. The binding of SRP54 with different ΔαN variants was assessed using the FRET tool and the maximally affected variant was found to be FtsYΔαN3. The apparent K_d values of the other two variants indicated that SRP54-binding was moderately compromised for FtsYΔαN2, whereas the ΔαN1 variant bound SRP54 like SRP54-FtsY binding in absence of RNA. The combinatorial GTPase activity of the SRP54-FtsY complex and its ΔαN variants further showed that the SRP54-FtsYΔαN3 complex was highly non-functional ($k_{cat}/K_m = 0.085 \pm 0.01 \times 10^6$ M^{-1} min^{-1}) in terms of GTP hydrolysis, whereas the SRP54-FtsYΔαN1 complex showed a slightly higher catalytic efficiency ($0.79 \pm 0.14 \times 10^6$ M^{-1} min^{-1}) as compared to the wildtype TC. Since αN1 helix was shown to be excluded from the functional association of crenarchaeal targeting complex (Wild et al., 2016), deletion of this specific segment probably could not affect the functionality of the targeting complex. The evident dynamic nature of this association led us to investigate the thermodynamic behavior of these complexes *in silico* by MD simulation using Open MM protocol. The resultant binding free energy values and the dynamic model corresponding to each complex were surprisingly indicative of a huge conformational rearrangement around the αN1 helix and the A domain preceding it. The SRP54-FtsY complex modeled by the AlphaFold2 Multimer program had the N-terminal 1-85 residues arranged in a helix-turn-helix motif, which was excluded from the previously solved crystal structure (5L3W, 5L3S) and proposed to be disordered in the A domain (1-71 residues) region. The simulated model showed very high conformational variations in the wildtype TC model, thus leading to a higher value of binding free energy (ΔG). SRP54-FtsYΔαN3 showed a positive value

for ΔG, drastically opposite to the experimental finding. This may be due to the severely affected binding interaction or the exclusion of interaction entropy from the calculation. However, deletion of all the αN helices together clearly seemed detrimental to the functional TC formation.

Bacterial FtsY has been studied extensively to pin the translocon binding and membrane targeting function on its A domain (de Leeuw et al., 2000; Draycheva et al., 2016) and to establish the minimal targeting sequence necessary for that function (Lam et al., 2010; Fu et al., 2017). Bacterial FtsY has been shown to prefer anionic phospholipids which tend to aggregate in presence of the receptor (de Leeuw et al., 2000). Although membrane interaction could be achieved by both A and NG domains (Draycheva et al., 2016), the dynamics of the interaction may be different. The native conformation of the A domain was found to be unfolded in solution which undergoes a random coil-helix transition in presence of anionic phospholipids (Stjepanovic et al., 2011) and this interaction is further strengthened when the receptor attains a stable complex with SRP-RNC (Lam et al., 2010; Fu et al., 2017), mostly mediated by the αN1 helix. In the present work, we sought to follow the changes, if any, incurred by the archaeal membrane lipid upon the different TC variants constructed on purpose. To identify changes in the secondary structure of the protein far-UV CD spectrum was obtained, with or without archaeosome, for receptor variants alone and in complex with SRP54. The alpha-helical contents of the wildtype and mutant TCs were found to decrease in presence of lipids, with the maximum effect in the wildtype complex with full-length FtsY. This observation clearly showed that unfolding of the initial A-αN1 region is triggered by archaeosome, contrary to the findings in bacterial FtsY. Similar observation could be obtained from the membrane stabilization assay where the fluidity of the lipid bilayer is measured by changes in steady-state fluorescence anisotropy of a bilayer-binding probe, DPH. A ~25% reduction in anisotropy only in presence of wildtype SRP receptor and receptor-SRP54 complex clearly hinted at the possible involvement of the A-αN1 region in membrane interaction.

5.5 CONCLUSION

The present work sought to identify the minimal domain of FtsY required to associate with SRP54 and archaeal cell membrane functionally. Deletion of the N-terminal alpha-helices resulted in truncated FtsY variants that bound to SRP54 with differing capacities. Also, the reciprocal GTPase activity by the complexes comprising SRP54 and FtsYΔαN variants was severely affected. The pattern of these observations suggested that deletion of all three helices is detrimental to native functions of FtsY, but deletion of the αN1 helix could retain considerable activities. The binding free energy of the wildtype and mutant targeting complexes were computationally calculated by MD simulation and compared with the experimental values, which further established the functionality of αN1 helix and the region preceding it (A domain) in the stabilization of targeting complex. Finally, the mutual influence of archaeal membrane and targeting complexes was analyzed by far-UV CD and DPH anisotropy. Both techniques successfully established that lipid interaction in archaea employs the N-terminal A-αN1 region of FtsY which probably gets relaxed of its helical constraints while associating with the membrane.

5.6 BIBLIOGRAPHY

Åqvist, J., Wennerström, P., Nervall, M., Bjelic, S., & Brandsdal, B. O. (2004). Molecular dynamics simulations of water and biomolecules with a Monte Carlo constant pressure algorithm. *Chemical Physics Letters*, *384*(4–6), 288–294.

Arantes, P. R., Polêto, M. D., Pedebos, C., & Ligabue-Braun, R. (2021). Making it Rain: Cloud-Based Molecular Simulations for Everyone. *Journal of Chemical Information and Modeling*, *61*(10), 4852–4856.

Ataide, S. F., Ataide, S. F., Schmitz, N., Shen, K., Ke, A., Shan, S., Doudna, J. A., & Ban, N. (2012). *The Crystal Structure of the Signal with Its Receptor*. *881*(2011).

Bahari, L., Parlitz, R., Eitan, A., Stjepanovic, G., Bochkareva, E. S., Sinning, I., & Bibi, E. (2007). *Membrane Targeting of Ribosomes and Their Release Require Distinct and Separable Functions of FtsY *. 282*(44), 32168–32175.

Bibi, E. (2001). Putative integral membrane SRP nomenclature for the subunits of eukaryotic DNA polymerase δ. *Trends in Biochemical Sciences*, *26*(1), 15–16.

Buskiewicz, I., Kubarenko, A., Peske, F., Rodnina, M. V., & Wintermeyer, W. (2005). Domain rearrangement of SRP protein Ffh upon binding 4.5S RNA and the SRP receptor FtsY. *Rna*, *11*(6), 947–957.

Darden, T., York, D., & Pedersen, L. (1998). Particle mesh Ewald: An N·log(N) method for Ewald sums in large systems. *The Journal of Chemical Physics*, *98*(12), 10089.

De Leeuw, E., Te Kaat, K., Moser, C., Menestrina, G., Demel, R., De Kruijff, B., Oudega, B., Luirink, J., & Sinning, I. (2000). Anionic phospholipids are involved in membrane association of FtsY and stimulate its GTPase activity. *EMBO Journal*, *19*(4), 531–541.

De Leeuw, Erik, Poland, D., Mol, O., Sinning, I., Ten Hagen-Jongman, C. M., Oudega, B., & Luirink, J. (1997). Membrane association of FtsY, the E. coli SRP receptor. *FEBS Letters*, *416*(3), 225–229.

Draycheva, A., Bornemann, T., Ryazanov, S., Lakomek, N. A., & Wintermeyer, W. (2016). The bacterial SRP receptor, FtsY, is activated on binding to the translocon. *Molecular Microbiology*, *102*(1), 152–167.

Draycheva, A., Lee, S., & Wintermeyer, W. (2018). Cotranslational protein targeting to the membrane : Nascent-chain transfer in a quaternary complex formed at the translocon. *Scientific Reports*, *March*, 1–12.

Eastman, P., Swails, J., Chodera, J. D., McGibbon, R. T., Zhao, Y., Beauchamp, K. A., Wang, L. P., Simmonett, A. C., Harrigan, M. P., Stern, C. D., Wiewiora, R. P., Brooks, B. R., & Pande, V. S. (2017). OpenMM 7: Rapid development of high performance algorithms for molecular dynamics. *PLOS Computational Biology*, *13*(7), e1005659.

Egea, P. F., Shan, S. O., Napetschnig, J., Savage, D. F., Walter, P., & Stroud, R. M. (2004). Substrate twinning activates the signal recognition particle and its receptor. *Nature*, *427*(6971), 215–221.

Egea, P. F., Tsuruta, H., de Leon, G. P., Napetschnig, J., Walter, P., & Stroud, R. M. (2008). Structures of the signal recognition particle receptor from the archaeon Pyrococcus furiosus: implications for the targeting step at the membrane. *PloS One*, *3*, e3619.

Evans, R., O'Neill, M., Pritzel, A., Antropova, N., Senior, A., Green, T., Žídek, A., Bates, R., Blackwell, S., Yim, J., Ronneberger, O., Bodenstein, S., Zielinski, M., Bridgland, A., Potapenko, A., Cowie, A., Tunyasuvunakool, K., Jain, R., Clancy, E., … Hassabis, D. (2021). Protein complex prediction with AlphaFold-Multimer. *BioRxiv*, 2021.10.04.463034.

Fu, Y. H., Huang, W. Y. C., Shen, K., Groves, J. T., Miller, T., Shan, S., & States, U. (2017). *Two-step membrane binding by the bacterial SRP receptor enable efficient and accurate Co-translational protein targeting*. 1–26.

Gao, F., Kight, A. D., Henderson, R., Jayanthi, S., Patel, P., Murchison, M., Sharma, P., Goforth, R. L., Kumar, T. K. S., Henry, R. L., & Heyes, C. D. (2015). Regulation of structural dynamics within a signal recognition particle promotes binding of protein targeting substrates. *Journal of Biological Chemistry*, *290*(25), 15462–15474.

Ghosh, A., Hartung, S., Van Der Does, C., Tainer, J. A., & Albers, S. V. (2011). Archaeal flagellar ATPase motor shows ATP-dependent hexameric assembly and activity stimulation by specific lipid binding. *Biochemical Journal*, *437*(1), 43–52.

Greenfield, N. J. (2007). Using circular dichroism spectra to estimate protein secondary structure. *Nature Protocols*, *1*(6), 2876–2890.

Gupta, S, Roy, M., & Ghosh, A. (2017). The Archaeal Signal Recognition Particle: Present Understanding and Future Perspective. *Current Microbiology*, *74*(2), 284–297.

Gupta, Sayandeep, Roy, M., Dey, D., Bhakta, K., Bhowmick, A., Chattopadhyay, D., & Ghosh, A. (2021). Archaeal SRP RNA and SRP19 facilitate the assembly of SRP54-FtsY targeting complex. *Biochemical and Biophysical Research Communications*, *566*, 53–58.

Haddad, A., Rose, R. W., & Pohlschröder, M. (2005). The Haloferax volcanii FtsY homolog is critical for haloarchaeal growth but does not require the A domain. *Journal of Bacteriology*, *187*, 4015–4022.

Hainzl, T., Huang, S., & Sauer-Eriksson, A. E. (2007). Interaction of signal-recognition particle 54 GTPase domain and signal-recognition particle RNA in the free signal-recognition particle. *Proceedings of the National Academy of Sciences of the United States of America*, *104*(38), 14911–14916.

Izadi, S., Anandakrishnan, R., & Onufriev, A. V. (2014). Building Water Models: A Different Approach. *The Journal of Physical Chemistry Letters*, *5*(21), 3863–3871.

Jagath, J. R., Rodnina, M. V, & Wintermeyer, W. (2000). Conformational changes in the bacterial SRP receptor FtsY upon binding of guanine nucleotides and SRP. *Journal of Molecular Biology*, *295*, 745–753.

Keenan, R. J., Freymann, D. M., Stroud, R. M., & Walter, P. (2001). The signal recognition particle. *Annual Review of Biochemistry*, *70*, 755–775.

Kollman, P. A., Massova, I., Reyes, C., Kuhn, B., Huo, S., Chong, L., Lee, M., Lee, T., Duan, Y., Wang, W., Donini, O., Cieplak, P., Srinivasan, J., Case, D. A., & Cheatham, T. E. (2000). Calculating Structures and Free Energies of Complex Molecules: Combining Molecular Mechanics and Continuum Models. *Accounts of Chemical Research*, *33*(12), 889–897.

Kremer, J. J., Sklansky, D. J., & Murphy, R. M. (2001). Profile of changes in lipid bilayer structure caused by β-amyloid peptide. *Biochemistry*, *40*(29), 8563–8571.

Lam, V. Q., Akopian, D., Rome, M., Henningsen, D., & Shan, S. (2010). Lipid activation of the signal recognition particle receptor provides spatial coordination of protein targeting. *Journal of Cell Biology*, *190*(4), 623–635.

Leipe, D. D., Wolf, Y. I., Koonin, E. V., & Aravind, L. (2002). Classification and evolution of P-loop GTPases and related ATPases. *Journal of Molecular Biology*, *317*(1), 41–72.

Lichi, T., Ring, G., & Eichler, J. (2004). Membrane binding of SRP pathway components in the halophilic archaea Haloferax volcanii. *European Journal of Biochemistry / FEBS*, *271*, 1382–1390.

Luirink, J., ten Hagen-Jongman, C. M., van der Weijden, C. C., Oudega, B., High, S., Dobberstein, B., & Kusters, R. (1994). An alternative protein targeting pathway in Escherichia coli: studies on the role of FtsY. *The EMBO Journal*, *13*(10), 2289–2296.

Miller, J. D., Bernstein, H. D., & Walter, P. (1994). Interaction of E. coli Ffh/4.5S ribonucleoprotein and FtsY mimics that of mammalian signal recognition particle and its receptor. *Nature*, *367*(6464), 657–659.

Mirdita, M., Schütze, K., Moriwaki, Y., Heo, L., Ovchinnikov, S., & Steinegger, M. (2022). ColabFold - Making protein folding accessible to all. *BioRxiv*, 2021.08.15.456425.

Moser, C., Mol, O., Goody, R. S., & Sinning, I. (1997). The signal recognition particle receptor of Escherichia coli (FtsY) has a nucleotide exchange factor built into the GTPase domain. *Proceedings of the National Academy of Sciences of the United States of America*, *94*(21), 11339–11344.

Peluso, P., Shan, S. O., Nock, S., Herschlag, D., & Walter, P. (2001). Role of SRP RNA in the GTPase cycles of Ffh and FtsY. *Biochemistry*, *40*(50), 15224–15233.

Peluso, Paul, Herschlag, D., Nock, S., Freymann, D. M., Johnson, A. E., & Walter, P. (2000). Role of 4.5S RNA in assembly of the bacterial signal recognition particle with its receptor. *Science*, *288*(5471), 1640–1643.

Powers, T., & Walter, P. (1995). Reciprocal stimulation of GTP hydrolysis by two directly interacting GTPases. *Science*, *269*(5229), 1422–1424.

Powers, T., & Walter, P. (1997). Co-translational protein targeting catalyzed by the Escherichia coli signal recognition particle and its receptor. *EMBO Journal*, *16*(16), 4880–4886.

Rosendal, K. R., Wild, K., Montoya, G., & Sinning, I. (2003). Crystal structure of the complete core of archaeal signal recognition particle and implications for interdomain communication. *Proceedings of the National Academy of Sciences of the United States of America*, *100*(25), 14701–14706.

Roy, M., Gupta, S., Patranabis, S., & Ghosh, A. (2018). The oligomeric plasticity of Hsp20 of Sulfolobus acidocaldarius protects environment-induced protein

aggregation and membrane destabilization. *Biochimica et Biophysica Acta - Biomembranes*, *1860*(12), 2549–2565.

Ryckaert, J.-P., Ciccotti+, G., & Berendsen, H. J. C. (1977). Numerical integration of the Cartesian Equations of Motion of a System with Constraints: Molecular Dynamics of n-Alkanes. *Journal Of Computational Physics*, *23*, 321–341.

Shan, S. O., Stroud, R. M., & Walter, P. (2004). Mechanism of association and reciprocal activation of two GTPases. *PLoS Biology*, *2*(10).

Shan, S., & Walter, P. (2005). Molecular Crosstalk between the Nucleotide Specificity Determinant of the SRP GTPase and the SRP Receptor. *Biochemistry*, *44*(16), 6214–6222.

Shan, S., Chandrasekar, S., & Walter, P. (2007). Conformational changes in the GTPase modules of the signal reception particle and its receptor drive initiation of protein translocation. *Journal of Cell Biology*, *178*(4), 611–620.

Shen, K., Arslan, S., Akopian, D., Ha, T., & Shan, S. O. (2012). Activated GTPase movement on an RNA scaffold drives co-translational protein targeting. *Nature*, *492*(7428), 271–275.

Shen, K., Wang, Y., Hwang Fu, Y. H., Zhang, Q., Feigon, J., & Shan, S. O. (2013). Molecular Mechanism of GTPase Activation at the Signal Recognition Particle (SRP) RNA Distal End. *Journal of Biological Chemistry*, *288*(51), 36385–36397.

Sheng, Y., Yin, Y., Ma, Y., & Ding, H. (2021). Improving the Performance of MM/PBSA in Protein–Protein Interactions via the Screening Electrostatic Energy. *Journal of Chemical Information and Modeling*, *61*(5), 2454–2462.

Stjepanovic, G., Kapp, K., Bange, G., Graf, C., Parlitz, R., Wild, K., Mayer, M. P., & Sinning, I. (2011). Lipids Trigger a Conformational Switch That Regulates Signal Recognition Particle (SRP) -mediated Protein Targeting * □. *Journal of Biological Chemistry*, *286*(26), 23489–23497.

Sun, H., Duan, L., Chen, F., Liu, H., Wang, Z., Pan, P., Zhu, F., Zhang, J. Z. H., & Hou, T. (2018). Assessing the performance of MM/PBSA and MM/GBSA methods. 7. Entropy effects on the performance of end-point binding free energy calculation approaches. *Physical Chemistry Chemical Physics*, *20*(21), 14450–14460.

Tian, C., Kasavajhala, K., Belfon, K. A. A., Raguette, L., Huang, H., Migues, A. N., Bickel, J., Wang, Y., Pincay, J., Wu, Q., & Simmerling, C. (2020). ff19SB: Amino-Acid-Specific Protein Backbone Parameters Trained against Quantum Mechanics Energy Surfaces in Solution. *Journal of Chemical Theory and Computation*, *16*(1), 528–552.

Van Den Berg, B., Clemons, W. M., Collinson, I., Modis, Y., Hartmann, E., Harrison, S. C., & Rapoport, T. A. (2004). X-ray structure of a protein-conducting channel. *Nature*, *427*(6969), 36–44.

Voigts-hoffmann, F., Schmitz, N., Shen, K., Shan, S., Ataide, S. F., & Ban, N. (2013). Article The Structural Basis of FtsY Recruitment and GTPase Activation by SRP RNA. *Molecular Cell*, *52*(5), 643–654.

Walter, P., & Johnson, A. E. (1994). Signal sequence recognition and protein targeting to the endoplasmic reticulum membrane. *Annual Review of Cell Biology*, *10*, 87–119.

Wang, E., Weng, G., Sun, H., Du, H., Zhu, F., Chen, F., Wang, Z., & Hou, T. (2019). Assessing the performance of the MM/PBSA and MM/GBSA methods. 10. Impacts of enhanced sampling and variable dielectric model on protein–protein Interactions. *Physical Chemistry Chemical Physics*, *21*(35), 18958–18969.

Wild, Klemens, Bange, G., Motiejunas, D., Kribelbauer, J., Hendricks, A., Segnitz, B., Wade, R. C., & Sinning, I. (2016). Structural Basis for Conserved Regulation and Adaptation of the Signal Recognition Particle Targeting Complex. *Journal of Molecular Biology*, *428*(14), 2880–2897.

Zelazny, A., Seluanov, A., Cooper, A., & Bibi, E. (1997). The NG domain of the prokaryotic signal recognition particle receptor, FtsY, is fully functional when fused to an unrelated integral membrane polypeptide. *Proceedings of the National Academy of Sciences of the United States of America*, *94*(12), 6025–6029.

Zhang, X., Kung, S., & Shan, S. (2008). *Demonstration of a Multistep Mechanism for Assembly of the SRP · SRP Receptor Complex : Implications for the Catalytic Role of SRP RNA*. *54*, 581–593.

Zhang, X., Schaffitzel, C., Ban, N., & Shan, S. O. (2009). Multiple conformational switches in a GTPase complex control co-translational protein targeting. *Proceedings of the National Academy of Sciences of the United States of America*, *106*(6), 1754–1759.

CHAPTER 6

Conclusion

to

summarize the findings

Archaea are unicellular life forms that constitute a separate domain of life other than bacteria and eukaryotes. From the evolutionary viewpoint, archaea represent a variety of interesting molecular features that usually combine homologous traits from the other two domains of life. Protein translocation is a critical process in the maintenance of cellular life. The translocation process has been critically addressed in eukaryotes and bacteria. However, little information is available regarding protein translocation across archaeal membranes. The Signal Recognition Particle (SRP), the ribonucleoprotein complex that plays an important role in the process of translocation, is a protein targeting machine conserved across all species that binds the signal peptide at the N-terminus of the nascent polypeptide chain. The archaeal SRP machinery bears high similarity with its eukaryotic counterpart with the proteins SRP54 and SRP19 primarily binding the 7S SRP RNA. Together this complex recognizes the signal peptide and binds the RNC, and then interacts with the membrane-associated receptor, FtsY, a homolog of its bacterial counterpart. Concomitant GTP hydrolysis by SRP and FtsY then delivers the polypeptide to the adjacent protein conducting channel. With very limited knowledge in hand, a proper elucidation of the protein-protein and protein-RNA interactions became a requirement to understand archaeal protein translocation.

The first objective of this study addresses the basics of the SRP system in *Sulfolobus acidocaldarius*, a thermoacidophilic crenarchaeon. To bridge the gap between the few available structural understandings and the actual biochemical details, the key components comprising the pathway were first cloned, expressed in *Escherichia coli* overexpression system, and purified to obtain recombinant SRP54 and SRP19 protein and 7S RNA. The binding of these proteins with SRP RNA was investigated using electrophoretic mobility shift assay and their affinity for the RNA was calculated. Since SRP54 possesses the classical motifs of a GTPase, its capacity for hydrolyzing GTP was assessed in lights of different reaction conditions, which included nucleotide specificity, optimal temperature, pH, specificity for divalent cations, etc. Computational modeling of SRP54 hinted at the possible changes in the conformation of the M domain of the protein upon binding the 7S RNA and predicted a battery of residues possibly involved in the RNA-protein interaction.

Mutational analyses of two such residues showed compromised RNA-binding ability, proving the importance of the M domain.

In the second objective, the functional association between SRP54 and FtsY was studied by using the fluorescence resonance energy transfer technique. The complex formation was found to be greatly enhanced in presence of 7S RNA and a non-hydrolyzable GTP analog. Furthermore, the reciprocal GTPase activity of the complex, carried out concomitantly by the two proteins, was characterized to kinetic details, and 7S RNA was proved to be facilitating the reaction. The addition of SRP19 hugely enhanced the overall kinetics of the dual GTPase activity, whereas full-length 7S RNA, instead of its minimum functional domain, seemed to be more effective. Together, it could be said that the formation of a functional targeting complex is catalyzed by the presence of full-length SRP RNA and SRP19, probably because the SRP54-RNA-SRP19 complex imparts huge conformational rearrangements in SRP54 that favors FtsY binding.

Powered by these arsenals of newer findings, the present work finally aimed to elucidate the structural motifs of FtsY required to interact with SRP54 and archaeal membrane lipids. The N-terminal acidic domain and subsequent αN helices have long been hailed to maintain such interactions in bacterial FtsY. We found that deletion of these domains greatly affected the functional targeting complex formation, as well as reciprocal GTPase action. Small-angle X-ray scattering analysis proved the structural integrity of the protein in solution which was then modeled in complex with SRP54. The model was further simulated using standard MD simulation protocol and incorporating various mutant FtsY lacking subsequent αN helices. The free energy of binding calculated from each simulation provided a clear understanding of the comparative stability of these FtsYΔαN variants. Effect of archaeal membrane lipids was tested by monitoring changes in protein's secondary structure and membrane fluidity by CD absorbance and anisotropy respectively. Cumulative findings suggest that the key functionalities of archaeal FtsY are maintained via the A domain and αN1 helix.

LIST OF PUBLICATION

Roy, M., Bhakta, K., Bhowmick, A., **Gupta, S.**, Ghosh, A., & Ghosh, A. (2022). Archaeal Hsp14 drives substrate shuttling between small heat shock proteins and thermosome: insights into a novel substrate transfer pathway. *The FEBS journal*, *289*(4), 1080–1104.

Gupta, S., Roy, M., Dey, D., Bhakta, K., Bhowmick, A., Chattopadhyay, D., & Ghosh, A. (2021). Archaeal SRP RNA and SRP19 facilitate the assembly of SRP54-FtsY targeting complex. Biochemical and Biophysical Research Communications, 566, 53-58.

Mukherjee, D., **Gupta, S.**, Ghosh, A., & Ghosh, A. (2020). Ustilago maydis secreted T2 ribonucleases, Nuc1 and Nuc2 scavenge extracellular RNA. Cellular Microbiology, 22(12), e13256.

Roy, M., **Gupta, S**., Patranabis, S., & Ghosh, A. (2018). The oligomeric plasticity of Hsp20 of Sulfolobus acidocaldarius protects environment-induced protein aggregation and membrane destabilization. Biochimica et Biophysica Acta (BBA)-Biomembranes, 1860(12), 2549-2565.

Gupta, S., Roy, M., & Ghosh, A. (2017). The archaeal signal recognition particle: present understanding and future perspective. Current microbiology, 74(2), 284-297.

Mukherjee, D., **Gupta, S.**, Saran, N., Datta, R., & Ghosh, A. (2017). Induction of apoptosis-like cell death and clearance of stress-induced intracellular protein aggregates: dual roles for Ustilago maydis metacaspase Mca1. Molecular microbiology, 106(5), 815-831.

Saha, S., Jana, S., **Gupta, S.**, Ghosh, A., & Nayek, H. P. (2016). Syntheses, structures and biological activities of square planar Ni (II), Cu (II) complexes. Polyhedron, 107, 183-189.

Curr Microbiol
DOI 10.1007/s00284-016-1167-9

REVIEW ARTICLE

The Archaeal Signal Recognition Particle: Present Understanding and Future Perspective

Sayandeep Gupta[1] · Mousam Roy[1] · Abhrajyoti Ghosh[1]

Received: 25 April 2016 / Accepted: 21 November 2016
© Springer Science+Business Media New York 2016

Abstract The signal recognition particle (SRP) and its receptor constitute universally conserved and essential cellular machinery that controls the proper membrane localization of nascent polypeptides with the transmembrane domain. In the past decade, there has been an immense advancement in our understanding of this targeting machine in all three domains of life. A significant portion of such progress came from the structural analysis of archaeal SRP components. Despite the availability of structural insights from different archaeal SRP components, little is known about protein translocation in this domain of life compared to either bacteria or eukaryotes. One of the primary reasons being limited availability of the genetic and cell biological tools in archaea. In the present review, an attempt has been made to explore the structural information available for archaeal SRP components to gain insights into the protein translocation mechanism of this group of organisms. Besides, many exciting avenues of archaeal research possible using the recently developed genetic and cell biological tools for some species have been identified.

Introduction

Protein translocation is a critical process in the maintenance of cellular life. Proteins are sorted to various intracellular destinations or secreted into the extracellular space from their sites of synthesis. A ribonucleoprotein complex, known as signal recognition particle (SRP), plays a significant role in executing protein sorting and translocation in all three domains of life. The SRP is a universally conserved protein-targeting machine that binds to the particular peptide sequence at the N-terminus of the nascent polypeptide chain and delivers it to the translocation system for further processing [31, 37]. The SRP–ribosome-nascent polypeptide complex (RNC) attaches to the cognate SRP receptor (SR) located on the targeted membrane [23]. The interaction between the GTPase domains associated with both the SR and SRP allows the delivery of the concerned protein into the adjacent protein-conducting channel (PCC). GTP hydrolysis empowers the process, and the SRP is available for another round of targeting process [51, 71] (Fig. 1).

In general, protein translocation occurs either in co- or post-translational manner in all three domains of life (Fig. 1). In eukaryotes, with few exceptions like fission yeast, proteins are transported co-translationally into the lumen of endoplasmic reticulum (ER). In this mode, a signal peptide that emerges from the ribosome is bound by SRP [75]. It has been shown recently that SRP typically binds the protein–ribosome complex after synthesis of initial 40–55 amino acids. Upon binding, the protein translation from the entire ternary complex RNC remains arrested until this complex interacts with the SRP receptor. The dynamicity of SRP–stalled RNC interaction has been recently demonstrated where it was shown that SRP bound RNCs expose signal peptide in multiple interconvertible conformations, each with a specific kinetic property [76]. The entire SRP–stalled RNC complex interacts with the SRP receptors SRα and SRβ on the ER membrane. Finally, at the ER membrane, ribosome docks onto the protein translocation channel (Sec61αβγ) and SRP is released from

✉ Abhrajyoti Ghosh
abhrajyoti.ghosh@jcbose.ac.in

[1] Department of Biochemistry, Bose Institute, Centenary Campus, P 1/12, C. I. T. Road, Scheme – VIIM, Kolkata 700054, West Bengal, India

Published online: 29 November 2016

Polyhedron 107 (2016) 183–189

Contents lists available at ScienceDirect

Polyhedron

journal homepage: www.elsevier.com/locate/poly

Syntheses, structures and biological activities of square planar Ni(II), Cu(II) complexes

Sudeshna Saha [a], Subhayan Jana [a], Sayandeep Gupta [b], Abhrajyoti Ghosh [b,*], Hari Pada Nayek [a,*]

[a] Department of Applied Chemistry, Indian School of Mines, Dhanbad 826004, Jharkhand, India
[b] Department of Biochemistry, Bose Institute, Centenary Campus, Kolkata 700054, West Bengal, India

ARTICLE INFO

Article history:
Received 14 November 2015
Accepted 25 January 2016
Available online 1 February 2016

Keywords:
Schiff base ligand
Nickel complex
Copper complex
Crystal structure
Biological activities

ABSTRACT

Ni(II) and Cu(II) complexes of a tridentate Schiff base ligand, *N*-(2-hydroxyphenyl)-3-methoxy-salicylideneamine (**H_2L**) have been synthesized and characterized by IR, NMR, UV–Vis spectroscopy and elemental analysis. The solid state structures of complexes have been determined by single crystal X-ray diffraction analyses. The molecular structures shows the formation of mononuclear complexes [(NiL(1Me-Im)] (**1**), [(CuL(1Me-Im)] (**2**) and [(NiL(PPh_3)] (**3**) (1Me-Im = 1-methylimidazole and PPh_3 = triphenylphosphine). The Ni(II) or Cu(II) ion is situated in a square planar environment and coordinated by the NO_2 donors of the Schiff base ligand and 1Me-Im (**1**–**2**) or PPh_3 (**3**). The interactions of complexes **1**–**3** with DNA have been investigated by EtBr displacement experiments and spectroscopic titrations. The MTT assay showed no significant toxicity of **1**, **3** and increasing toxicity of **2** at lower concentration.

© 2016 Elsevier Ltd. All rights reserved.

1. Introduction

In recent years, the study of the interaction of DNA with metal complexes has been tremendously appreciated in chemical and biological science [1,2]. It explores the possibility of designing effective anticancer drugs and chemotherapeutic agents. Metal complexes bind DNA through both covalent and non-covalent interactions such as electrostatic interactions, intercalation as well as direct coordination bond formation [3]. Initially, platinum based compounds which binds the DNA covalently, have been used for the treatment of cancers [4]. However, their intense side effects bound their applications [5]. Therefore, a tremendous attention is being paid for the synthesis of new less-toxic, more effective and target specific metal-based anticancer drugs as an alternative of platinum drugs. Many metal complexes have been synthesized and screened as a potential DNA binding agent [6,7]. First-row transition metal complexes containing bio-essential metal ions such as Ni(II), Cu(II) and Zn(II) have been proven to be an effective DNA binding agent with potential cytotoxic activity [8–11]. Of course, the organic ligands play important role to determine favourable interactions and activities between metal complexes and DNA. A variety of polydentate organic ligands have been used [12]. In this context, metal complexes of Schiff base ligands have been investigated extensively [13–15]. Metal complexes with salicylidene Schiff base ligands showed effective interactions with DNA [16,17]. However, planar ligands or metal complexes prefer intercalative DNA binding whereas non-planar compounds prefer groove binding. In this context, square planner metal complexes of Schiff base ligand has attracted enormous attention. For instance, Ni(II) and Co(II) complexes of (2-hydroxyl-benzylidene) hydrazide has been synthesized and their interactions with DNA have been reported [18]. Metal complexes based on amino-alcohol, amino acids and thiosemicarbazones derived Schiff base ligands were synthesized and their cytotoxic effect on cancerous cell line and interactions with DNA were investigated [19–21]. Highly cytotoxic DNA binding Cu(II) complexes of various Schiff base have recently been documented [22]. Several Ni(II) complexes of Schiff base ligands containing meso-1,2-diphenylethylenediamine moiety exhibited excellent interactions with a tetramolecular DNA quadruplex [23]. Square planar NI(II) complexes of 1-phenyl-3-((2-(piperidin-4-yl)ethyl)imino)but-1-en-1-ol and 4-((2-(piperazin-1-yl)ethyl)imino)pent-2-en-2-ol have been synthesized and their DNA binding abilities have been investigated [24].

Persisting our study on the syntheses of metal complexes using the ONO and N_2O_2 donor ligands we have recently reported homo or heteronuclear metal complexes with interesting magnetic properties and biological activities [25–27]. Here, we report the results obtained by the reaction of a Schiff-base ligand *N*-(2-hydroxyphenyl)-3-methoxy-salicylideneamine (**H_2L**) with hydrated Ni (II) and Cu(II) salts in the presence of an ancillary ligand,

* Corresponding authors. Tel.: +91 33 25693225; fax: +91 33 23553886 (A. Ghosh), tel.: +91 326 2235756; fax: +91 326 2296563 (H.P. Nayek).
E-mail addresses: abhrajyoti.ghosh@jcbose.ac.in (A. Ghosh), hpnayek@yahoo.com (H.P. Nayek).

http://dx.doi.org/10.1016/j.poly.2016.01.034
0277-5387/© 2016 Elsevier Ltd. All rights reserved.

Molecular Microbiology (2017) 106(5), 815–831 ■
doi:10.1111/mmi.13848
First published online 16 October 2017

Induction of apoptosis-like cell death and clearance of stress-induced intracellular protein aggregates: dual roles for *Ustilago maydis* metacaspase Mca1

Dibya Mukherjee,[1] Sayandeep Gupta,[2] N. Saran,[1] Rahul Datta[1] and Anupama Ghosh [1]*

[1]*Division of Plant Biology, Bose Institute, Centenary Campus, P1/12 C.I.T. Road, Scheme VIIM, Kolkata 700054, India.*

[2]*Department of Biochemistry, Bose Institute, Centenary Campus, P1/12 C.I.T. Road, Scheme VIIM, Kolkata 700054, India.*

Summary

Metacaspases primarily associate with induction and execution of programmed cell death in protozoa, fungi and plants. In the recent past, several studies have also demonstrated cellular functions of metacaspases other than cell death in different organisms including yeast and protozoa. This study shows similar dual function for the only metacaspase of a biotrophic phytopathogen, *Ustilago maydis*. In addition to a conventional role in the induction of cell death, Mca1 has been demonstrated to play a key role in maintaining the quality of the cellular proteome. On one hand, Mca1 could be shown to bring about apoptosis-like phenotypic changes in *U. maydis* on exposure to oxidative stress, on the other hand, the protein was found to regulate cellular protein quality control. *U. maydis* metacaspase has been found to remain closely associated with the insoluble intracellular protein aggregates, generated during an event of stress exposure to the fungus. The study, therefore, provides direct evidence for a role of *U. maydis* metacaspase in the clearance of the stress-induced intracellular insoluble protein aggregates. Furthermore, host infection assays with *mca1* deletion strain also revealed a role of the protein in the virulence of the fungus.

Accepted 21 September, 2017. *For correspondence. E-mail: ghosh.anupama@jcbose.ac.in; Tel. 9903888166; Fax +91-33-23553886.

© 2017 John Wiley & Sons Ltd

Introduction

Metacaspases are a class of cysteine proteases that cleave their substrates after an arginine/lysine residue at P_1 position (Vercammen *et al.*, 2007). These are found in plants, fungi and protozoa (Uren *et al.*, 2000). Like caspases, metacaspases also possess a conserved cysteine-histidine catalytic dyad that is required for catalysis by cysteine proteases (Uren *et al.*, 2000). Metacaspases play diverse functions across the kingdoms. For instance in plants, they have been found to be involved in more conventional functions associated with metacaspases or caspases, namely regulation or execution of cell death pathways (Coll *et al.*, 2010). Trypanosomatid metacaspases, however, lack a role in cell death regulation (Proto *et al.*, 2013) and exhibit unconventional functions like the generation of membrane-associated pseudopeptidase virulence factors (Proto *et al.*, 2011). Likewise, *Trypanosoma brucei* metacaspases have been demonstrated to be essential for the survival of bloodstream forms of the parasite (Helms *et al.*, 2006). Evidence of non-cell death roles of metacaspases is also available in the fungal homologs of the protein in literature. For instance, yeast metacaspase Yca1 functions in both the induction of programmed cell death in response to oxidative stress (Madeo *et al.*, 2002, Khan *et al.*, 2005), and in clearance of insoluble protein aggregates in logarithmically growing cells (Lee *et al.*, 2010). Besides *Saccharomyces cerevisiae*, functions of metacaspases have also been explored in certain other fungi like *Candida albicans* (Jung and Kim, 2014), *Aspergillus flavus* (Wang *et al.*, 2014) and *Podospora anserine* (Hamann *et al.*, 2007; Strobel and Osiewacz, 2013). In most of these cases, however, metacaspase function has been found to be associated with either stress induced or age-induced apoptosis. In this study, we investigate the function of the only metacaspase Mca1 of a biotrophic fungal pathogen, *Ustilago maydis* that causes smut disease of maize. To our knowledge, this is the first report of the functional characterization of a metacaspase gene from a phytopathogenic fungus. Unlike most of the fungal metacaspases, Mca1

BBA - Biomembranes 1860 (2018) xxx–xxx

Contents lists available at ScienceDirect

BBA - Biomembranes

journal homepage: www.elsevier.com/locate/bbamem

The oligomeric plasticity of Hsp20 of *Sulfolobus acidocaldarius* protects environment-induced protein aggregation and membrane destabilization

Mousam Roy, Sayandeep Gupta, Somi Patranabis[1], Abhrajyoti Ghosh*

Department of Biochemistry, Bose Institute, Centenary Campus, P 1/12, C. I. T. Road, Scheme - VIIM, Kolkata 700054, West Bengal, India

ARTICLE INFO

Keywords:
Small heat-shock protein 20 (Hsp20)
Aggregation protection
Membrane stabilization
Oligomerization
Crenarchaea
Sulfolobus acidocaldarius

ABSTRACT

Small heat shock proteins (sHsps) are a ubiquitous family of molecular chaperones that rescue misfolded proteins from irreversible aggregation during cellular stress. Many such sHsps exist as large polydisperse species in solution, and a rapid dynamic subunit exchange between oligomeric and dissociated forms modulates their function under a variety of stress conditions. Here, we investigated the structural and functional properties of Hsp20 from thermoacidophilic crenarchaeon *Sulfolobus acidocaldarius*. To provide a framework for investigating the structure-function relationship of Hsp20 and understanding its dynamic nature, we employed several biophysical and biochemical techniques. Our data suggested the existence of a ~24-mer of Hsp20 at room temperature (25 °C) and a higher oligomeric form at higher temperature (50 °C–70 °C) and lower pH (3.0–5.0). To our surprise, we identified a dimeric form of protein as the functional conformation in the presence of aggregating substrate proteins. The hydrophobic microenvironment mainly regulates the oligomeric plasticity of Hsp20, and it plays a key role in the protection of stress-induced protein aggregation. In *Sulfolobus* sp., Hsp20, despite being a non-secreted protein, has been reported to be present in secretory vesicles and it is still unclear whether it stabilizes substrate proteins or membrane lipids within the secreted vesicles. To address such an issue, we tested the ability of Hsp20 to interact with membrane lipids along with its ability to modulate membrane fluidity. Our data revealed that Hsp20 interacts with membrane lipids via a hydrophobic interaction and it lowers the propensity of in vitro phase transition of bacterial and archaeal lipids.

1. Introduction

During the process of evolution, a network of proteins emanated to protect cells against stress conditions (e.g., heat, cold, oxidative, pH, etc.) [1]. A predominant group of such stress response proteins is the molecular chaperones, which include different classes based on their molecular mass and evolutionary history [2]. Small heat shock proteins (sHsps) are one of the least conserved and least understood among these molecular chaperones [3,4]. The importance of sHsps is manifested by their almost ubiquitous expression in all three domains of life (archaea, bacteria, and eukaryotes) and their dramatic up-regulation in response to various signals including protein aggregation [5]. The present view of the mode of action of sHsp is that they bind to unfolding 'substrate' proteins in the cells and prevent their irreversible aggregation [6,7]. Most sHsps form large molecular assemblies with variable quaternary structure and the reversible dissociation of their oligomers has been reported to be important for their enhanced chaperone activity at elevated temperatures [8–11]. The common characteristic feature of sHsps is the presence of a conserved 'α-crystallin domain' (ACD) that consists of two β-sheets at the center, flanked by a C-terminal segment and preceded by a highly variable N-terminal region [4]. Several studies revealed that the ACD is involved in the formation of large oligomeric ensembles of mass ranging from 200 to 800 kDa and is highly important for oligomerization via an interaction with a conserved IXI motif in the C-terminal domain of neighboring subunits through a hydrophobic interaction [12]. The oligomeric plasticity of sHsps and its importance in the activity of these chaperones, however, remains poorly understood.

Thermal stress in living cells induces multiple changes that ultimately affect membrane structure and function by altering the membrane fluidity and denaturing membrane proteins. It has been shown that heat shock and ethanol stress could exert membrane-disruptive effects as well as promote denaturation of membrane proteins resulting in changes in the plasma membrane protein composition [13]. Some sHsps have been shown to bring about distinct alterations in certain characteristics of the membrane lipids, such as fluidity and permeability, and can thereby assist in the maintenance of membrane stability

* Corresponding author.
E-mail address: abhrajyoti.ghosh@jcbose.ac.in (A. Ghosh).
[1] Present address: Amity University, Kolkata, India.

https://doi.org/10.1016/j.bbamem.2018.09.005
Received 14 June 2018; Received in revised form 29 August 2018; Accepted 5 September 2018
Available online 07 September 2018
0005-2736/ © 2018 Elsevier B.V. All rights reserved.

Received: 2 May 2020 | Accepted: 18 August 2020

DOI: 10.1111/cmi.13256

RESEARCH ARTICLE

WILEY

Ustilago maydis secreted T2 ribonucleases, Nuc1 and Nuc2 scavenge extracellular RNA

Dibya Mukherjee[1] | **Sayandeep Gupta**[2] | **Abhrajyoti Ghosh**[2] | **Anupama Ghosh**[1]

[1]Division of Plant Biology, Bose Institute Centenary Campus, Kolkata, India

[2]Department of Biochemistry, Bose Institute Centenary Campus, Kolkata, India

Correspondence
Anupama Ghosh, Division of Plant Biology, Bose Institute Centenary Campus, 1/12 C.I.T. Road, Scheme VIIM, Kolkata 700054, India.
Email: ghosh.anupama@jcbose.ac.in

Funding information
Department of Science and Technology, Ministry of Science and Technology, India, Grant/Award Number: IFA13-LSPA16 (DST-INSPIRE Faculty Scheme)

Abstract

Ustilago maydis genome codes for many secreted ribonucleases. The contribution of two among these belonging to the T2 family (Nuc1 and Nuc2) in the pathogen virulence, has been assessed in this study. The *nuc1* and *nuc2* deletion mutants showed not only reduced pathogenicity compared to the SG200 WT strain but also exhibited significant delay in the completion of the pathogenic lifecycle. Both the proteins were also tested for their nucleolytic activities towards RNA substrates from maize and yeast. This also yielded valuable insights into the ability of the ribonucleases to utilise extracellular RNA as a nutrient source. Our study therefore established a role of two T2 type secreted ribonucleases of a phytopathogen in the acquisition of nutrient for the first time. This study also provides evidence that maize apoplast contains RNA, which can be utilised as a substrate by both Nuc1 and Nuc2.

KEYWORDS

effector proteins, extracellular RNA, T2 ribonucleases, *Ustilago maydis*, *Zea mays*

1 | INTRODUCTION

T2 ribonucleases are widely distributed across kingdoms and exhibit nucleolytic activities in the pH range of 4–5 (Irie, 1999). These ribonucleases, therefore, localise mostly within acidic cellular compartments like vacuoles and lysosomes (Deshpande & Shankar, 2002). Some of the T2 ribonucleases also exhibit secretory properties and hence confine within the extracellular milieu. An array of different biological functions has been found associated with T2 ribonucleases (Luhtala & Parker, 2010). Scavenging of RNA as a source of the nutrient is one of the tasks of T2 ribonucleases that have been observed quite often mostly in plants (Abel, Nurnberger, Ahnert, Krauss, & Glund, 2000; Bariola et al., 1994; Kock, Stenzel, & Zimmer, 2006; Nurnberger, Abel, Jost, & Glund, 1990). Secreted ribonucleases belonging to different families have also been reported in many of the fungal phytopathogens (Brown, Antoniw, & Hammond-Kosack, 2012; Espino et al., 2010). Most interestingly the expression of these ribonucleases is found to be induced several folds upon infection when compared to that in the axenic culture. This indicate important role of these ribonucleases during in-planta growth of the pathogen. Like for instance in *Zymoseptoria tritici* a small secreted RNase belonging to N1/T1 class, Zt6 has recently been shown to exhibit cytotoxic activities against bacteria, yeast, tobacco and even wheat cells (Kettles et al., 2018). It is hypothesised that Zt6 provides selective growth advantage to *Z. tritici* during infection of wheat. It is also hypothesised that an antitoxin yet to be identified probably also exists that might inhibit Zt6 activity against *Z. tritici* itself. In another instance a ribonuclease like secreted effector protein from *Blumeria graminis*, CSEP0064/BEC1054 has been shown to inhibit host cell death through its interaction with host ribosomes. CSEP0064/BEC1054 binds to host ribosome thereby inhibiting the action of plant ribosome inhibiting proteins that otherwise lead to host cell death (Pennington et al., 2019). This study also investigates the biological function of two secreted T2 type ribonucleases, Nuc1 and Nuc2 from *Ustilago maydis*. In *U. maydis* these two ribonucleases are found to be involved in scavenging nutrients from plant apoplastic RNA sources. Both the proteins are found to be efficiently secreted by the pathogen during infection and can act upon maize extracellular RNA. Moreover, each of the two proteins is also essential for the survival of *U. maydis* in-planta as their absence is associated with reduced virulence of the fungus.

 © 2020 John Wiley & Sons Ltd

Biochemical and Biophysical Research Communications 566 (2021) 53–58

Contents lists available at ScienceDirect

Biochemical and Biophysical Research Communications

journal homepage: www.elsevier.com/locate/ybbrc

Archaeal SRP RNA and SRP19 facilitate the assembly of SRP54-FtsY targeting complex

Sayandeep Gupta [a], Mousam Roy [a], Dhritiman Dey [b], Koustav Bhakta [a], Arghya Bhowmick [a], Dhrubajyoti Chattopadhyay [c], Abhrajyoti Ghosh [a, *]

[a] Department of Biochemistry, Bose Institute, Kolkata, India
[b] Department of Natural Products, National Institute of Pharmaceutical Education and Research, Kolkata, India
[c] Sister Nivedita University, Kolkata, India

ARTICLE INFO

Article history:
Received 25 May 2021
Accepted 26 May 2021

Keywords:
Signal recognition particle
Archaea
SRP RNA
Targeting complex (TC)
SRP54
SRP19
FtsY

ABSTRACT

The signal recognition particle (SRP) plays an essential role in protein translocation across biological membranes. Stable complexation of two GTPases in the signal recognition particle (SRP) and its receptor (SR) control the delivery of nascent polypeptide to the membrane translocon. In archaea, protein targeting is mediated by the SRP54/SRP19/7S RNA ribonucleoprotein complex (SRP) and the FtsY protein (SR). In the present study, using fluorescence resonance energy transfer (FRET), we demonstrate that archaeal 7S RNA stabilizes the SRP54·FtsY targeting complex (TC). Moreover, we show that archaeal SRP19 further assists 7S RNA in stabilizing the targeting complex (TC). These results suggest that archaeal 7S RNA and SRP19 modulate the conformation of the targeting complex and thereby reinforce TC to execute protein translocation via concomitant GTP hydrolysis.

© 2021 Elsevier Inc. All rights reserved.

1. Introduction

The signal recognition particle (SRP) and its receptor constitute essential cellular machinery required to execute cotranslational translocation of nascent polypeptides across the membranes in all three domains of life. The signal sequence at the N-terminus of the nascent polypeptide chain is recognized and bound by SRP. After that, it forms a complex with a cognate receptor (SR, in eukaryotes; FtsY, in prokaryotes) located on the target membrane. Such interaction is followed by a series of conformational rearrangements in the SRP-FtsY complex that leads to the delivery of the ribosome-nascent chain complex (RNC) to the nearby translocon (SecYEG). Once the RNC is released, the SRP-FtsY complex dissociates through concomitant GTP hydrolysis by both the proteins [1]. The SRP shares its structural and functional similarity across different domains of life. Mammalian SRP consists of six proteins (SRP54, SRP19, SRP68, SRP72, SRP9, and SRP14) and a 7S RNA, whereas the bacterial counterpart consists of only one protein (Ffh, SRP54 homolog) and a 4.5S RNA [1]. The ribonucleoprotein complex's functional core comprises the RNA and SRP54 protein that performs signal recognition, receptor interaction, and GTP hydrolysis. Archaea, being a true mosaic of eukaryotic and prokaryotic features, shares the similarities of mammalian SRP54, SRP19, and 7S RNA and the bacterial SRP receptor [2,3]. The 7S RNA and GTP, the key regulators in the evolutionarily conserved targeting process, are bound by the M domain and NG domain in SRP54, respectively. The catalytic NG domain is also the interacting domain for both SRP54 and FtsY, and the G domain shares the motifs of the classic P-loop GTPases [1]. SRP19 contacts the helices 6 and 8 of the 7S RNA and induce the side-by-side alignment of these two helices, which supposedly favors the conformational rearrangements in the asymmetric loop of helix 8 necessary for SRP54 binding [1]. However, SRP19-independent SRP54-7S RNA binding has been shown in *Haloferax volcanii,* where the cells could grow normally even after the deletion of the *srp19* gene implying the dispensable nature of SRP19 [4]. SRP RNA is crucial to signal sequence recognition and binding and plays a vital role in the interaction of the two GTPases in bacteria. Kinetic analyses have shown that bacterial 4.5S RNA does not affect the basal GTPase activity of Ffh but is required for a successful association with FtsY [5]. Though the stable assembly of the two proteins is GTP-dependent, it is initiated by an early GTP-independent complex which is significantly stabilized by 4.5S

* Corresponding author. Department of Biochemistry, Bose Institute P1/12, CIT Road, Scheme VIIM, Kolkata-700054, West Bengal, India.
E-mail address: abhrajyoti.ghosh@jcbose.ac.in (A. Ghosh).

https://doi.org/10.1016/j.bbrc.2021.05.087
0006-291X/© 2021 Elsevier Inc. All rights reserved.

Check for updates

The FEBS Journal

FEBS PRESS science publishing by scientists

Archaeal Hsp14 drives substrate shuttling between small heat shock proteins and thermosome: insights into a novel substrate transfer pathway

Mousam Roy[1], Koustav Bhakta[1], Arghya Bhowmick[1], Sayandeep Gupta[1], Anupama Ghosh[2] and Abhrajyoti Ghosh[1]

1 Department of Biochemistry, Bose Institute, Kolkata, India
2 Division of Plant Biology, Bose Institute, Kolkata, India

Keywords
aggregation protection; protein folding; heat shock protein; subunit exchange; *Sulfolobus acidocaldarius*

Correspondence
A. Ghosh, Department of Biochemistry, Bose Institute, P1/12 C.I.T., Scheme VIIM, Kolkata- 700054, India
Tel: +91 7044287317
E-mails: abhrajyoti.ghosh@jcbose.ac.in; aghosh78@gmail.com

Mousam Roy and Koustav Bhakta contributed equally to this article.

(Received 19 April 2021, revised 26 August 2021, accepted 11 October 2021)

doi:10.1111/febs.16226

Heat shock proteins maintain protein homeostasis and facilitate the survival of an organism under stress. Archaeal heat shock machinery usually consists of only sHsps, Hsp70, and Hsp60. Moreover, Hsp70 is absent in thermophilic and hyperthermophilic archaea. In the absence of Hsp70, how aggregating protein substrates are transferred to Hsp60 for refolding remains elusive. Here, we investigated the crosstalk in the heat shock response pathway of thermoacidophilic crenarchaeon *Sulfolobus acidocaldarius*. In the present study, we biophysically and biochemically characterized one of the small heat shock proteins, Hsp14, of *S. acidocaldarius*. Moreover, we investigated its ability to interact with Hsp20 and Hsp60 to facilitate the substrate proteins' folding under stress conditions. Like Hsp20, we demonstrated that the dimer is the active form of Hsp14, and it forms an oligomeric storage form at a higher temperature. More importantly, the dynamics of the Hsp14 oligomer are maintained by rapid subunit exchange between the dimeric states, and the rate of subunit exchange increases with increasing temperature. We also tested the ability of Hsp14 to form hetero-oligomers via subunit exchange with Hsp20. We observed hetero-oligomer formation only at higher temperatures (50 °C–70 °C). Furthermore, experiments were performed to investigate the interaction between small heat shock proteins and Hsp60. We demonstrated an enthalpy-driven direct physical interaction between Hsp14 and Hsp60. Our results revealed that Hsp14 could transfer sHsp-captured substrate proteins to Hsp60, which then refolds them back to their active form.

Introduction

A living cell often suffers abrupt changes in its surroundings, putting the cell under stress. The ability to cope with such environmental stresses is crucial for the survival of any organism. One of the significant effects of stress is the denaturation of protein, followed by aggregation. Protein aggregates are toxic and could be fatal for the cells if not adequately dealt with [1–4]. A group of proteins known as heat shock proteins or chaperones has evolved mainly to prevent aggregate formation by unfolded proteins [5]. Heat shock proteins can be classified into five major classes depending on their molecular weight, such as Hsp100, Hsp90, Hsp70,

Abbreviations
ANS, 8-anilino-1-naphthalenesulfonic acid; CIP, calf intestinal phosphatase; DLS, dynamic light scattering; FITC, fluorescein isothiocyanate; Hsp, heat shock protein; ITC, isothermal titration calorimetry; LDH, lactate dehydrogenase; pNP, para-nitrophenol; pNPP, para-nitrophenyl phosphate; sHsp, small heat shock protein; TRITC, tetramethylrhodamine-5-isothiocyanate.